Faculty of Science and Engineering

Magnetic Nanostructures for Selective Detection of Zinc Ions in Aqueous Solutions

Ghazaleh Pourfallah
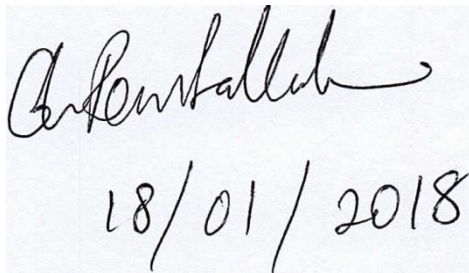
This thesis is presented for the Degree of
Doctor of Philosophy
of
Curtin University

January 2018

DECLARATION

To the best of my knowledge and belief this thesis contains no material previously published by any other person except where due acknowledgment has been made.

This thesis contains no material which has been accepted for the award of any other degree or diploma in any university.

Ghazaleh Pourfallah

January 18th 2018

ABSTRACT

This thesis reports on the synthesis and characterization of novel magnetic nanostructure fluorescent chemosensors as well as their potential applications in sensing and detection of heavy metals. The nanostructures obtained in this study were carefully designed by employing a core-shell approach which was advantageous by offering stability hydrophilicity and recoverability.

For this purpose, magnetic Iron oxide (Fe_3O_4) was prepared through a well-stablished co-precipitation procedure followed by coating a thin layer of silica shell (SiO_2) around nanoparticle cores. Functionalised polyethylene glycol (PEG) was further attached to the core-shell nanostructure via a silane linker either 3-aminopropyl)triethoxysilane (APS) or (3-glycidyloxypropyl) trimethoxylsilane (GPS), which was further conjugated with selected flouorophores. Incorporating PEG on the surface of silica coated nanoparticles provides wettability and hydrophilicity and improves the mobility of the fluorophore moiety and spatially separates the fluorophore from the magnetic core, therefore reducing the probability of core-fluorophore interactions. Further, the peglated core-shell nanostructure was covalently attached to fluorophore moiety for sensing purposes. The first fluorophore applied in this study was 5-(dimethylamino) naphthalene-1-sulfonyl chloride (with a trade name of dansyl chloride (DnCl)) to produce Fe_3O_4@SiO_2-PEG-DnS nanochemosensors. Dansyl chloride (DnCl) is a well-established fluorophore with a large Stockes shift, high quantum yield and charge transfer ability. The sizeand morphology of the resulting nanostructure system were characterised using transmission electron microscopy (TEM). The successful fabrication of the dansylated nanochemosensors was also confirmed by various spectroscopic techniques such as Furrier transform infra-red (FTIR), UV-visible absorption, Thermogravimetric analysis (TGA) and X-ray diffraction (XRD) analysis. The photophysical

properties of the produced nanochemosensor were further investigated in aqueous solution by fluorescence spectrometer. The results revealed a noticeable selectivity for $Fe_3O_4@SiO_2$-PEG-DnS towards Zn^{2+} cation by significantly quenching the fluorescent intensity. The complexation of the fluorescent nanochemosensor with Zn^{2+} ion is believed to occur through the electron pair-containing nitrogen in naphthalene ring.

An aminoquinoline derivative nanochemosensor namely $Fe_3O_4@SiO_2$-PEG-4AQ was also fabricated by utilising the 4-isomer of aminoquinoline (4AQ) as a fluorophore. The design of this novel nanochemosensor was based on the unusual chemical properties of 4AQ in comparison with other aminoquinoline derivatives. The produced nanochemosensor was also fully characterised to confirm the prosperous structure as well as the size and morphology of the nanoparticles. The photophysical properties were also investigated in aqueous solution revealing a 13.5-fold fluorescence enhancement upon complexation with Zn^{2+} resulted from tuned ICT.

The other photophysical properties such as sensitivity of the chemosensor, detection limit, pH dependence, quantum yield, molar stoichiometric ratio (Job plot), competition study with other metal cations as well as reusability and recoverability of both synthesised nanochemosensors were also determined using fluorescence and UV-vis spectrometers. Both nanochemosensors were able to distinguish Zn^{2+} from Cd^{2+} which is beneficial as Cd^{2+} often demonstrates coordination properties similar to those of Zn^{2+} due to both having a full d^{10} electron configuration. The influence of PEG spacer on both prepared nanochemosensors was further investigated by comparing their photophysical properties with a similar nanostructure with no PEG attached to the surface of nanoparticles. The results demonstrated a significantly improved sensitivity and selectivity towards zinc ions.

The crystalline structure of one of the chemosensors was studied by using a short length PEG spacer covalently grafted on dansyl chloride (DnCl) fluorophore. For this purpose, the single

crystals of PEG-DnS were prepared by reacting mPEG with DnCl in dry acetone followed by solvent evaporation. The crude product was repeatedly washed and single crystals were obtained by slow evaporation of solvent at room temperature and purified by recrystallization. The single crystals were then characterized by nuclear magnetic resonance (^{1}HNMR), FTIR and UV-Vis. The crystallography study was also performed by single crystal X-ray Diffraction (XRD) to support the hypothesised coordination mode between the fluorophore and Zn^{2+} ion. The obtained results evident the complexation between electron donor nitrogen atom of naphthalene ring in fluorophore structure and Zn^{2+} and also supported the obtained 2:1 stoichiometric ratio between the chemosensor and zinc cation. The photophysical properties of PEG-DnS was also investigated which was in agreement with that of obtained for $Fe_3O_4@SiO_2$-PEG-DnS previously.

This thesis is ultimately aimed at the development of an entirely novel, stable and more importantly recyclable as an environmentally friendly nanochemosensors for detection of Zn^{2+} cation. The methodology and results presented in this dissertation shall provide a better understanding of nanostructure surface modification and functionalisation for design and development of nanochemosensors. It also offers a feasible and cost effective procedure for heavy metal detections with high sensitivity and selectivity in different applications such as mining industry, biological and environmental areas.

ACKNOWLEDGEMENTS

PUBLICATIONS

Journal publications:

1. Pourfallah, G., Lou, X. (2016) A novel recyclable magnetic nanostructure for highly sensitive, selective and reversible detection of zinc ions in aqueous solutions. Sensors and Actuators B: Chemical, 223, 379-387.

   Doi:https://doi.org/10.1016/j.snb.2016.04.087

   (This paper is based on work presented in Chapter 2)

Contribution: The research and work was primarily designed, executed, interpreted and written by the author, with guidance from Professor Xia Lou, the thesis supervisor.

2. Pourfallah, G., Lou, X. (2018), The Synthesis and Characterisation of Quinoline Functionalized Magnetic Nanostructure for Selective and Sensitive Detection of Zn^{2+} in Aqueous Solutions. Accepted for publishing in Dyes and Pigments Journal.

   Doi: https://doi.org/10.1016/j.dyepig.2018.05.021, November 2018

   (This paper is based on the work presented in Chpater 3)

Contribution: The research and work was primarily designed, executed, interpreted and written by the author, with guidance from Professor Xia Lou, the thesis supervisor.

3. Pourfallah, G., Lou, X. Synthesis, Characterization and Crystallography of PEG Conjugated Dansyl Fluorophore. This manuscript is in preparation based on the work presented in Chapter 5.

Contribution: The research and work was primarily designed, executed, interpreted and written by the author, with guidance from Professor Xia Lou, the thesis supervisor.

Conference Presentations:

A novel dansylated magnetic nano-structure for selective detection of Zn^{2+}, Pourfallah, G., Lou, X. A poster presentation at the 12th International Conference on Materials Chemistry (MC12), University of York, UK, July 2015.

Contribution: The research and work was primarily designed, executed, interpreted and written by the author, with guidance from Professor Xia Lou, the thesis supervisor.

TABLE OF CONTENTS

List of Figures

List of Tables

Chapter 1

Introduction and Overview

1.1.   General introduction to fluorescence spectroscopy

Fluorescence is the light emitted by an atom or molecule after absorption of a limited duration of electromagnetic energy which promotes an electron from the ground state to an unoccupied orbital after absorption of a photon (Albani 2008). Basically, when molecules are exposed to light, some of the light energy absorbed could be promoted to a higher energy orbital. This electron promotion is often from the highest occupied molecular orbital (HOMO), usually the singlet ground state to the lowest unoccupied molecular orbital (LUMO), and the resulting species is called the singlet excited state (Lakowicz and Masters 2008). The $n - \pi^*$ and $\pi - \pi^*$ are the two lowest energy transitions that can be achieved as a result of the energy available from the photons as shown in Figure 1-1.
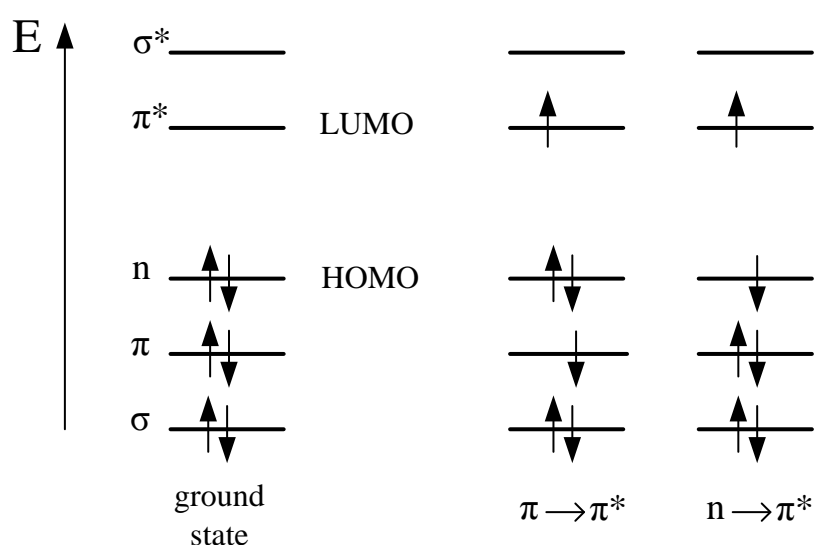
Figure 1-1. Energy transition levels

Generally, fluorescence is a result of a three-step process which occurs in a fluorescent molecule. Figure 1-2 demonstrates this process based on Jablonski diagram (Frackowiak 1988):

1. Excitation: A photon is absorbed by the fluorophore which creates an excited singlet state (S'_1).

2. Excited state: During a short period of time (1-10 nanoseconds), the fluorophore undergoes conformational changes and the energy of S'_1 is partially dissipated which yields a singlet excited state (S_1).

3. Fluorescent emission: Fluorescence emission originates from S_1 energy state. A photon of energy is emitted, returning the fluorophore to its ground state S_0. The difference in energy or wavelength between the absorbed and emitted photon is called the Stokes shift.
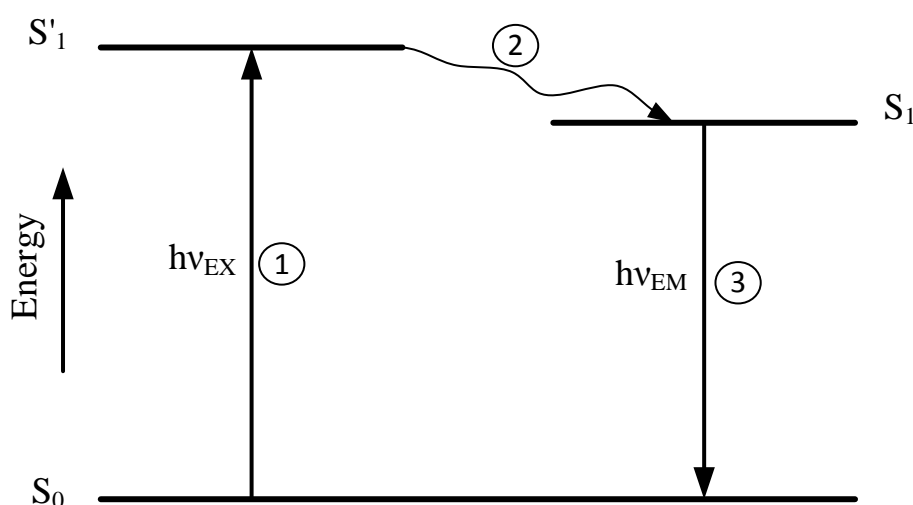
Figure 1-2. Jablonski diagram for the three-step fluorescence process

1.1.1. Fluorescence spectroscopy as a tool for sensing

Fluorescence spectroscopy has been widely investigated for sensing of transition metals for several decades. Most of the applications were in biology or medicine; however, it can be also used in environmental studies, water or mining industry. Development of simpler, faster

and more reliable methods to be cost-effective as well is of major interest in the field of sensing and detection of transition metals. Fluorescence spectroscopy possesses many attractive characteristics for sensing applications such as high sensitivity which can go down even to nano-range, simplicity of the method and being relatively cheaper compare to other sensing instrumentations (Valeur and Brochon 2012). The use of fluorescent molecules as detection probes is of corporate approach for the purpose of sensing. The very first fluorescent molecules were used for labelling of biomolecules such as DNA and proteins in the biomedical applications (Weiss 1999).

The ideal fluorescent probe should own all the following parameters (Basabe-Desmonts, Reinhoudt et al. 2007):

- Water solubility: for biological application and environmentally friendly purposes.

- High selectivity: to be able to distinguish only one target among others

- High sensitivity: to give the intense signal change in case of interaction with the target

- Luminescent properties in the visible region: to be able to detect the target by means of common source of light with the least interference with biological samples.

Fluorescent chemical sensors, also named as "chemosensors", have been proved to be able to overcome many of the restrictions that other sensory devices might have had and meet all the above criteria to be count as the ideal fluorescent probe. Chemosensors are also valuable since they are feasible to make, user friendly and cost-effective. Figure 1-3 exhibits a simple structure of a chemosensor.
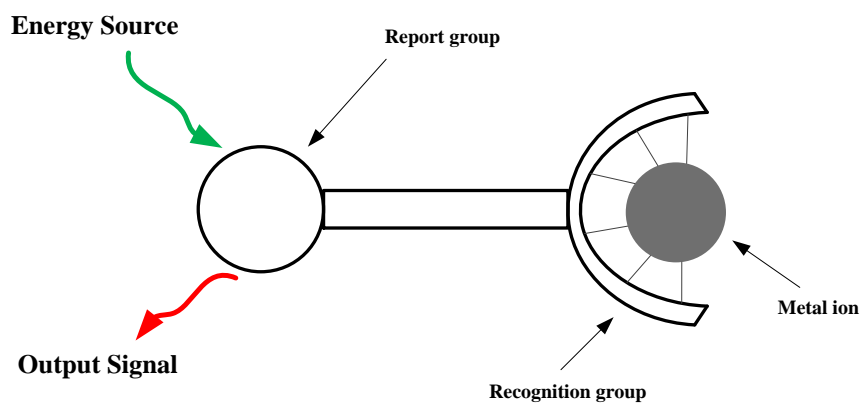
Figure 1-3. Chemosensor structure (combination of metal ions and change of the output signal)

1.2. Chemosensors

1.2.1. The need of Chemosensors

A chemosensor is a molecule that connects with the species such as a transition metal ion to produce a detectable change. There are numerous analytical methods for the detection of analytes, however they are expensive and often require large amount of sample (Czarnik 1993). Therefore, molecular sensors gain significant importance in this field. Chemosensors consist of fluorophore and ion receptor, while the receptor complex with a guest, a signal can be observed by the fluorophore (Figure 1-4). Among all type of chemosensors, fluorescent chemosensor is very important which utilizes fluorescence light as the output signal and offers many advantages such as high sensitivity, low cost, ease in application, versatility, etc. The main advantage of fluorescent chemosensor is its high sensibility. This is so because the emitted fluorescence signal is proportional to the analytes concentration even at very low ranges (Ueno and Nagano 2011).
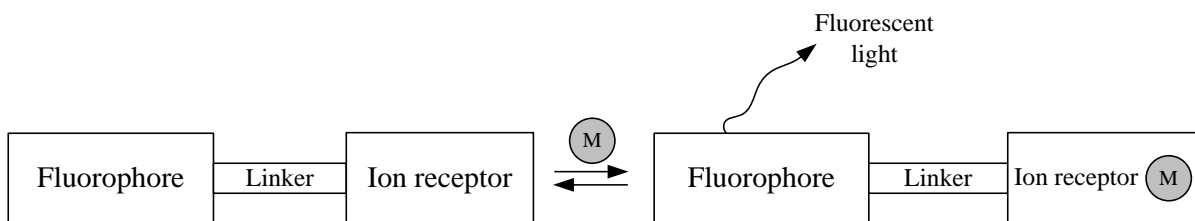
Figure 1-4. Chemosensor behaviour upon metal ion complexation

The photophysical properties of a fluorophore can be modulated by many approaches such as the introduction of proton, energy and electron-transfer processes, the presence of heavy atoms, changes in electronic density, and destabilisation of non-emissive n-π^* excited states (Valeur and Leray 2000).

The final goal of a luminescent chemosensor is to convert a chemical signal, represented by the concentration of the target (transition metal) into a luminescence signal, which can be quantitatively measured. Chemosensors have a broad range of applications such as biochemistry, clinical and medical sciences, cell biology, analytical chemistry and environmental sciences. The point of safety for the use in biological application is due to the fact that samples are neither affected nor damaged during the measurements and there is no hazardous by-product is generated (Valeur and Berberan-Santos 2012).

1.2.2. Design principles for chemosensors

The concept of "chemosensor" was first introduced by Czarnik in 1993 (Czarnik 1993) and was defined as "a compound of abiotic origin that complexes to an analyte reversibly with a concomitant fluorescent signal transduction'' and it constitutes only the active transduction unit of a sensor". For decades, the design of fluorescent chemosensors was composed of two moieties a receptor responsible for the molecular recognition and a fluorescent dye responsible of signalling the recognition event integrated into the same molecule which results in the term of "small molecule chemosensor". For transition metals to be detected by fluorescence there must be some observable changes in the fluorescent emission by the

5

fluorophore. One approach contains an enhancement in fluorescent intensity in the presence of metal ion. The other approach is fluorescence quenching and is when the chemosensor shows high fluorescence in the absence of the metal ion however, it could be reduced or no fluorescence in the presence of metal ion (Valeur and Berberan-Santos 2012).

1.2.3. Mechanism of fluorescence intensity upon binding with metal ion

Binding an analyte to a receptor may lead to a significant change in the photophysical properties of the fluorophore. Design of a chemosensor determines the type of alteration might be observed in the fluorescence signal after complexing with the target. These alterations could be a form of amplification or quenching of the fluorescence signal as well as shift in the emission wavelength (Desvergne and Czarnik 2012).

1.2.3.1.   Enhancement of fluorescence intensity

The three major mechanisms of fluorescence sensing include ICT (intermolecular charge transfer), PET (photoinduced electron transfer) and FRET (fluorescence resonance energy transfer) (Demchenko 2008). The ICT mechanism is well-known for designing ratiometric fluorescent chemosensors. In this mechanism, the receptor which is often an amino group, directly interact with a conjugation system. The system would then have an electron rich and electron poor ends. The electron charge transfer occurs from the electron donor to the receptor and cause an enhancement in ICT once the light is excited (De Silva, Gunaratne et al. 1997). The interaction of the receptor with the metal cation provides additional strength to the push‑pull effect and leads to a red shift in emission (Qian, Xiao et al. 2010).

PET mechanism, on the other hand, often uses a linker which contains no more than three carbon atoms between the fluorescence group to the receptor. Upon excitation by photons the electron of the highest occupied molecular orbital (HOMO) of the fluorophore is promoted to

the local lowest unoccupied molecular orbital (LUMO); but when the electron pair is interacted with a metal ion, there would be an interruption in electron transfer and the fluorescence is turned on (Fabbrizzi, Licchelli et al. 1996, Thiagarajan, Ramamurthy et al. 2005).

Recently, the fluorescence resonance energy transfer (FRET) is more of interest in designing sensors. Sensors with FRET mechanism usually enclose with two fluorophores which connected to each other by a spacer through covalent bonds. (Shang, Gao et al. 2008, Yuan, Lin et al. 2013).

1.2.3.2. Quenching of fluorescence intensity

Fluorescence quenching states any processes that cause a decrease in the fluorescence intensity of sample. Fluorescence quenching typically occurs through either the mechanism of static or dynamic (collisional) quenching (Rehm and Weller 1970). In dynamic quenching, the contact between quencher and fluorophore takes place during the excited state and the fluorophore returns to its ground state, without emitting (Figure 1-5) (Chen, McBranch et al. 1999).

Absorption

Fluorescence
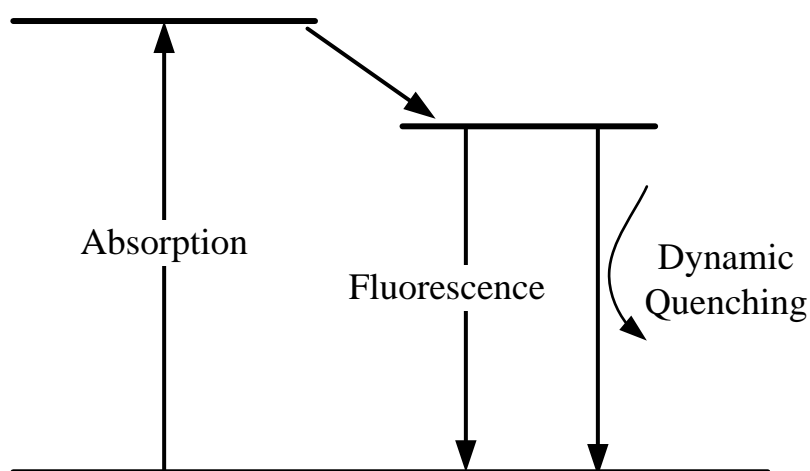
Dynamic
Quenching

Figure 1-5. Dynamic quenching of fluorescence signal

In static quenching however, complexation forms between the fluorophore and the quencher which this complex is non-fluorescent (Laws and Contino 1992).

$$\text{Fluor} + \text{Q} \; \rightleftharpoons \; \text{Fluor} \cdot \text{Q}$$

1.2.4. Small molecule chemosensors for transition metals

A pioneering work regarding fluorescent chemosensors for transition metals was reported by Parker et al (Parker and Williams 1995). They showed the fluorescence behaviour of two macrocyclic ligands incorporating naphthyl fluorophores. The two synthesized ligands exhibited a two-fold increase in the intensity of the naphthyl fluorescence in the presence of Zn^{2+}, however, the addition of Pb^{2+}, Ni^{2+} and Cu^{2+} quenched the fluorescent intensity.

Later on, Czarnik and co-workers (Desvergne and Czarnik 1997) prepared two ligands namely: 2- and 9-anthracene derivatives bearing the N-methylthiohydroxamate. The ligands exhibited strongly quenched fluorescence after binding with Pb^{2+} arising from the mechanism of photo-induced electron transfer. The experiments were done over a few competitive metal ions such as Ag^{+}, Co^{2+} and Hg^{2+}, but this was still one of the first attempts on detecting Pb^{2+}.

Prodi et al. (Prodi, Montalti et al. 2001) designed and synthesized 5-chloro-8-methoxyquinoline appended diaza-18-crown-6 as a chemosensor for Cd^{2+} detection. The fluorophore demonstrated very weak fluorescent emission in methanol solution, however, the fluorescence was enhanced 94-fold and 30 nm red shifted in the presence of Cd^{2+}.

Lin and co-workers (Lin, Cao et al. 2010) fabricated a novel fluorescence turn-on Hg^{2+} sensor containing a thiol atom and an alkene segment for sensing application. The chemosensor was highly selective to Hg^{2+} and showed a 1000-fold enhancement in fluorescent emission with Hg^{2+} in PBS buffer.

1.2.5. Conjugated polymer florescent chemosensor for transition metals

Apart from small molecule fluorescent chemosensors, conjugated polymer chemosensors also have been used and investigated for the detection of transition metals in a variety range of applications. Conjugated polymer fluorescent chemosensors have shown several important advantages over the small molecule chemosensors. The combination of polymer and small molecule structures would be able to provide new opportunities for design and development of new sensors (Kimura, Horai et al. 1998). A very vital advantage is that a conjugated polymer chain with small organic chemosensor is able to enhance the binding affinity and selectivity for specific target. Also, the amplification of the fluorescence signal could be induced by the polymer conjugation. Polymers offer a great deal of flexibility to the conjugated structure as well as structural modification and stability (Fan, Zhang et al. 2009). Studies show that different types of polymers have been used as a conjugated chemosensor to obtain enhanced photophysical properties and sensitivity of the chemosensor. Lu et al. (Li, Xu et al. 2009) designed and synthesized quinoline derivatives with methacrylate moieties to make it soluble in organic solvents as well as their application in fluorescent devices. The obtained polymer conjugated quinoline derivative displayed high selectivity and sensitivity towards Fe^{3+} with noticeable quenching effect of fluorescence in comparison with other tested transition-metal ions such as Zn^{2+}, Ni^{2+}, Cu^{2+}, and Co^{2+} in different organic solvents. Su et al. (Wang, Liu et al. 2009) also used free radical copolymerization for preparation of a hydrophilic polymer with coumarin for sensing Ni^{2+}. The conjugated chemosensor was seen as an effective on and off probe in the range of pH: 3.02–12.08, and was highly selective for Ni^{2+} by turning on the fluorescence. Tian et al. (Guo, Zhu et al. 2009) reported a water soluble co-polymer by employing a dicyanomethylene- 4H-pyran (DCM) segment to be used as a fluorescent sensor for Cu^{2+}. They chose the hydrophilic copolymer P3 (Figure 1-6) poly(2-hydroxyethyl methacrylate) (PHEMA) to improve the hydrophilicity and permeability

9

of the polymer backbone. The conjugated chemosensor turned-off fluorescent emission in the presence of Cu^{2+}.
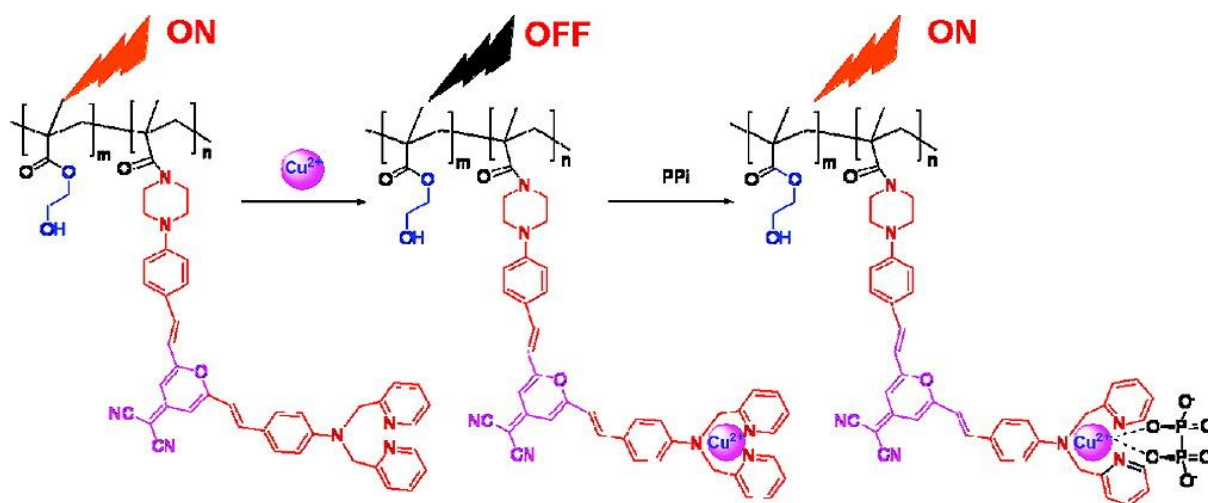
Figure 1-6. chemosensor based on the fluorescence ''off–on'' of P3 and P3-Cu^{2+} (Guo, Zhu et al. 2009)

Liu et al. (Hu, Li et al. 2009) constructed a sensitive hydrophilic block co-polymer chemosensor which was sensitive to pH, Hg^{2+} ions and temperature by using RAFT polymerization method. Poly(ethylene oxide)-b-poly(N-isopropyl acrylamide-co-RhBHA) (P4), (PEO-b-P(NIPAM-co-RhBHA)), which are hydrophilic copolymers, were able to sense Hg^{2+} by having rhodamine derivative in their thermo-sensitive block. They found that at higher temperatures the sensitivity of the chemosnsor could be improved for sensing Hg^{2+} ions and pH.

1.2.6. Nanostructure chemosensors

Design and development of nanoscale material in chemical sensing has recently been of a progressive interest in biological and bioanalytical applications. Nanomaterials with their unique properties, varied size and shape and their high surface area offer promoted chemical and physical properties specifically in the field of chemosensor and biosensors by improving their sensitivity (Prodi 2005). Silica nanoparticles (SiNPs), gold (AUNPs), silver (AgNPs)

and iron oxide nanoparticles (Fe_2O_3/Fe_3O_4) have been used in a wide range of sensors by having unique optical and magnetic properties. Polymer-nanoparticles have been studied in recent years as they are chemically inert material for fluorescent applications. The first group who has proposed this matrices system was Kopelman and Rosenzweig (Buck, Xu et al. 2004). They described the nanoparticle matrix as a protection for sensor from any interference with the cellular content. Montalti and co-workers (Montalti, Prodi et al. 2002) investigated silica nanoparticles chemosensor and reported on photophysical processes that can be collected from two different fluorescent molecules connected to the surface of the silica nanoparticles. Rampazzo et al. (Rampazzo, Brasola et al. 2005) reported on an effective and new fabrication of coated silica nanoparticle chemosensor. The sensor was able to detect Cu (II) ion by quenching the fluorescence (Figure 1-7).
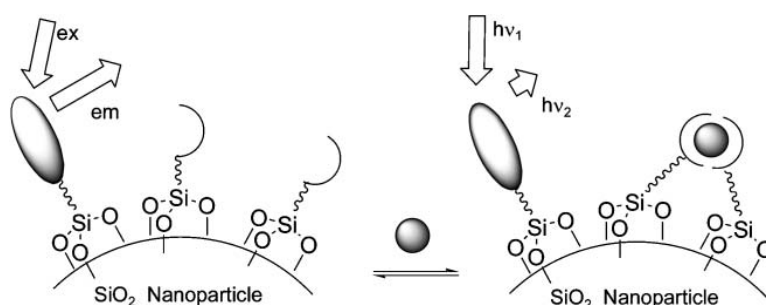
Figure 1-7. Coated silica nanoparticles based fluorescence chemosensors (Rampazzo, Brasola et al. 2005)

Larpent and coworkers (Méallet-Renault, Pansu et al. 2004) also reported on nanoparticles with two fluorescent dyes: cyclam ligand and borondipyrromethane (BODIPY). They showed major fluorescence signal in the presence of Cu(II) by fluorescent quenching.

1.2.6.1. Core-shell nanostructure

Core-shell nanoparticles have also attracted a wide range of interests recently by offering magnetic, structural, optical, electrical and chemical properties in bio-sensing application

specifically (Arfsten, Armes et al. 2007). It is worth to mention that core-shell nanomaterials are different than those nanoparticles with an organic coated layer. Core-shell nanomaterials basically contain a core and a shell which both are in nano scale and their synthesise is performed in consequent steps (Ghosh Chaudhuri and Paria 2011). The core is often a metal oxide and the shell can be an organic, inorganic, organic-inorganic hybrid or polymeric nanomaterial. Core-shell nanostructure offers biocompatibility, functionality and increased nanoparticle flexibility by having elevated surface area (Yoon, Yu et al. 2006).

Lee et al. (Cho, Lee et al. 2010) used a porphyrin-functionalized $Au@SiO_2$ core-shell nanoparticles to fabricate chemosensor prepared by the sol–gel method. The produced chemosensor was highly selective for Hg^{2+} when tested among the other metal ions.

Park and co-workers (Park, Seo et al. 2010) prepared a new type of fluorescent chemosensor containing $Ni@SiO_2$ core-shell nanoparticles functionalized with nitrobenzofuran. The fabricated chemosensor was selective to Cu^{2+} and was effective in detecting Cu^{2+} in human blood and drinking water.

Montoya et al. (Delgado-Pinar, Montoya et al. 2010) reported on fabrication of $Al@SiO_2$ core-shell nanostructure. They grafted the nanoparticles by the fluorophoric polyamines from condensation of TEOS and $Al(NO_3)_3$-$9H_2O$ in ethanol. The resultant product was found to be an Hg^{2+} selective nanosensor as a consequence of PET mechanism in aqueous solution at pH = 5 among a range of transition metals.

1.2.6.2.   Magnetic core-shell nanostructure

Magnetic core-shell nanostructure has recently attracted even more interests over other nanosensors due to offering extra advantages. The most interesting benefit that magnetic core-shell nanoparticles ($Fe_3O_4@SiO_2$) are able to offer is recyclability or reusability by applying an external magnet. They also have controllable sizes ranging from a few

nanometres up to tens of nanometres which are the perfect size in nanoscale for providing high surface to volume ratio in different applications (Jung, Lee et al. 2011). Magnetic core-shell structures have been using in a broad range of applications including biomedical and biotechnological applications because they are biocompatible, easily renewable and stable against degradation. For example, they have been utilized in targeted drug delivery, magnetic resonance imaging (MRI), labelling and sorting of cells and separation and purification of biological products (Pankhurst, Connolly et al. 2003).

More recently, the magnetic Fe_3O_4 core with outer shell of silica as hybrid nanomaterial has obtained increasing attention in chemo-sensing applications due to improved functionalities and offering a promising approach in detecting toxic metal ions at very low concentrations (Nogués, Skumryev et al. 2006). An inert silica coating improves the stability of nanoparticles and also prevents their aggregation in solution. It also offers protection, biocompatibility as well as hydrophilicity to magnetic nanoparticles so they would be able to conjugate with organic fluorescent molecules or polymer spacers (Frey, Peng et al. 2009).

Peng and co-workers (Peng, Wang et al. 2011) designed and synthesized a functionalized magnetic core-shell $Fe_3O_4@SiO_2$ nanostructure as a fluorescent chemosensor for Hg(II) in CH_3CN (Figure 1-8). They showed their produced chemosensor with high affinity, selectivity and sensitivity upon the presence of mercury.
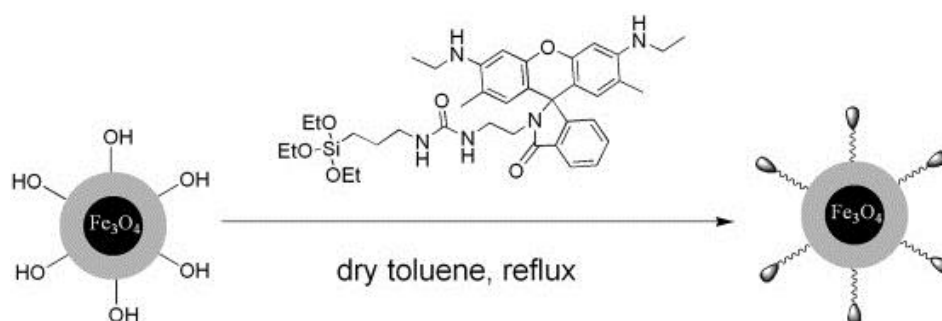
Figure 1-8. Fabrication of functionalized $Fe_3O_4@SiO_2$ nanostructure (Peng, Wang et al. 2011)

Liu et al. (Liu, Wu et al. 2011) reported on the preparation of bifunctional magnetic-luminescent dansylated $Fe_3O_4@SiO_2$ nanoparticles by the nucleophilic substitution of dansyl chloride with primary amines of aminosilane-modified $Fe_3O_4@SiO_2$ core–shell nanostructures. They used the produced nanosensor for cancer cell imaging either by magnetic resonance (MR) or fluorescent imaging.

Song et al. (Song, Li et al. 2013) synthesized a bifunctional polydopamine-Fe_3O_4 magnetic core-shell structure as shown in Figure 1-9. The polymeric nanosensor was able to simultaneously detect Pb^{2+} and Cd^{2+}. They investigated the magnetic nanosensor with high stability and low cost with high sensitivity for practical applications.
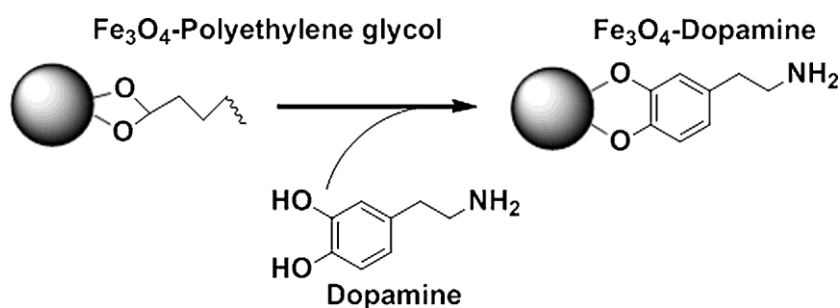
Figure 1-9. Fe_3O_4-Dopamine nanostructure (Song, Li et al. 2013)

Jeong et al. (Jeong, Shin et al. 2015) prepared magnetic core–shell nanoparticles for detection of metal ions. They fabricated metal – amine complex by using four different heavy metal ions (Co^{2+}, Cu^{2+}, Fe^{2+} and Hg^{2+}) interacted with their produced APTES–Fe@SiO_2 (Figure 1-10). The result showed that their magnetic core-shell sensor is selective to Co^{2+} by producing new absorption peaks at the range of 500-700 nm followed by a colour change which was evident by the formation of a strong chelating complex via amine group towards Co^{2+}.
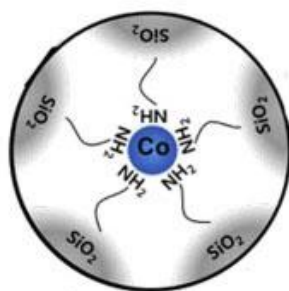
Figure 1-10. Schematic diagram for detection mechanism of core–shell nanoparticles

Wang and co-workers (Wang, Zhang et al. 2015) designed and develop a magnetic core-shell nanostructure fluorescent probe in conjugation with poly(m-phenylenediamine) namely Fe_3O_4@PmPDs for the detection of Cr(IV) ion. They illustrated a significant enhancement in absorption intensity which was attributed to the protonation of amino group within the nanostructure. They also suggested that the newly developed probe has a great potential in treating Cr(IV) – contaminated water.

Zeng et al. (Zeng, Xu et al. 2017) synthesized an inorganic/organic hybrid Fe_3O_4@SiO_2 nanostructure covalently attached to a rhodamine fluorescent probe. The nanosensor was selective towards Hg^{2+} by showing naked-eye colour change in water/methanol solution. The detection limit for sensing Hg^{2+} was reported to be 1×10^{-6} M.

Mao et al. (Mao and Liu 2018) also reported on fabrication of a magnetic core coated with silica shell and attached to rhodamine derivatives as their fluorescent probe. The synthesized magnetic core-shell nanochemosensor was able to detect Hg^{2+} by increasing the emission intensity with a detection limit of 11 μM. Their fabricated nanosensor was recyclable by using EDTA solution.

1.2.6.3. Magnetic core-shell nanostructure for selective detection of Zn(II)

1.2.6.3.1. The importance of Zn (II) detection

Zinc is the 23rd most found element in the Earth's crust having atomic number 30 and atomic weight 65.37 is one of the vital element in living systems. Zinc can be found in most rocks and minerals in various amounts and it enters the air, water and soil through both natural processes and human activities. It forms a variety of compounds, such as zinc chloride, zinc oxide, and zinc sulphate that are used in a wide variety of applications (Salgueiro, Zubillaga et al. 2000).

Metallic zinc is a very applicable metal in manufacturing. One of the most famous uses of zinc is the protection from corrosion and rust by coating steel and iron metals.

Metallic zinc is also utilising in dry batteries in the form of alloys when combined with other metals. Zinc ion can also be used for dying fabrics and to preserve woods. Likewise in making ceramics and white paints. (Xu and Pascoe 1994).

Zinc is an important divalent cation that is vital for many biological and physiological processes. Zinc is a trace element required for growth and development, proper immune function and good health (Roohani, Hurrell et al. 2013). Zinc is also the second most abundant transition metal found in human body after iron. It is a d-block metal which plays critical role in many biological processes such as brain function, gene and DNA transcription, immune function and reproductive system. Zn^{2+} is spectroscopically silent due to its specific d^{10} electron configuration (Endre, Beck et al. 1990).

The environmental impact of zinc must also be considered and it is a naturally occurring element in the environment. Very low and very high concentration of zinc in environment may produce undesirable impacts. The uncomplexed, free zinc ion (Zn^{2+}) can be the source of toxicity in the environment, water and soil. Zn^{2+} can also be found in hazardous wastes. Zinc

in air should be constant and as low as possible. Usually, manufacturing areas could have upper levels of zinc in the air. Some people in special industries are more potential for high levels of Zn^{2+} exposure such as in zinc mining, welding, brass and bronze alloys manufactures, rubber, plastic, ceramic and dyes industries. Drinking water can also be contaminated by high level of Zn^{2+}. Urban runoff, mine drainage and industrial wastes are sources of zinc in water (Kaur, Gupta et al. 2014).

Human bodies can be exposed to high level of zinc through food and water, inhaling dust and fumes and very small amount from the skin. However, the most likely source of zinc toxicity in human bodies is through drinking water specially children living near industrial areas. Thus, the detection of zinc is crucial for environment as well as human health.

The available analytical techniques such as UV-vis spectroscopy, flame atomic absorption spectrometry (AAS) and potentiometric are still limited for detection of Zn(II) due to the $3d^{10}4s^{0}$ not giving any spectroscopic signal (De Leon-Rodriguez, Lubag et al. 2012).

1.2.6.3.2. Nanochemosensors for Zn^{2+} based on magnetic core-shell structure

Zhou et al. (Xu, Zhou et al. 2013) reported on designing magnetic core–shell $Fe_3O_4@SiO_2$ nanostructure modified with rhodamine-B ($Fe_3O_4@SiO_2$-Rho) derivatives (Figure 1-11). The nanostructure served as a fluorescent OFF-ON nanosensor was used to detect Zn^{2+}. The inorganic/organic hybrid fluorescent chemosensor $Fe_3O_4@SiO_2$-Rho nanostructure exhibited selective "turn-on" type fluorescent enhancements with Zn^{2+} at room temperature.
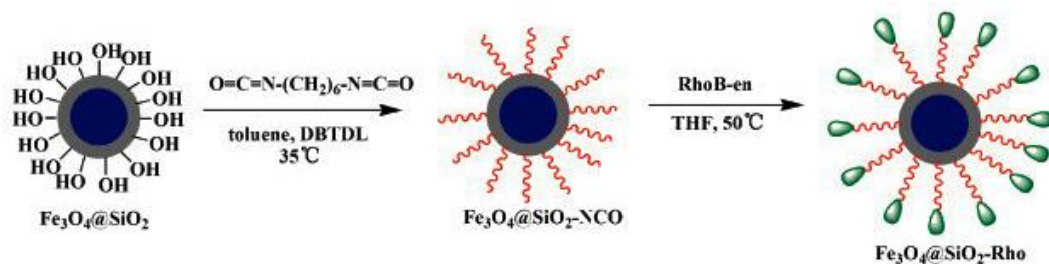
Figure 1-11. Functionalization of $Fe_3O_4@SiO_2$ NPs with rhodamine-B (Xu, Zhou et al. 2013)

Peng et al. (Wang, Peng et al. 2012) fabricated a magnetic core-shell nanosensor by 3,5-di-tert-butyl-2-hydroxybenzaldehyde (DTH) covalently grafted onto the surface of magnetic core-shell $Fe_3O_4@SiO_2$ nanoparticles (DTH-$Fe_3O_4@SiO_2$) using the silanol hydrolysis approach (Figure 1-12). The DTH-$Fe_3O_4@SiO_2$ inorganic-organic hybrid nanosensor exhibited fluorescence response towards Zn^{2+} by significant fluorescent enhancement (25-fold).
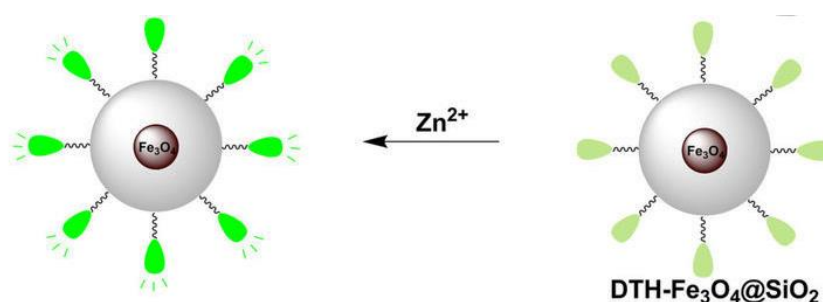
Figure 1-12. Syntheses of DTH-APTES and DTH-$Fe_3O_4@SiO_2$ (Wang, Peng et al. 2012)

Tian et al. (Tian, Dong et al. 2013) reported on designing highly selective and sensitive method for recognition of Zn^{2+} in aqueous solution by grafting a quinoline fluorescent sensor on the surface of magnetic silica nanoparticles ($Fe_3O_4@SiO_2$) (Figure 1-13). The produced chemosensor displayed high selectivity and sensitivity for Zn^{2+} by significantly enhancing the fluorescence emission signal based on electron transfer mechanism. They also used the chemosensor-Zn complex for the detection of H_2S.
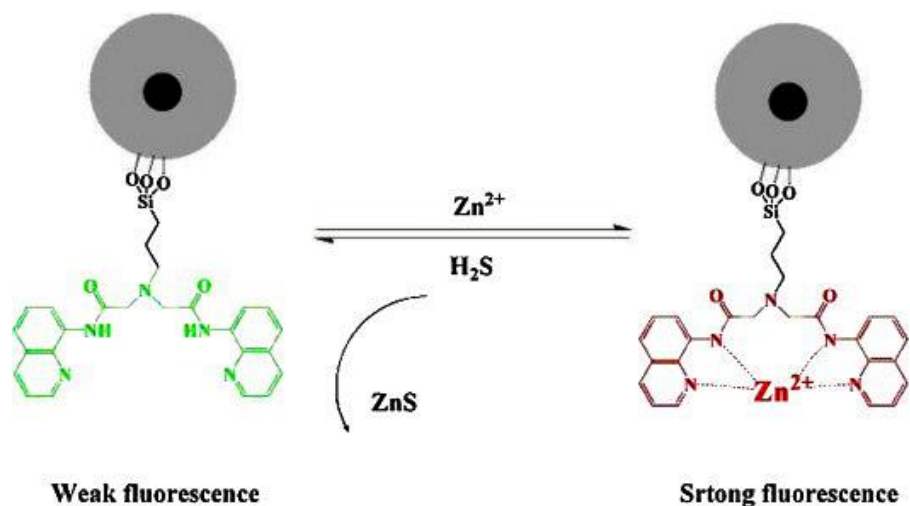
Figure 1-13. Complexation mechanism of the nanochemosensor with Zn^{2+}

Zhou et al (Xu, Zhou et al. 2013) reported on functionalization of $Fe_3O_4@SiO_2$ nanoparticles by 8-chloroacetylaminoquinoline (CAAQ) as a fluorescent chemosensor for detection and removal of Zn^{2+} as shown in Figure 1-14. The hybrid fluorescent material ($Fe_3O_4@SiO_2$-CAAQ) showed an efficient removal of Zn^{2+} from 100 ppm to as low as 7.63 ppm at room temperature (92.37%) and exhibited excellent magnetic properties for further biological and environmental applications.
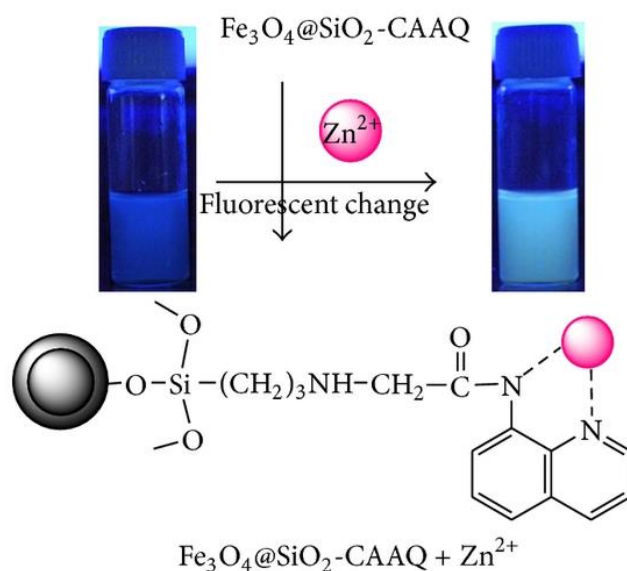
Figure 1-14. The complexation modeof $Fe_3O_4@SiO_2$-CAAQ and Zn^{2+} (Xu, Zhou et al. 2013)

Zeng et al. (Zeng, Zhou et al. 2014) also reported on development of $Fe_3O_4@SiO_2$ nanoparticles functionalized with di(2-picolyl)amine for detecting and removing Zn^{2+} in solution (Figure 1-15). The inorganic/organic hybrid magnetic network displayed sensitivity and selectivity to Zn^{2+} in acetonitrile solution with a detection limit of 10^{-5} M level of Zn^{2+} ion. Significant visual colour change from colorless to pink-red of $Fe_3O_4@SiO_2$–DPA nanosensor was observed by irradiation with 365 nm UV lamp upon the addition of zinc ions.
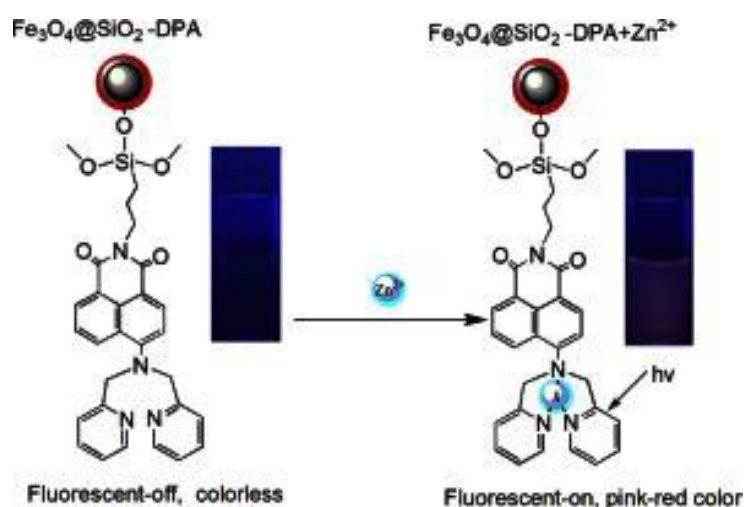
Figure 1-15. The complexation of Zn^{2+} to $Fe_3O_4@SiO_2$–DPA

Sun et al. (Sun, Li et al. 2015) developed a multifunctional core–shell magnetic silica nanospheres ($Fe_3O_4@SiO_2@KCC-1$) sensing probe for detection and removal of Zn^{2+}. They employed 8-aminoquinoline (AQ) as the fluorescent molecule to fabricate AQ-$Fe_3O_4@SiO_2@KCC-1$ and its complex with Zn^{2+} as AQ-$Fe_3O_4@SiO_2@KCC-1$–Zn^{2+}. Their results demonstrated a selective and sensitive fluorescent probe for Zn^{2+} with a detection limit of 1.08×10^{-7} M.

Bazrafshan (Bazrafshan, Hajati et al. 2015) fabricated a novel and simple Zn^{2+} selective sensor based on magnetic nanostructure ($Fe_3O_4@SiO_2$) using hydroxy-3-

methoxybenzaldehyde (2-H-3-MBA). Their results illustrated a selective fluorescent nanostructure towards Zn^{2+} with a detection limit of 2.5×10^{-6} M.

Kim and co-workers (Kim, Yoon et al. 2017) applied magnetics nanoparticles to prepare a hybrid nanochemosensor by employing dopamine–naphthalimide–dipicolylamine (DPA) as a fluorescent dye. The results demonstrate that their synthesized nanochemosensor was selective to Zn^{2+} by significantly increasing the fluorescent intensity. The detection limit was found to be 0.0345 ppb.

1.3. Scope of the research

In the recent past, growing concern over the environmental impacts and biological issues has promoted the fabrication of environmentally friendly chemosensors for heavy metal detections. Magnetic core-shell structures in particular, are being increasingly preferred over small molecule probes due to their biocompatibility as well as recyclability by using an external magnet. Previously used small molecule sensors suffer from high selectivity and sensitivity with the lack of biocompatibility and stability especially when the ions of zinc, cadmium and mercury co-exist, some show reduced fluorescence as a consequence of quenching, limiting the sensors' applicability Most of Shiff-base derivatives suffer from water solubility. Magnetic core-shell chemosensors have been found to provide improved selectivity and sensitivity and reusability to overcome such these limitations. Chemosensors consist of polymer spacer are yet able to offer extra advantages for detection of transition metals. Therefore, the conjugation of magnetic core-shell structure with a polymer spacer can be hypothesised to be a very promising approach in the case of sensing and detection of transition metals.

This study is ultimately targeted at the development of novel magnetic nanochemosensors involving polymer spacer that would have tuned photophysical properties and recyclability

and stability against degradation. Plain magnetic nanoparticles will be synthesised and functionalised with different silane coupling agents. Dansyl chlorides (5-(dimethylamino) naphthalene-1-sulfonyl chloride) as well as 4-amino-2-methyl-8-(trifluoromethyl) quinoline will be used as the organic fluorophores which is attached to the core-shell structure by a PEG spacer. The photophysical properties of these nanochemosensors will be also compared with their pristine structure with no PEG spacer involved. The emission and absorption properties of nanochemosensors shall be investigated through a series of experiments to determine their selectivity and sensitivity over the transition metal ions. The dependence of the fluorescent properties of nanochemosensors on pH value will also be investigated. Moreover, the quantum yield of nanochemosensors will be calculated by comparison with a reference compound. The stoichiometric mole ratio of metal-ligand complexation shall be then acquired by constructing job plot.

1.3.1. Aims and Objectives:

The purpose of this dissertation was to synthesis magnetic core-shell nanochemosensors for selective detection of Zn^{2+} cation, applying different fluorophores: dansyl chloride and 4-aminoquinoline derivative. $Fe_3O_4@SiO_2$-PEG-DnS was synthesised using a facile synthetic approach. A core-shell nanoparticulate system was developed for the purpose of recyclability and reusability. The core was to comprise of a hybrid, magnetic, iron oxide (Fe_3O_4) material, wrapped by a silica shell and attached to a dansyl chloride based fluorescent molecule and polyethylene glycol. Also, Synthesis of quinolone-derivative magnetic core-shell nanostructure: $Fe_3O_4@SiO_2$-PEG-4AQ through a similar pathway. The objectives of this research include: (1) Investigate the effect of polymer spacer between the organic fluorescent molecule and nanostructure: $Fe_3O_4@SiO_2$-PEG-DnS and $Fe_3O_4@SiO_2$-PEG-4AQ. (2) Study the selectivity of the nanosensors over a series of the metal cations as well as their sensitivity

and detection limit. (3) Determine the photophysical properties of the produced nanochemosensors such as quantum yield, stoichiometric molar ratio (Job's plot) and pH sensitivity. (4) Obtain the understanding about the crystalline structure of the polymer-fluorophore conjugation and its complexation mode with zinc cation.

1.3.2. Research Methodology

A detailed flow chart of the thesis work is presented below. In brief, preparation method of nanoparticles will determine the size, shape, distribution as well as the magnetic properties and surface chemistry of nanoparticles. Co-precipitation from a homogeneous solution of ferric and ferrous iron solution under controlled conditions has been known as a widely used method for magnetic nanoparticle preparation. Particular attention must be paid to the particle growth in the precursor (Tartaj, Veintemillas-Verdaguer et al. 2003, Roca, Costo et al. 2009). Adjusting the pH and stoichiometric ratio of ingredients are the main key points for the size and distribution control. This co-precipitation is illustrated in the below reaction:

$$FeCl_2.\ 4H_2O + FeCl_3.6H_2O \longrightarrow Fe_3O_4$$
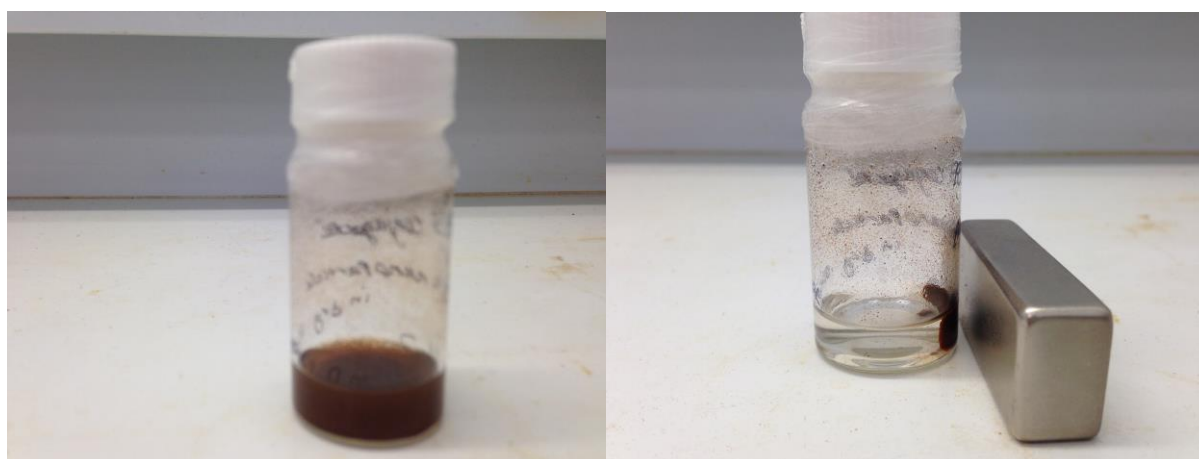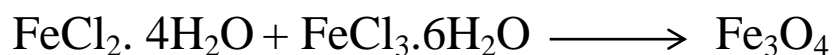
Figure 1-16. Magnetic Fe$_3$O$_4$ nanoparticles in aqueous solution

Coating magnetic nanoparticles with a silica shell is one of the most promising approaches in the development of functionalized magnetic nanoparticles. The coated silica shell is able to

improve the dispersion of magnetic nanoparticles in aqueous media, improve further functionalization and provide an inert surface for magnetic nanoparticles (Deng, Wang et al. 2005). Silanisation of nanoparticles for surface modifications have been widely used in our research group for a variety of applications (Feng, Zhang, et al, 2013, Feng, Zhang, et al. (2015), Patel, Raj, et al. 2016, Patel, Raj, et al. 2017).

This procedure of silanisation of magnetic nanoparticles relies on the hydrolysis of tetraethyl orthosilicate (TEOS) for coating Fe_3O_4 nanoparticles ($Fe_3O_4@SiO_2$). The thickness of the silica layer can be controlled by varying the concentration of the sol-gel precursor solution (Shao, Ning et al. 2012). Polyethylene glycol (PEG) is a coiled polymer of repeating ethylene ether units with dynamic conformations (Otsuka, Nagasaki et al. 2003). Addition of PEG offers solubility, hydrophilicity, flexibility to magnetic nanoparticles (Otsuka, Nagasaki et al. 2003, Jokerst, Lobovkina et al. 2011). PEGlation of Fe_3O_4 nanoparticles can be carried out using a PEG that have two functional groups at the end of the PEG chain, of which one would couple with the −OH groups of the silica coated magnetic nanoparticles, the other couple with the intended florescent moiety in a separate stage. A schematic illustration of the chemical synthesis is shown in Figure 1-17.
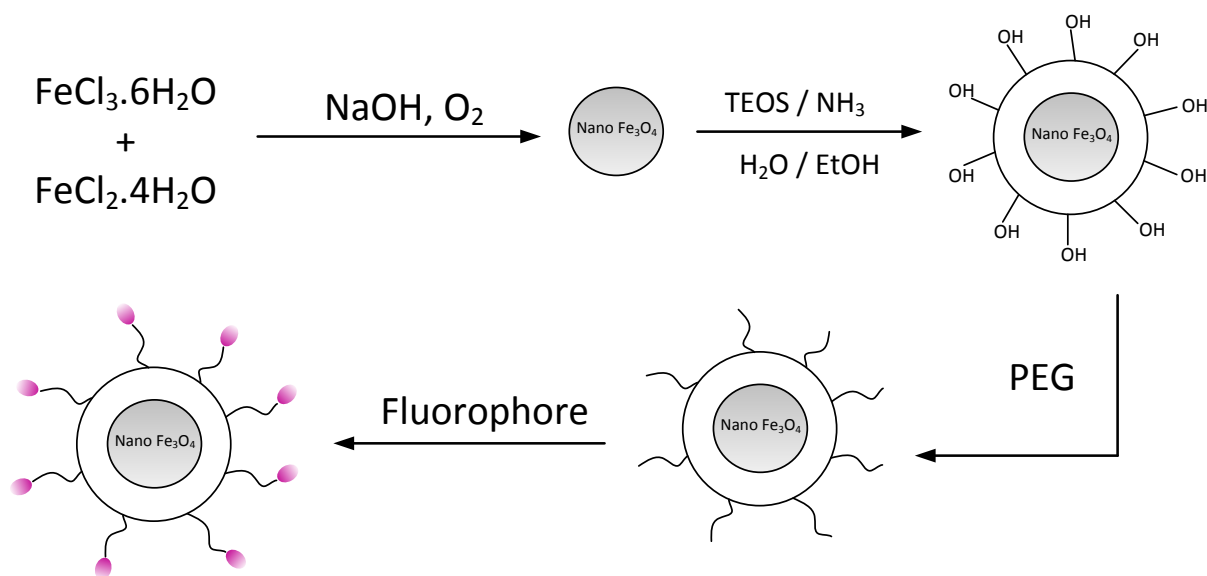
Figure 1-17. Schematic illustration of the chemical synthesis

Detailed physiochemical characterisation scheme shall be employed for the investigation of the synthetic products. Transition electron microscopy (TEM), and dynamic light scattering (DLS) will be used to analyse morphology and size distribution. Various spectroscopic techniques will be utilized to confirm the surface chemistry conjugations step by step including Furrier transform infra-red (FTIR), ultra violet – visible (UV-Vis) absorption, X-ray diffraction (XRD) and nuclear magnetic resonance (NMR). Thermo gravimetric analysis (TGA) will also be used to quantify the functional groups attached to the surface of magnetic nanoparticles. Fluorescence experiments will be conducted by a PerkinElmer L55 fluorescence spectrometer with an excitation source set at 325 nm and a scanning rate of 5 nm/min. The sensitivity and selectivity of the produced nanostructure sensor will obtain from fluorescent studies. The fluorescence quantum yield will also be calculated which is basically the ratio of fluorescence photons emitted to photons absorbed. Fluorescent quantum yield can be examined by the measurement of fluorescence efficiency relative to that of a standard solution. Job plot will also be performed to illustrate the binding stoichiometry of metal ion to

the fluorophore. Job plot can be presented by plotting UV absorption versus mole fraction of the compound which will express the molar stoichiometry between fluorophore and Zn^{2+} ion. Recovery test will also be done in this research as it's the most important feature of the produced nanochemosensors in this study to be recyclable and consequently environmentally friendly. The recovery test will be carried out by utilising EDTA through 4 cycles.

1.4. The overall structure of thesis

```
┌─────────────────────────┐
│ Introduction and Overview│
│      (Chapter 1)         │
└─────────────────────────┘

                              ┌──────────────────────────────────────┐
                              │ preparation of magnetic silica core-shell│
                              │ nanostructure to obtain Fe₃O₄@SiO₂      │
                              └──────────────────────────────────────┘

                              ┌──────────────────────────────────────┐
                              │ Functionalisation of Core-shell structure to│
                              │ produce Fe₃O₄@SiO₂-APS and Fe₃O₄@SiO₂-│
                              │ GPS,                                   │
                              └──────────────────────────────────────┘

┌─────────────────────────┐   ┌──────────────────────────────────────┐
│ Selective detection of Zn²⁺ by│ Develop the dansyl-base fluorescent   │
│ developing dansylated magnetic│ nanochemosensor by conjugating PEG spacer│
│ nanostructure fluorescent│   │ and esterification with dansyl chloride to│
│ chemosensor             │   │ obtain Fe₃O₄@SiO₂-PEG-DnS             │
│      (Chapter 2)         │   └──────────────────────────────────────┘
└─────────────────────────┘
                              ┌──────────────────────────────────────┐
                              │ Investigate the Physicochemical        │
                              │ characterization of produced           │
                              │ nanochemosensor: UV-visible, FTIR, X-ray,│
                              │ TGA, TEM                               │
                              └──────────────────────────────────────┘

                              ┌──────────────────────────────────────┐
                              │ Evaluate the photophysical properties of│
                              │ nanochemosensor: selectivity, sensitivity│
                              │ towards Zn²⁺ ion, pH dependence, Job plot,│
                              │ quantum yield, reversibility           │
                              └──────────────────────────────────────┘
```

$Fe_3O_4@SiO_2$

$Fe_3O_4@SiO_2$-APS and $Fe_3O_4@SiO_2$-GPS,

Develop the dansyl-base fluorescent nanochemosensor by conjugating PEG spacer and esterification with dansyl chloride to obtain $Fe_3O_4@SiO_2$-PEG-DnS

Investigate the Physicochemical characterization of produced nanochemosensor: UV-visible, FTIR, X-ray, TGA, TEM

Evaluate the photophysical properties of nanochemosensor: selectivity, sensitivity towards Zn^{2+} ion, pH dependence, Job plot, quantum yield, reversibility

Selective detection of Zn^{2+} by developing dansylated magnetic nanostructure fluorescent chemosensor (Chapter 2)

Synthesis and investigation of Quinoline based magnetic nanostructure for selective Detection of Zn^{2+} (Chapter 3)

Preparation of nano-magnetic core-shell structure containing functional precursors of 3-glycidyloxypropyl siloxane to produce $Fe_3O_4@SiO_2$-GPS

Grafting 4-aminoquinoline fluorescent to the conjugated system of PEG-attached magnetic nanostructure to develop $Fe_3O_4@SiO_2$-PEG-4AQ

Characterization of produced nanochemosensor to confirm the structure by UV-visible, FTIR, X-ray, TGA, TEM

Determination the fluorescent properties of the nanochemosesnsor: selective detection of Zn^{2+} ion, sensitivity and detection limit, quantum yield, pH dependence, recyclability

Crystallography study of PEG conjugated Dansyl fluorophore (Chapter 4)

Attaching methoxy polyethylene glycol (mPEG-160) to dansyl chloride to resemble the PEG-DnS moiety in $Fe_3O_4@SiO_2$-PEG-DnS

Confirmation of crystal structure of by FTIR, ^1H NMR, UV-Vis spectroscopy and XRD analysis.

Investigate the photophysical properties of produced crystal structure of PEG-DnS before and after complexation with Zn^{2+}

Crystallography study on the produced PEG-DnS by X-ray crystallographic analysis.

Conclusion (Chapter 5)

1.5. References

Albani, J. R. (2008). Principles and applications of fluorescence spectroscopy, John Wiley & Sons.

Arfsten, N. J., S. Armes, et al. (2007). Core-shell nanoparticles, Google Patents.

Basabe-Desmonts, L., D. N. Reinhoudt, et al. (2007). "Design of fluorescent materials for chemical sensing." Chemical Society Reviews **36**(6): 993-1017.

Bazrafshan, A., S. Hajati, et al. (2015). "Improvement in the performance of a zinc ion-selective potentiometric sensor using modified core/shell $Fe_3O_4@SiO_2$ nanoparticles." RSC Advances **5**(128): 105925-105933.

Buck, S. M., H. Xu, et al. (2004). "Nanoscale probes encapsulated by biologically localized embedding (PEBBLEs) for ion sensing and imaging in live cells." Talanta **63**(1): 41-59.

Chen, L., D. W. McBranch, et al. (1999). "Highly sensitive biological and chemical sensors based on reversible fluorescence quenching in a conjugated polymer." Proceedings of the National Academy of Sciences **96**(22): 12287-12292.

Cho, Y., S. S. Lee, et al. (2010). "Recyclable fluorimetric and colorimetric mercury-specific sensor using porphyrin-functionalized $Au@SiO_2$ core/shell nanoparticles." Analyst **135**(7): 1551-1555.

Czarnik, A. W. (1993). Fluorescent chemosensors for ion and molecule recognition, ACS Publications.

De Leon-Rodriguez, L., A. J. M. Lubag, et al. (2012). "Imaging free zinc levels in vivo–What can be learned?" Inorganica chimica acta **393**: 12-23.

De Silva, A. P., H. N. Gunaratne, et al. (1997). "Signaling recognition events with fluorescent sensors and switches." Chemical Reviews **97**(5): 1515-1566.

Delgado-Pinar, E., N. Montoya, et al. (2010). "Preparation of Hg^{2+} selective fluorescent chemosensors based on surface modified core–shell aluminosilicate nanoparticles." New Journal of Chemistry **34**(3): 567-570.

Demchenko, A. P. (2008). Introduction to fluorescence sensing, Springer Science & Business Media.

Deng, Y.-H., C.-C. Wang, et al. (2005). "Investigation of formation of silica-coated magnetite nanoparticles via sol–gel approach." Colloids and Surfaces A: Physicochemical and Engineering Aspects **262**(1): 87-93.

Desvergne, J.-P. and A. W. Czarnik (1997). <u>Chemosensors of ion and molecule recognition</u>, Springer Science & Business Media.

Desvergne, J.-P. and A. W. Czarnik (2012). <u>Chemosensors of ion and molecule recognition</u>, Springer Science & Business Media.

Endre, L., F. Beck, et al. (1990). "The role of zinc in human health." <u>The Journal of trace elements in experimental medicine</u> **3**(4): 337-375.

Fabbrizzi, L., M. Licchelli, et al. (1996). "Fluorescent Sensors for Transition Metals Based on Electron-Transfer and Energy-Transfer Mechanisms." <u>Chemistry–A European Journal</u> **2**(1): 75-82.

Fan, L.-J., Y. Zhang, et al. (2009). "Fluorescent conjugated polymer molecular wire chemosensors for transition metal ion recognition and signaling." <u>Coordination Chemistry Reviews</u> **253**(3): 410-422.

Frackowiak, D. (1988). "The jablonski diagram." <u>Journal of Photochemistry and Photobiology B: Biology</u> **2**(3): 399.

Frey, N. A., S. Peng, et al. (2009). "Magnetic nanoparticles: synthesis, functionalization, and applications in bioimaging and magnetic energy storage." <u>Chemical Society Reviews</u> **38**(9): 2532-2542.

Ghosh Chaudhuri, R. and S. Paria (2011). "Core/shell nanoparticles: classes, properties, synthesis mechanisms, characterization, and applications." <u>Chemical Reviews</u> **112**(4): 2373-2433.

Guo, Z., W. Zhu, et al. (2009). "Hydrophilic copolymer bearing dicyanomethylene-4 H-pyran moiety as fluorescent film sensor for Cu^{2+} and pyrophosphate anion." <u>Macromolecules</u> **43**(2): 739-744.

Hu, J., C. Li, et al. (2009). "Hg2+-reactive double hydrophilic block copolymer assemblies as novel multifunctional fluorescent probes with improved performance." <u>Langmuir</u> **26**(2): 724-729.

Jeong, U., H. H. Shin, et al. (2015). "Functionalized magnetic core–shell $Fe@SiO_2$ nanoparticles as recoverable colorimetric sensor for Co^{2+} ion." <u>Chemical Engineering Journal</u> **281**: 428-433.

Jokerst, J. V., T. Lobovkina, et al. (2011). "Nanoparticle PEGylation for imaging and therapy." <u>Nanomedicine</u> **6**(4): 715-728.

Jung, J. H., J. H. Lee, et al. (2011). "Functionalized magnetic nanoparticles as chemosensors and adsorbents for toxic metal ions in environmental and biological fields." <u>Chemical Society Reviews</u> **40**(9): 4464-4474.

Kaur, K., R. Gupta, et al. (2014). "Zinc: the metal of life." Comprehensive Reviews in Food Science and Food Safety **13**(4): 358-376.

Kim, K. T., S. A. Yoon, et al. (2017). "Synthesis of fluorescent naphthalimide-functionalized Fe_3O_4 nanoparticles and their application for the selective detection of Zn^{2+} present in contaminated soil." Sensors and Actuators B: Chemical **243**: 1034-1041.

Kimura, M., T. Horai, et al. (1998). "Fluorescence chemosensor for metal ions using conjugated polymers." Advanced Materials **10**(6): 459-462.

Lakowicz, J. R. and B. R. Masters (2008). "Principles of fluorescence spectroscopy." Journal of Biomedical Optics **13**(2): 029901.

Laws, W. R. and P. B. Contino (1992). "[21] Fluorescence quenching studies: Analysis of nonlinear Stern-Volmer data." Methods in enzymology **210**: 448-463.

Li, N., Q. Xu, et al. (2009). "A polymeric chemosensor for Fe 3+ based on fluorescence quenching of polymer with quinoline derivative in the side chain." Materials Chemistry and Physics **114**(1): 339-343.

Lin, W., X. Cao, et al. (2010). "A reversible fluorescent Hg^{2+} chemosensor based on a receptor composed of a thiol atom and an alkene moiety for living cell fluorescence imaging." Organic & biomolecular chemistry **8**(16): 3618-3620.

Liu, G., H. Wu, et al. (2011). "Synthesis and applications of fluorescent-magnetic-bifunctional dansylated $Fe_3O_4@SiO_2$ nanoparticles." Journal of materials science **46**(18): 5959-5968.

Mao, H. and Z. Liu (2018). "Two emissive-magnetic composite platforms for Hg (II) sensing and removal: The combination of magnetic core, silica molecular sieve and rhodamine chemosensors." Spectrochimica Acta Part A: Molecular and Biomolecular Spectroscopy **189**: 366-373.

Méallet-Renault, R., R. Pansu, et al. (2004). "Metal-chelating nanoparticles as selective fluorescent sensor for Cu^{2+}." Chemical communications(20): 2344-2345.

Montalti, M., L. Prodi, et al. (2002). "Solvent-induced modulation of collective photophysical processes in fluorescent silica nanoparticles." Journal of the American Chemical Society **124**(45): 13540-13546.

Nogués, J., V. Skumryev, et al. (2006). "Shell-driven magnetic stability in core-shell nanoparticles." Physical review letters **97**(15): 157203.

Otsuka, H., Y. Nagasaki, et al. (2003). "PEGylated nanoparticles for biological and pharmaceutical applications." Advanced drug delivery reviews **55**(3): 403-419.

Pankhurst, Q. A., J. Connolly, et al. (2003). "Applications of magnetic nanoparticles in biomedicine." Journal of physics D: Applied physics **36**(13): R167.

Park, M., S. Seo, et al. (2010). "Functionalized Ni@ SiO$_2$ core/shell magnetic nanoparticles as a chemosensor and adsorbent for Cu^{2+} ion in drinking water and human blood." Analyst **135**(11): 2802-2805.

Parker, D. and J. G. Williams (1995). "Luminescence behaviour of cadmium, lead, zinc, copper, nickel and lanthanide complexes of octadentate macrocyclic ligands bearing naphthyl chromophores." Journal of the Chemical Society, Perkin Transactions 2(7): 1305-1314.

Peng, X., Y. Wang, et al. (2011). "Functionalized magnetic core–shell Fe$_3$O$_4$@SiO$_2$ nanoparticles as selectivity-enhanced chemosensor for Hg (II)." Dyes and Pigments **91**(1): 26-32.

Prodi, L. (2005). "Luminescent chemosensors: from molecules to nanoparticles." New Journal of Chemistry **29**(1): 20-31.

Prodi, L., M. Montalti, et al. (2001). "Characterization of 5-chloro-8-methoxyquinoline appended diaza-18-crown-6 as a chemosensor for cadmium." Tetrahedron Letters **42**(16): 2941-2944.

Qian, X., Y. Xiao, et al. (2010). ""'Alive'' dyes as fluorescent sensors: fluorophore, mechanism, receptor and images in living cells." Chemical communications **46**(35): 6418-6436.

Rampazzo, E., E. Brasola, et al. (2005). "Surface modification of silica nanoparticles: a new strategy for the realization of self-organized fluorescence chemosensors." Journal of Materials Chemistry **15**(27-28): 2687-2696.

Rehm, D. and A. Weller (1970). "Kinetics of fluorescence quenching by electron and H-atom transfer." Israel Journal of Chemistry **8**(2): 259-271.

Roca, A., R. Costo, et al. (2009). "Progress in the preparation of magnetic nanoparticles for applications in biomedicine." Journal of physics D: Applied physics **42**(22): 224002.

Roohani, N., R. Hurrell, et al. (2013). "Zinc and its importance for human health: An integrative review." Journal of Research in Medical Sciences **18**(2): 144-157.

Salgueiro, M. J., M. Zubillaga, et al. (2000). "Zinc as an essential micronutrient: a review." Nutrition Research **20**(5): 737-755.

Shang, G.-Q., X. Gao, et al. (2008). "A novel Hg^{2+} selective ratiometric fluorescent chemodosimeter based on an intramolecular FRET mechanism." Journal of fluorescence **18**(6): 1187.

Shao, M., F. Ning, et al. (2012). "Preparation of $Fe_3O_4@SiO_2$ layered double hydroxide core–shell microspheres for magnetic separation of proteins." Journal of the American Chemical Society **134**(2): 1071-1077.

Song, Q., M. Li, et al. (2013). "Bifunctional polydopamine@ Fe_3O_4 core–shell nanoparticles for electrochemical determination of lead (II) and cadmium (II)." Analytica chimica acta **787**: 64-70.

Sun, Z., H. Li, et al. (2015). "A multifunctional magnetic core–shell fibrous silica sensing probe for highly sensitive detection and removal of Zn^{2+} from aqueous solution." Journal of Materials Chemistry C **3**(18): 4713-4722.

Tartaj, P., S. Veintemillas-Verdaguer, et al. (2003). "The preparation of magnetic nanoparticles for applications in biomedicine." Journal of physics D: Applied physics **36**(13): R182.

Thiagarajan, V., P. Ramamurthy, et al. (2005). "A novel colorimetric and fluorescent chemosensor for anions involving PET and ICT pathways." Organic letters **7**(4): 657-660.

Tian, X., Z. Dong, et al. (2013). "A quinoline group modified $Fe_3O_4@SiO_2$ nanoparticles for sequential detection of Zn^{2+} and hydrogen sulfide in aqueous solution and its logic behavior." Sensors and Actuators B: Chemical **183**: 446-453.

Ueno, T. and T. Nagano (2011). "Fluorescent probes for sensing and imaging." Nature methods **8**(8): 642.

Valeur, B. and M. N. Berberan-Santos (2012). Molecular fluorescence: principles and applications, John Wiley & Sons.

Valeur, B. and J.-C. Brochon (2012). New trends in fluorescence spectroscopy: applications to chemical and life sciences, Springer Science & Business Media.

Valeur, B. and I. Leray (2000). "Design principles of fluorescent molecular sensors for cation recognition." Coordination Chemistry Reviews **205**(1): 3-40.

Wang, B. Y., X. Y. Liu, et al. (2009). "Synthesis and photophysical behavior of a water-soluble coumarin-bearing polymer for proton and Ni2+ ion sensing." Polymer International **58**(6): 703-709.

Wang, T., L. Zhang, et al. (2015). "Synthesis of core–shell magnetic $Fe_3O_4@poly$(m-phenylenediamine) particles for chromium reduction and adsorption." Environmental science & technology **49**(9): 5654-5662.

Wang, Y., X. Peng, et al. (2012). "Highly selective fluorescent chemosensor for Zn^{2+} derived from inorganic-organic hybrid magnetic core/shell $Fe_3O_4@SiO_2$ nanoparticles." Nanoscale research letters **7**(1): 86.

Weiss, S. (1999). "Fluorescence spectroscopy of single biomolecules." Science **283**(5408): 1676-1683.

Xu, Q. and D. Pascoe (1994). "The importance of food and water as sources of zinc during exposure of Gammarus pulex (Amphipoda)." Archives of Environmental Contamination and Toxicology **26**(4): 459-465.

Xu, Y., Y. Zhou, et al. (2013). "A fluorescent sensor for zinc detection and removal based on core-shell functionalized $Fe_3O_4@SiO_2$ nanoparticles." Journal of Nanomaterials **2013**.

Xu, Y., Y. Zhou, et al. (2013). "Highly sensitive and selective OFF-ON fluorescent sensor based on functionalized $Fe_3O_4@SiO_2$ nanoparticles for detection of Zn^{2+} in acetonitrile media." Applied Surface Science **276**: 705-710.

Yoon, T. J., K. N. Yu, et al. (2006). "Specific targeting, cell sorting, and bioimaging with smart magnetic silica core–shell nanomaterials." small **2**(2): 209-215.

Yuan, L., W. Lin, et al. (2013). "FRET-based small-molecule fluorescent probes: rational design and bioimaging applications." Accounts of chemical research **46**(7): 1462-1473.

Zeng, X., Y. Xu, et al. (2017). "An inorganic/organic hybrid magnetic network as a colorimetric fluorescent nanosensor and its recognizing behavior toward Hg^{2+}." Applied Surface Science **423**: 1103-1110.

Zeng, X., Y. Zhou, et al. (2014). "Selective Zn (II) chemosensor based on di (2-picolyl) amine functionalized inorganic/organic hybrid magnetic network." Chemical Engineering Journal **244**: 75-81.

Chapter 2

Synthesis and Characterisation of Dansylated Magnetic Nanostructure for Reversible Detection of Zn^{2+} in Aqueous Solution

2.1. Introduction

Selective detection of Zn^{2+} at low concentrations in aqueous solution has always been attractive due to the broad range of zinc applications in biological science, mineral and environmental exploration. Studies show that developing fluorescent sensors is the most promising detection method with moderately high selectivity and sensitivity. In chapter, a novel magnetic core-shell nanostructure has been developed for sensing Zn^{2+} in aqueous solution which offers many advantages over other type of sensors:

1) Introducing silica shell commonly provides stability and hydrophilicity to the magnetic nanoparticles as well as feasibility for further functionalization.

2) Various silicane precursors can be covalently bonded to the surface of magnetic nanoparticles through simple steps

34

3) Magnetic core-shell nanosensor offers recyclability/reusability via an external magnetic field.

The fluorescent nanosensor has been designed and developed in this work contains dansyl chloride as the fluorescent molecule attached to core-shell nanostructure via a polymer (PEG) spacer. Dansyl chloride (DnCl) is a well-established fluorophore that has been widely used for the labelling and detection of amino acids, proteins and drugs. Dansyl chloride was originally described in Weber's study as a very advantageous sensing probe in biochemical researches (Weber 1952). Dansyl chloride displays a large Stokes shift (Lakowicz and Masters 2008), a charge-transfer character (Montalti, Prodi et al. 2002) with high emission quantum yield (Chen and Chen 2005) and the synthetic flexibility of the sulfonic acid group. Dansyl groups can be excited at around 325-350 nm, the emission spectrum of the dansyl moiety is highly sensitive to solvent polarity and giving emission maxima typically near 510 nm. Dansyl chloride as a small molecule chemosensor has been widely used in biological applications. Schuster et al. (Schuster and Šandor 1996) reported on development of N-dansyl-N'-ethylthiourea (DET) fluorophore containing dansyl chloride moieties. The complexation of the produced sensor with Ni^{2+} and Cu^{2+} resulted in a quench in fluorescent emission signal. They also investigated the pH dependence as well as protonation/deprotonation of dansyl based sensor on the luminescence properties. In another study, Shankar and co-workers (Shankar and Ramaiah 2011) fabricated a number of dansylated chemosensors with different spacer groups and investigated the metal ion binding with different chemosensors. The chemosensor demonstrated an effective interaction with Cu^{2+} ion by quenching of the emission intensity opposing PET mechanism.

This study also investigates the influence of PEG spacer on luminescence properties of the dansylated core-shell nanosensor. PEG spacer is chemically inert and offers hydrophilicity and solubility to the nanostructure chemosensor. Incorporation PEG onto the surface of core-

shell nanostructure can effectively improve the stability of the magnetic core; it can also improve the mobility of the dansyl moiety and also spatially separating the dansyl fluorophore from the magnetic core, therefore, reducing the probability of core-fluorophore interactions.

This chapter explains the facile synthetic pathway of dansylated magnetic nanostructure which is displayed in Scheme 2-1. This pathway involves firstly the preparation of magnetic iron oxide (Fe_3O_4) nanoparticles which are coated with a thin layer of silica (SiO_2) shell to obtain $Fe_3O_4@SiO_2$. The core-shell nanostructure will be secondly functionalized by either 1-aminopropyl or 3-glycidyloxypropyl functional groups for further functionalization to produce $Fe_3O_4@SiO_2$-APS and $Fe_3O_4@SiO_2$-GPS, respectively. The functionalized nanoparticles shall then be conjugated with PEG spacer ($Fe_3O_4@SiO_2$-PEG) and finally esterified with dansyl chloride to produce dansylated magnetic nanosensor namely $Fe_3O_4@SiO_2$-PEG-DnS. A similar structure namely $Fe_3O_4@SiO_2$-DnS that contains no PEG spacer also shall be synthesised and investigated along with $Fe_3O_4@SiO_2$-PEG-DnS to determine the influence of polymer spacer on luminescence properties of the nanosensor. Both nanochemosensors are entirely characterized confirming their chemical structure and morphology. The photophysical properties are also fully investigated including the selectivity and sensitivity of the nanosensors, their detection limit, quantum yield, ligand-metal stoichiometric ratio as well as their recyclability.
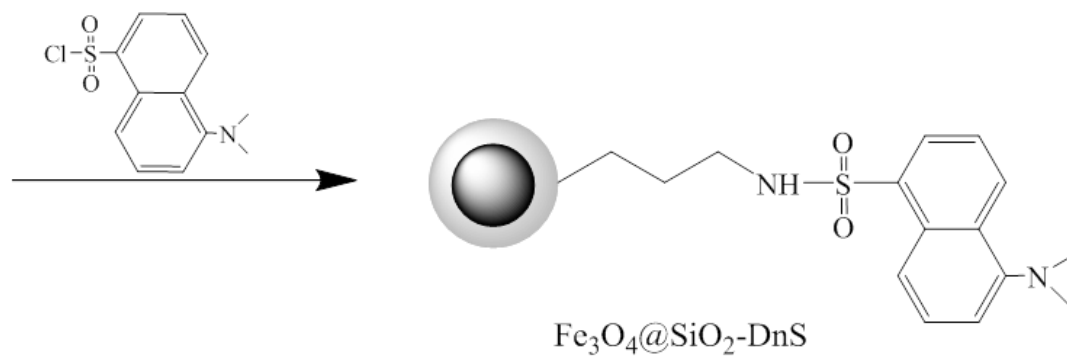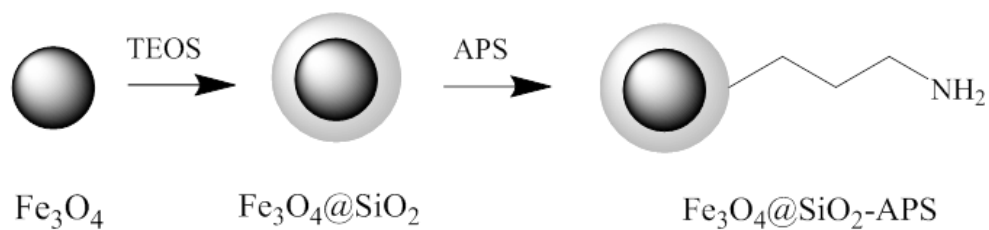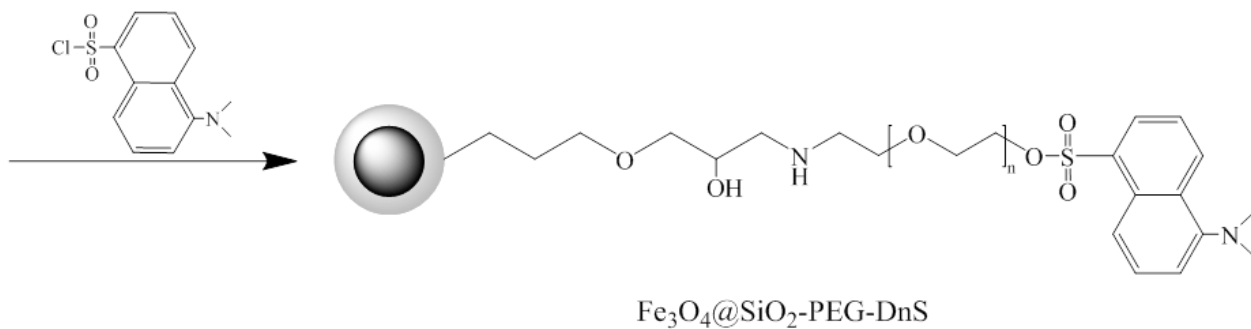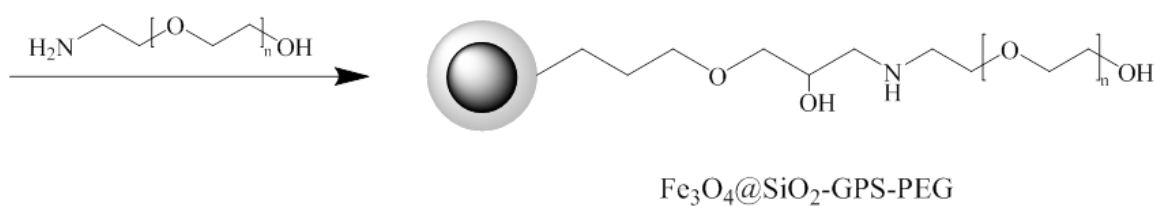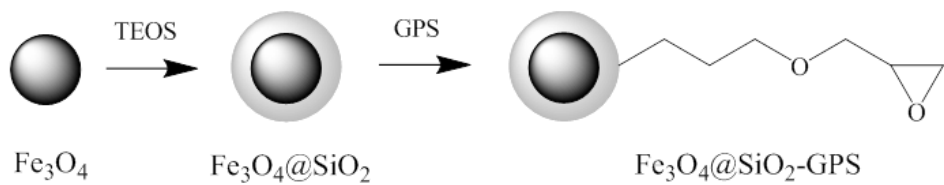
Scheme 2-1. Synthetic pathway of the dansylated magnetic nanochemosensors

37

2.2. Material and method

2.2.1. Material

All the chemicals were purchased from Sigma Aldrich Australia: Ferric chloride hexahydrate ($FeCl_3.6H_2O$, 99.99%), ferrous chloride tetrahydrate ($FeCl_2.4H_2O$, 99.99%), citric acid (99.5%), dansyl chloride (DnCl), Triethylamine (99.5%), tetraethoxysilane (TEOS) (99.99%), (3-glycidyloxypropyl) trimethoxylsilane (GPS) (98%), (3-aminopropyl) triethoxysilane (APS) (98%), ethanol (99.5%), O-(2-aminoethyl) polyethylene glycol ($M_w = 3000$), ammonium hydroxide (99.99%). All reagents were used, as received, without further purification. Deionised (D.I.) water was used in all experiments.

2.2.2. Synthesis of magnetic Fe_3O_4 nanoparticles

$FeCl_3.6H_2O$ (2.7 g, 10 mmol) and $FeCl_2.4H_2O$ (0.99 g, 5 mmol) were dissolved in 10 ml HCl solution (2 M) under vigorous stirring and nitrogen bubbling. The Fe^{2+}/Fe^{3+} solution was then added, dropwise, to 50ml sodium hydroxide solution (0.5 M) and allowed to proceed under mechanical stirring for 1 hr. After completion of the reaction, the black precipitate was isolated via an external magnet and washed sequentially four times, with 20 ml deionised water then 20 ml ethanol each time. In order to obtain well-dispersed magnetic nanoparticles, particles were added to 2 ml citric acid solution (0.1 M) with ultrasonic treatment for 30 min. Then the mixture was maintained at room temperature for 12 hr. Finally, nanoparticles were rinsed with D.I. water (4×20 ml), collected from the reaction mixture by an external magnet and dispersed as a suspension in D.I. water.

2.2.3. Synthesis of core/shell-structured Fe₃O₄@SiO₂-APS and Fe₃O₄@SiO₂-GPS

Silanisation of the produced Fe_3O_4 nanoparticles was carried out using a previously reported method (Feng, Zhang et al. 2013, Feng, Zhang et al. 2015). Fe_3O_4 nanoparticles (0.5 g, 2.16 mmol) were dispersed in a mixture of ethanol/water (30 ml, 2:1 ratio) and 1 ml ammonium hydroxide solution (25 wt%) under mechanical stirring for 1 hr. TEOS (0.5 ml, 2.25 mmol) was mixed with 5 ml ethanol and the mixture was added, dropwise, to the prepared dispersion of Fe_3O_4 nanoparticles. The reaction was then allowed to proceed for 2 hr, under stirring at room temperature, to obtain silica-coated Fe_3O_4 nanoparticles: $Fe_3O_4@SiO_2$. Amino functionalisation of $Fe_3O_4@SiO_2$ was achieved by the dropwise addition of a mixture of APS (1.05 ml, 4.5 mmol) and 5 ml ethanol into the $Fe_3O_4@SiO_2$ solution, and the reaction was carried out for further 2 hr under stirring. The obtained functionalised magnetic nanoparticles, $Fe_3O_4@SiO_2$-APS, were removed from the reaction mixture by applying an external magnet. They were washed sequentially with D.I. water and ethanol, each 4×20 ml, and suspended in D.I. water.

Epoxy-functionalised nanoparticles, $Fe_3O_4@SiO_2$-GPS, were also prepared by adding a solution of GPS (1.17 ml, 4.5 mmol) to the mixture, following the same procedure as for $Fe_3O_4@SiO_2$-APS. The resultant and purified $Fe_3O_4@SiO_2$-GPS also was suspended in D.I. water for further analyses.

2.2.4. Synthesis of Fe₃O₄@SiO₂-DnS

$Fe_3O_4@SiO_2$-APS (15 mg) was dispersed in 30 ml dry acetone. (The dry acetone was prepared through distillation of acetone after drying with calcium chloride overnight). Triethylamine (0.5 ml, 3.58 mmol) was then added to the dispersion, and the solution was sonicated for 30 min. DnCl (45 mg, 0.166 mmol) was dissolved in 20 ml dry acetone and

then added to the $Fe_3O_4@SiO_2$-APS dispersion. The mixture was then stirred at room temperature in the dark for 24 hr. The product, $Fe_3O_4@SiO_2$-DnS, was separated from the solution via an external magnet and washed sequentially with acetone, ethanol and D.I. water, each 4×20 ml.

2.2.5. Synthesis of $Fe_3O_4@SiO_2$-PEG-DnS

The synthesis of $Fe_3O_4@SiO_2$-PEG-DnS was carried out in two stages. Firstly, pegylated $Fe_3O_4@SiO_2$-GPS was prepared by dispersing 0.45 g of $Fe_3O_4@SiO_2$-GPS in 10 ml D.I. water, to which O-(2-aminoethyl) polyethylene glycol (0.135 g dissolved in 10 ml D.I. water) was added under stirring at 65ºC and further stirred for 6 hr at the same temperature. After collection via external magnet, the resultant $Fe_3O_4@SiO_2$-GPS-PEG was repeatedly washed with fresh D.I. water (4 × 20 ml). Then the deionised water was sequentially substituted with acetone and dry acetone prior to the dansylation. Dansylation of the $Fe_3O_4@SiO_2$-GPS-PEG nanoparticles was carried out using the same procedure that was applied to $Fe_3O_4@SiO_2$-APS. The final product, $Fe_3O_4@SiO_2$-PEG-DnS, was then washed and kept as a suspension in D.I. water.

2.2.6. Physicochemical Characterisation

The chemical structure and morphology of the preparation of nanochemosensors were revealed by FTIR, UV-vis, XRD and TEM step by step.

Fourier transform infrared (FTIR) spectra of the products were obtained using Thermo Scientific Nicolet iS50 for the qualitative analysis of the synthesised nanostructures. All spectra were recorded in the range of 400‑4000 cm^{-1}. X-ray diffraction (XRD) analysis was performed using a Bruker AXS diffractometer with Co Kα radiation (λ = 1.79 Å). A scan rate

of 0.015º/s was used to record the patterns in a 2θ range of 20–80º, and the accelerating voltage and current were 35 kV and 40 mA, respectively.

The produced samples also were examined using a Lambda 25 Perkin Elmer UV‑Vis Spectroscope. Scans were recorded in the wavelength range from 200 to 800 nm with a band width of 1 nm. The size, distribution and morphology of the synthesised nanoparticles were examined using a Transmission Electron Microscope (TEM, (JEOL JSM 2011)) that was equipped with a Gatan Digital Camera. Samples were suspended in ethanol and distributed onto a carbon-coated copper grid. The TEM images were recorded at an accelerating voltage of 200 kV. For nanoparticles size measurement, thirty particles were randomly selected and the average of the thirty measurements was representatively used as the size of nanoparticles.

2.2.7. Fluorescence measurements

A PerkinElmer L55 fluorescence spectrometer was used, with an excitation source set at 325 nm and a scanning rate of 5 nm/min. The emission intensities of $Fe_3O_4@SiO_2$-DnS at 0.3 μM of the fluorophore (0.1 mg mL^{-1}) and $Fe_3O_4@SiO_2$-PEG-DnS at 0.3 μM of the fluorophore (0.043 mg mL^{-1}) were measured before and after being mixed with a number of metal ions, namely Ag^+, Li^+, Cu^{2+}, Ni^{2+}, Co^{2+}, Ca^{2+}, Cd^{2+}, Hg^{2+}, Mg^{2+}, Fe^{2+}, Mn^{2+}, Al^{3+}, Cr^{3+} and Fe^{3+} in an aqueous solution (0.9 μM). A competition study was also carried out using aqueous solutions containing mixed metal ions.

2.2.8. Quantum yield measurements

Fluorescence quantum yield is among the most important selection criteria for fluorophores in fluorescence spectroscopy. The fluorescence quantum yield of a fluorophore (Φ) is basically the ratio of fluorescence photons emitted to photons absorbed (Sauer, Hofkens et al. 2011).

Fluorescent quantum yield can be examined by the measurement of fluorescence efficiency relative to that of a standard solution namely quinine sulfate dihydrate solution, using reported methods (Crosby and Demas 1971, Lakowicz and Masters 2008). In brief, the stock solution (100 mg/L) was made by dissolving 5 mg quinine sulfate dihydrate in 50 ml 0.1 M H_2SO_4 solution. UV-Vis and fluorescent spectra (excited at 325 nm) were measured for the same solution. The two newly produced nanochemosensors were dispersed in aqueous solution and further diluted to 1 mg/L then subjected to the same measurements. Equation 2-1 was used to calculate the quantum yields of the nanochemosensors

$$\Phi = \Phi_R \frac{I \, A_R \, n^2}{I_R \, A \, n_R^2} \tag{2-1}$$

where Φ is the quantum yield of the nanosesor, I is the integrated intensity, A is the optical density from the UV-vis measurement and n is the refractive index of the solvent. The subscript, R, refers to the reference fluorophore, quinine sulfate dihydrate, with a known quantum yield (Lakowicz and Masters 2008). In this expression it is assumed that the sample and reference are excited at the same wavelength, so that it is not necessary to correct for the different excitation intensities of different wavelengths.

2.2.9. Job plot measurements

One potential method to determine binding stoichiometry of metal-complex is known as the continuous variation method or Job's plot (Huang 1982). Paul Job (Job 1928) showed that plotting UV absorption versus mole fraction of a compound shall express the molar stoichiometry.

In this study, various volumes (5, 4.5, 4, 3.5, 3, 2.5, 2, 1.5, 1 and 0.5 ml) of the produced nanochemosensors solution (0.3 μM, aqueous) were taken and transferred to vials, to which Zn^{2+} solutions (0.3 μM, aqueous) were added with volumes of 0, 0.5, 1, 1.5, 2, 2.5, 3, 3.5, 4

and 4.5 ml, respectively. Each vial had a total volume of 5 ml mixed solution. The fluorescent intensity of each solution was recorded and plotted against the molar fraction of Zn^{2+}.

2.2.10.   Recovery test

The recovery of $Fe_3O_4@SiO_2$-PEG-DnS was carried out by following these four steps: 1) preparing 5 ml suspension of $Fe_3O_4@SiO_2$-PEG-DnS (0.3 μM) into a vial; 2) mixing with 5 ml Zn^{2+} solution (0.9 μM); 3) adding equivalent amount of EDTA (5 ml, 0.9 μM) into the step 2 mixture; and 4) recovered and resuspended $Fe_3O_4@SiO_2$-PEG-DnS in 5 ml water (recovery from step 3 was by an external magnet followed by washing (3×5 ml D.I. water). Florescent intensity was recorded at each step. The procedure was repeated on the recovered nanosensor for another 4 cycles. In each cycle, three paralleled vials were used. The average of three measurements was used for comparison. The mass of the recovered nanosensor was also recorded at the end of cycles 1, 3 and 5 using one vial sample only.

2.3.   Results and Discussions

2.3.1. Characterization of $Fe_3O_4@SiO_2$-DnS and $Fe_3O_4@SiO_2$-PEG-DnS

The morphology, size and distribution of nanoparticles in each synthetic stage of preparation of both nanochemosensors were obtained from TEM micrographs which are shown in Figure 2-1.

The average size of the plain Fe_3O_4 nanoparticles was obtained to be 8 ± 3 nm. However, the size of nanoparticles increased at each subsequent stage of the chemical reactions, due to the added silica coating and organic functional groups on the surfaces of the nanoparticles. For the final products, $Fe_3O_4@SiO_2$-PEG-DnS and $Fe_3O_4@SiO_2$-DnS, the particle sizes were 33 $\pm$ 6 and 28 ± 4 nm respectively. The presence of silica shell was well-demonstrated in all coated nanoparticles and is also shown in the EDS spectrum of $Fe_3O_4@SiO_2$-GPS in comparison with the EDS spectrum of plain Fe_3O_4 nanoparticles.
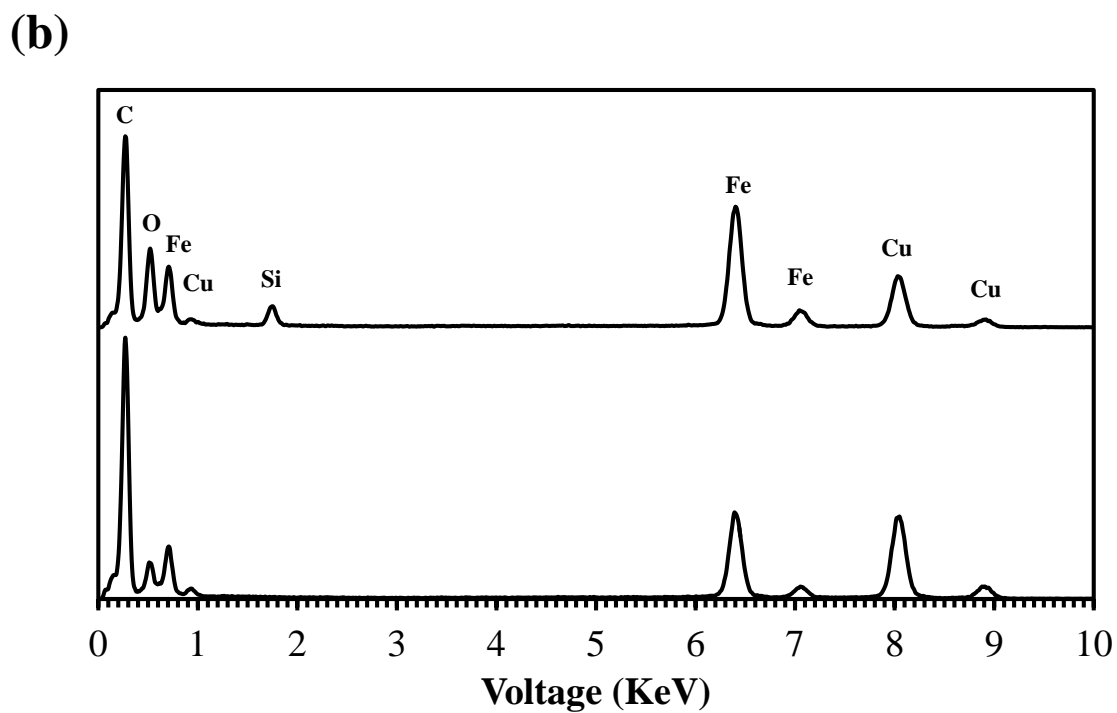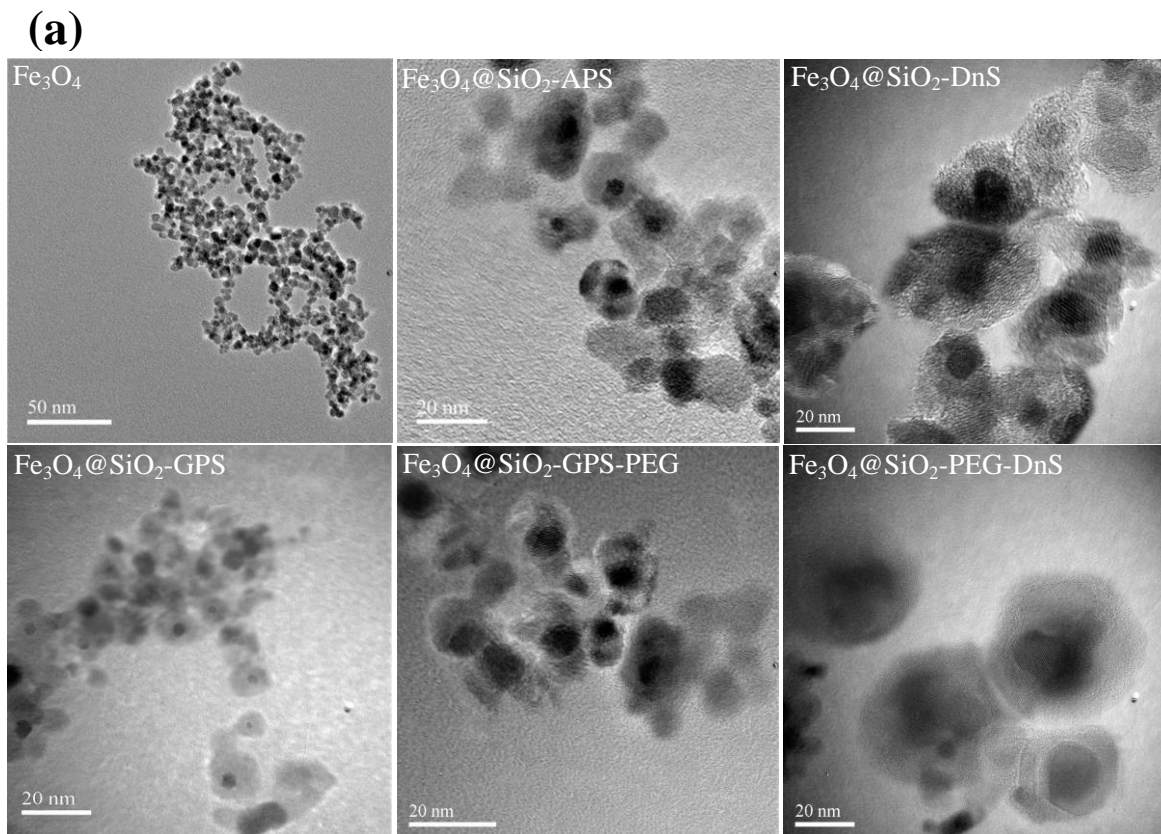
Figure 2-1. (a) TEM images of magnetic nanoparticles, (b) EDS spectrum of Fe_3O_4 and

$Fe_3O_4@SiO_2$-GPS. Cu and C in EDS spectrum are from the copper grid and carbon coating

on the copper, respectively

The successful synthesis of nanochemosensors was confirmed by FTIR (Figure 2-2). The FTIR spectra of $Fe_3O_4@SiO_2$-DnS and the related compounds are shown in Figure 2-2(a). An absorbance at 561 cm^{-1}, which can be seen in all compounds, is associated with the stretching and vibration of Fe-O. The typical vibration and stretching band of Si-O-Si at 1079 cm^{-1} can be seen in both $Fe_3O_4@SiO_2$-APS and $Fe_3O_4@SiO_2$-DnS. For the former, absorption bands at 2927 and 2861 cm^{-1} can be attributed to the C–H asymmetric and symmetric stretching vibrations of the C-H within the APS. The characteristic band at 1524 cm^{-1} is attributable to the N–H bending of primary amines. For $Fe_3O_4@SiO_2$-DnS,the S-O stretching vibrations at 1210 cm^{-1} and the C-N vibrations at 1150 cm^{-1} due to the presence of the dansylate group are well-demonstrated.

Fig. 2-2(b) displays FTIR spectra of all compounds related to the production of $Fe_3O_4@SiO_2$-PEG-DnS. The existence of GPS on $Fe_3O_4@SiO_2$ is confirmed by the presence of a new band at 903 cm^{-1}, representing the epoxy group. Absorption bands at 2927 and 2861 cm^{-1} also can be observed, attributable to the C–H stretching vibrations of GPS. After conjugation of PEG moieties onto the $Fe_3O_4@SiO_2$-GPS, the absorption band corresponding to the epoxy group is removed and an additional band at 3248 cm^{-1} is added, which supports the existence of N-H bending of the secondary amine. The stretching vibrations of S-O at 1210 cm^{-1} and C-N at 1150 cm^{-1} also can be seen in the spectra, denoting the attachment of dansyl groups.

(a)
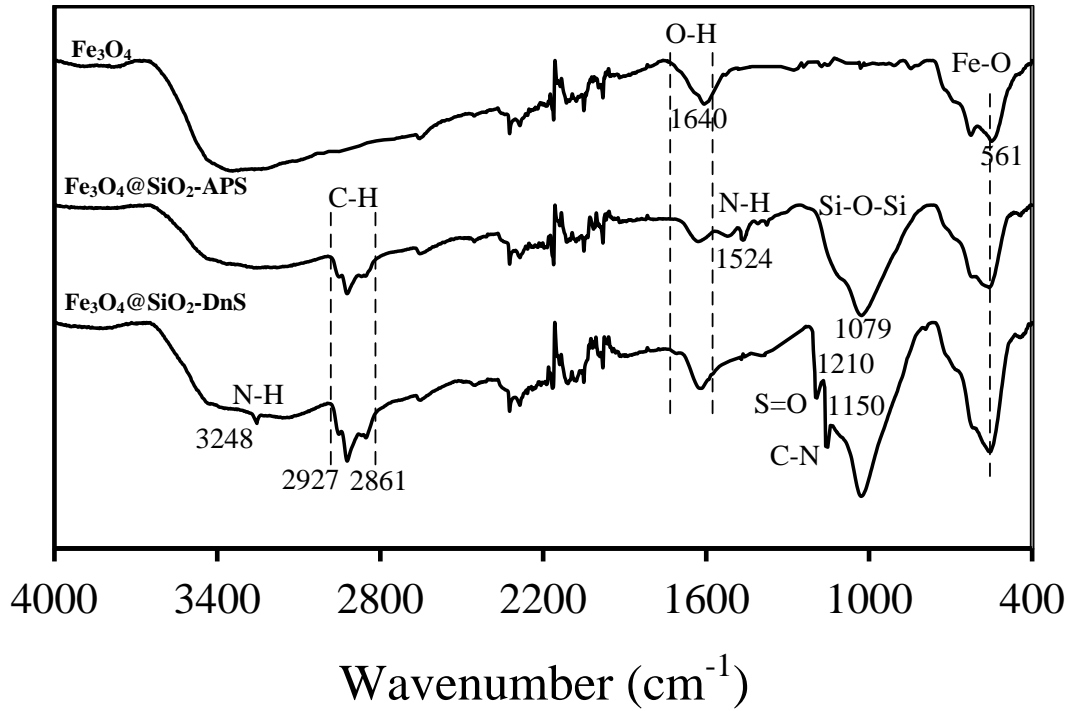
(b)
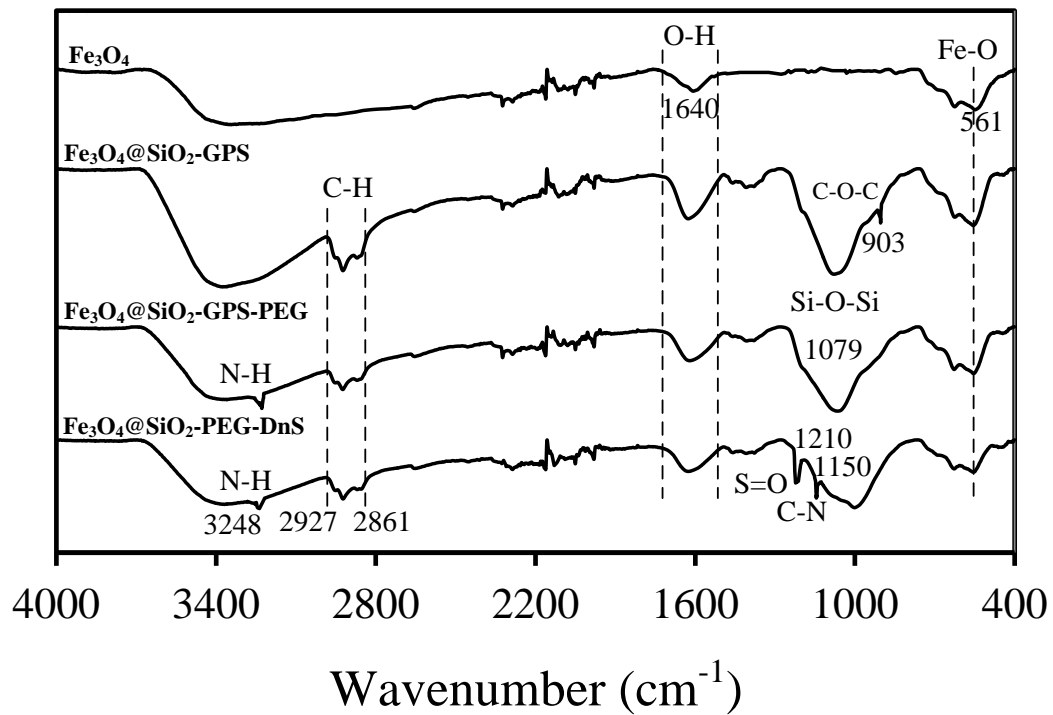
Figure 2-2. FTIR spectra of all nanoparticles related to (a) $Fe_3O_4@SiO_2$-DnS and

(b) $Fe_3O_4@SiO_2$-PEG-DnS

The powder X-ray diffraction patterns of Fe_3O_4 nanoparticles and the functional nanosensors Fe_3O_4@SiO_2-DnS and Fe_3O_4@SiO_2-PEG-DnS are shown in Figure 2-3. As can be seen, all samples possess the characteristic diffraction peaks at (2 2 0), (3 1 1), (4 0 0), (4 2 2), (5 1 1) and (4 4 0), which are in good agreement with pure cubic Fe_3O_4 (Feng, Mao et al. 2011). The broad peak appeared at 20‑28º in the two nanosensors corresponds to the amorphous-state silica layer and the spacer/linker attached to it, which indicates Fe_3O_4 magnetic cores are successfully coated by SiO_2 layer and other functional groups. The XRD patterns of the nanosensors are similar to that of plain Fe_3O_4, demonstrating the organic modification process does not induce any phase change of Fe_3O_4 nanoparticles.

Figure 2-3. XRD patterns of Fe_3O_4, Fe_3O_4@SiO_2-DnS and Fe_3O_4@SiO_2-PEG-DnS

The UV-vis spectra displayed in Figure 2-4(a) further reveal the successful synthesis of $Fe_3O_4@SiO_2$-DnS and $Fe_3O_4@SiO_2$-PEG-DnS. As can be seen from the figure, free dansyl chloride exhibits absorption bands at $\lambda_{max} = 230$ and 325 nm that correspond to π-π^* and n-π^* orbital transitions, respectively (Liu, Wu et al. 2011). Both bands appear in $Fe_3O_4@SiO_2$-DnS and $Fe_3O_4@SiO_2$-PEG-DnS, due to the formation of dansylated species.

TGA analysis of $Fe_3O_4@SiO_2$-PEG-DnS, and its intermediates 2-4(b), revealed a weight loss at 35-100 °C, corresponding to the evaporation of the physically adsorbed water, and a more significant weight loss at the temperature range of 200°C to 800 °C. An estimation based on these data indicates that the mole concentration of dansyl group on the surface of $Fe_3O_4@SiO_2$-PEG-DnS is approximately 6.66×10^{-6} mmol/mg nanoparticles. A similar analysis was performed on $Fe_3O_4@SiO_2$-DnS. The obtained mole concentration of dansyl group was 3.13×10^{-6} mmol/mg nanoparticles. This is half the value of the DnS moles attached to $Fe_3O_4@SiO_2$-PEG-DnS.

The presence of the DnS fluorophore on the surfaces of nanoparticles was further quantified by establishing a UV-vis calibration curve with different molar concentrations of DnCl at $\lambda_{max} = 325$ nm. The numbers of DnCl attached to chemosensors were then calculated by taking the ratio of the molar concentration of DnCl obtained from the UV-calibration curve (at $\lambda = 325$ nm) to each of the initial mass concentrations of chemosensors, resulting in the numbers of DnCl attached to $Fe_3O_4@SiO_2$-DnS and $Fe_3O_4@SiO_2$-PEG-DnS, respectively, being 3.00×10^{-6} mmol/mg and 6.92×10^{-6} mmol/mg. These results are in agreement with those obtained from TGA.

The number of DnS attached to a unit mass of $Fe_3O_4@SiO_2$-PEG-DnS is two times the value for $Fe_3O_4@SiO_2$-DnS. This could be attributed to the presence of the PEG spacer in the former. Having PEG as an inert and hydrophilic spacer causes the dansylation reaction to be more facile in an aqueous environment. On the other hand, the direct attachment of DnS onto

the surface of the core-shell nanostructure could be sterically hindered. For the examinations via fluorescent microscope, discussed in the following sections, equal molar concentrations of DnS fluorophore were used for comparison.

(a)

(b)
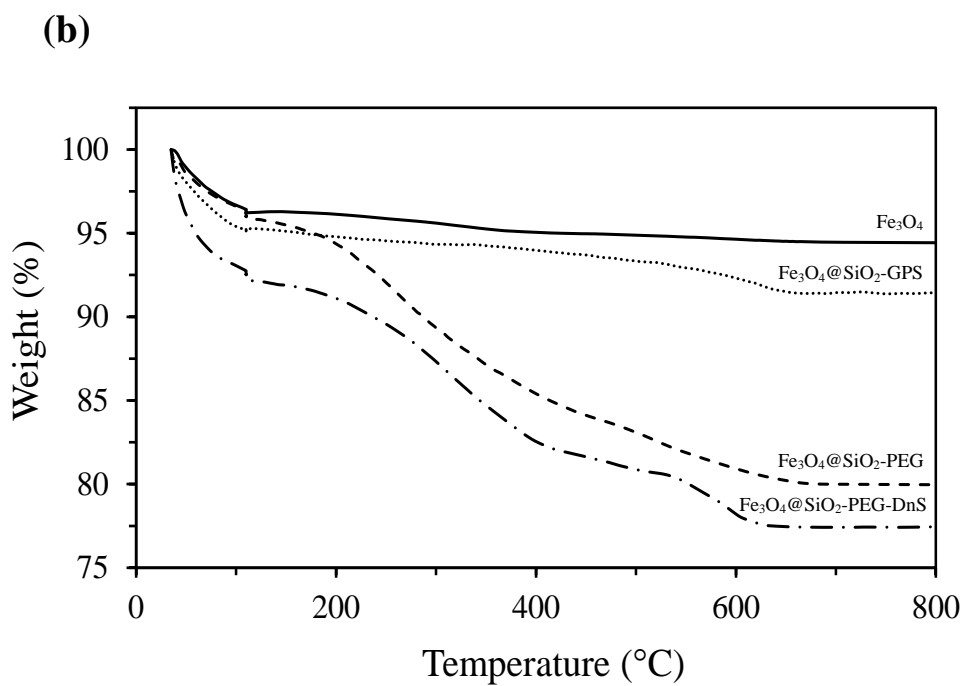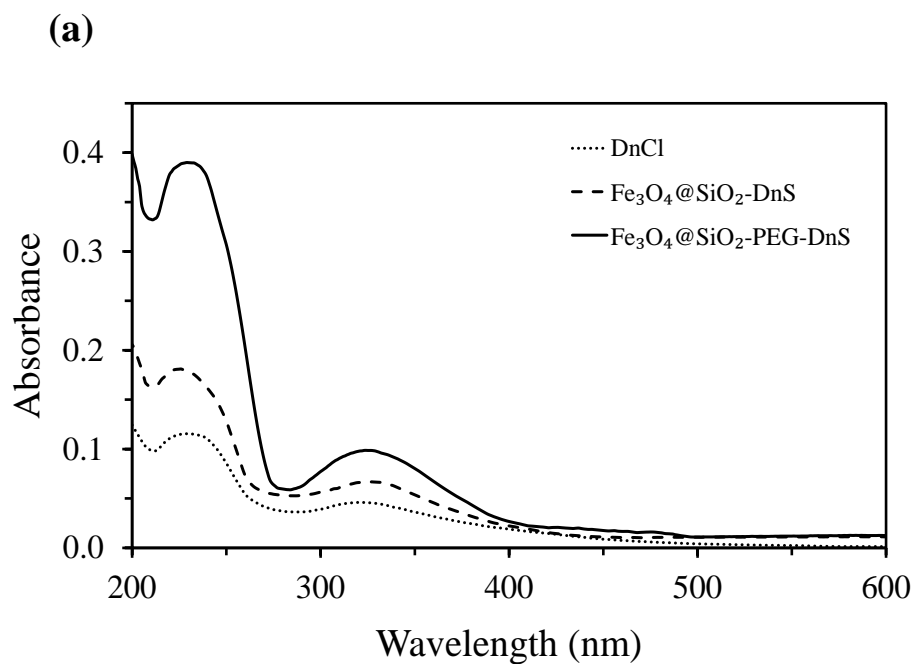
Figure 2-4. (a) UV-Vis spectra of DnCl, Fe$_3$O$_4$@SiO$_2$-DnS and Fe$_3$O$_4$@SiO$_2$-PEG-DnS and

(b) thermal curves showing thermogravimetric loss of Fe$_3$O$_4$@SiO$_2$-PEG-DnS at various

temperature ranges

2.3.2. Fluorescence studies

Figure 2-5(a) illustrates the fluorescent responses of DnCl, $Fe_3O_4@SiO_2$-PEG, $Fe_3O_4@SiO_2$-DnS and $Fe_3O_4@SiO_2$-PEG-DnS in aqueous solutions. The fluorescent spectra were obtained using compounds containing the same amounts of DnS (0.3 μM), with the exception of $Fe_3O_4@GPS$-PEG, which contained no DnS. As can be seen from the figure, $Fe_3O_4@SiO_2$-PEG shows no emission, due to its lack of fluorophore. An emission at λ_{max} = 498 nm was observed for DnCl, originating from a charge transfer state from the amine group of the dansyl to the naphthalene ring (Prodi, Bolletta et al. 2000, Lakowicz and Masters 2008). An enhanced fluorescence was observed for $Fe_3O_4@SiO_2$-DnS, which is likely to be due to intermolecular charge transfer (ICT) from the electron donor dimethylamino group to the electron withdrawal sulfonamide group (Scheme 2-2 (a)) (Prodi, Bolletta et al. 2000, Tharmaraj and Pitchumani 2012). A further increase in the fluorescence intensity was observed for $Fe_3O_4@SiO_2$-PEG-DnS at the maximum of 509 nm. The bonding of PEG with the dansyl group is through the more electronegative oxygen atom, thereby increasing the electron withdrawal capacity of the $-SO_2-$ group. This results in enhancement of the push-pull effect and, therefore, increased fluorescence (Scheme 2-2 (b)). The increased charge transfer also decreases the energy gap between the highest occupied molecular orbital (HOMO) and the lowest unoccupied molecular orbital (LUMO), leading to red shifting of the emission wavelength (Maeda, Maeda et al. 2012).

Figures 2-5(b) and (c) show the fluorescent spectra of the two chemosensors, $Fe_3O_4@SiO_2$-DnS and $Fe_3O_4@SiO_2$-PEG-DnS, after the separate addition of 3.0 molar equivalent metal cations of each of Zn^{2+}, Cu^{2+}, Ni^{2+}, Co^{2+}, Mg^{2+}, Mn^{2+}, Fe^{3+}, Cd^{2+}, Hg^{2+}, Ca^{2+}, Li^+ and Ag^+ (chlorides) in deionised water with (pH = 5.6). A strong and selective quenching was demonstrated after the addition of Zn^{2+} to both sensors. The intensity values displayed in the inserts of the figures are an average of three measurements. The quenching effect was found

to be much more significant in the case of $Fe_3O_4@SiO_2$-PEG-DnS (12.5-fold) than for $Fe_3O_4@SiO_2$-DnS (2.9-fold). The dramatic reduction in florescent intensity is likely to be due to the interactions of Zn^{2+} with the dansyl moiety through complexation with the electron pair-containing nitrogen in the dimethylamine group (Scheme 2-2 (b)), resulting in a reduction in the electron donating nature of this group to the naphthalene ring. In fact, the large fluorescent intensity before the addition of Zn^{2+} would have been due to the high electron density caused by the injection of electrons from the electron donor dimethylamine group into the π antibonding orbital of the naphthalene ring (Weber and Farris 1979). So, the complexation between dimethylamine and Zn^{2+} resulted in diminishment of electron injection, leading to the observed quenching of fluorescent intensity.
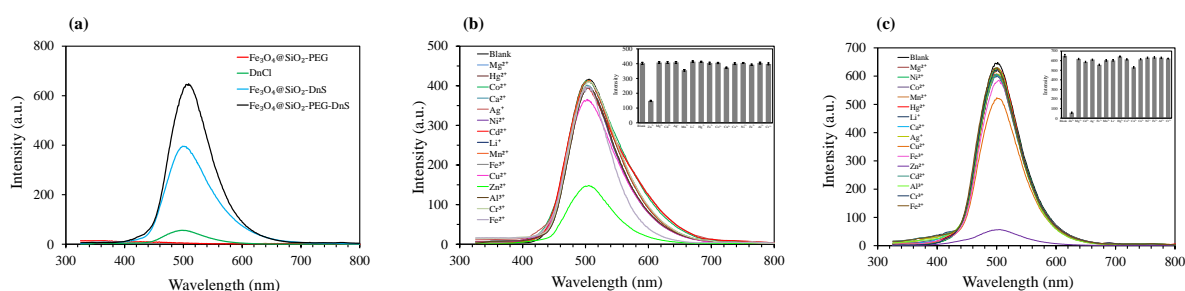
Figure 2-5. Fluorescent emission spectra of (a) DnCl, $Fe_3O_4@SiO_2$-PEG, $Fe_3O_4@SiO_2$-DnS and $Fe_3O_4@SiO_2$-PEG-DnS, and both (b) $Fe_3O_4@SiO_2$-DnS and (c) $Fe_3O_4@SiO_2$-PEG-DnS towards different metal cations
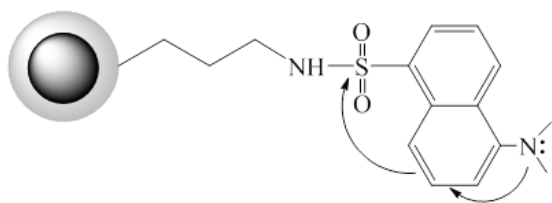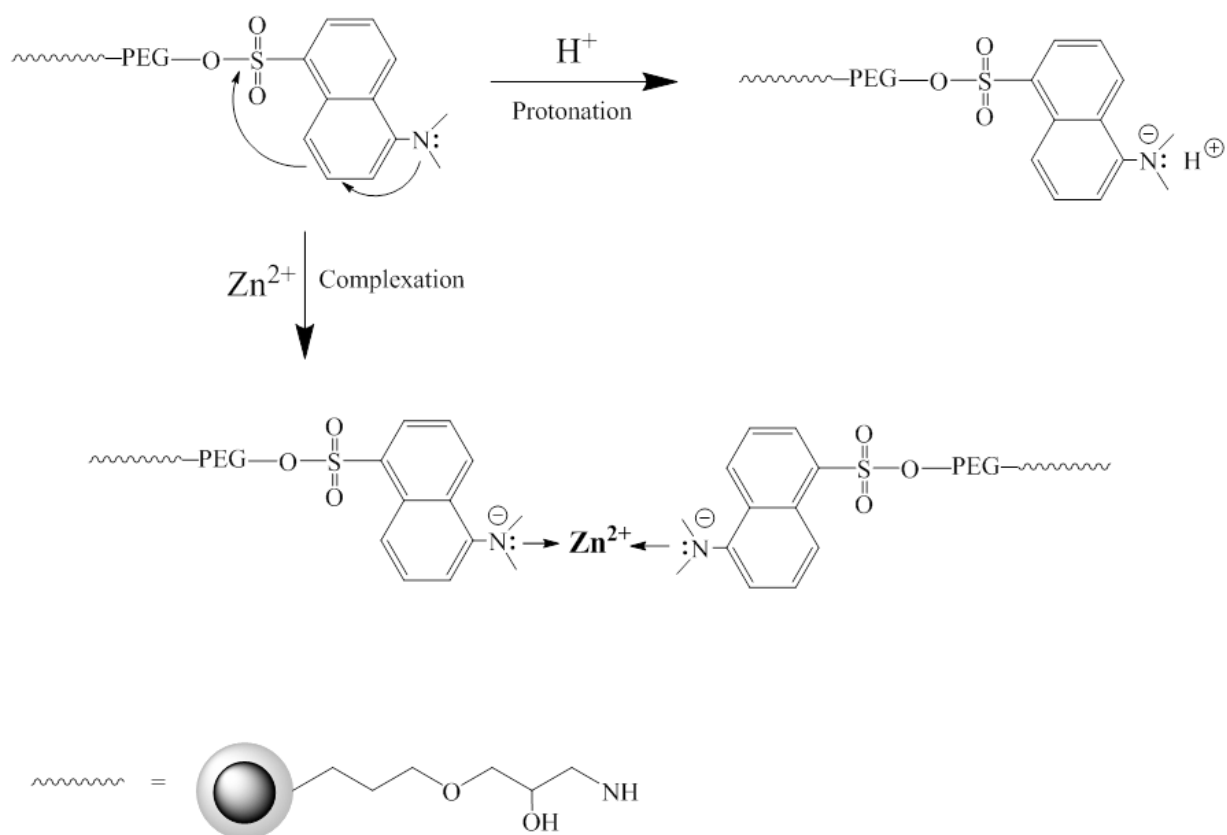
Scheme 2-2. Illustration of enhanced push-pull effect in (a) Fe$_3$O$_4$@SiO$_2$-DnS and (b)

Fe$_3$O$_4$@SiO$_2$-PEG-DnS, showing the hypothesised protonation and Zn^{2+} complexation

mechanisms

Further investigation of the pH-dependence of both the pure $Fe_3O_4@SiO_2$-PEG-DnS nanochemosensor and the nanosensor in the presence of added zinc cations was carried out under the same conditions. Results are shown in Figure 2-6 (a). A quenching effect is clearly presented in the pH range of 4 to 7.4, even without the presence of Zn^{2+}. This is most likely due to the protonation of the dimethylamino group of the chemosensor, as shown in Scheme 2-2 (b). Protonation of dansylated fluorophores has been widely investigated, and has demonstrated a reduced charge transfer from the electron donor dimethylamino group to the electron withdrawal sulfonate group which, therefore, leads to reduced fluorescent intensity (Schuster and Šandor 1996, Prodi, Bolletta et al. 1999, Montalti, Prodi et al. 2002). No quenching can be seen when the pH value is greater than 7.4. The fluorescent intensity of the nanosensor plus Zn^{2+} in the same pH range also is shown in Fig. 6(a). While the reduction observed in fluorescent intensity for pH values above 5.6 is attributable to the interaction of dimethylamino with Zn^{2+}, the changes in the low pH range could be due to a synergistic effect of protonation and zinc cation interaction with the nanosensor. The complexation of Zn^{2+} with chemosensors was evident also in the absorption spectra of the chemosensors (Figure 2-6(b)). As shown in the figures, the main n-π* absorption band at 325 nm in $Fe_3O_4@SiO_2$-PEG-DnS is diminished due to the complexation of dimethylamine with Zn^{2+} at pH = 5.6. A new band appeared at ~ 255 nm resembling the π-π* absorption band of the naphthalene ring (Montalti, Prodi et al. 2002). Also shown in the figure is the influence of the pH value upon the absorption wavelength. The n-π* absorption band at λ = 325 nm completely disappeared at pH = 4. Only the π-π* transition of the naphthalene ring is present. However, at pH = 6 and 9, there are no significant changes in the absorption spectra, indicating no modification within the naphthalene ring (Prodi, Bolletta et al. 1999, Montalti, Prodi et al. 2002). Similar results were observed for $Fe_3O_4@SiO_2$-DnS.

(a)

(b)
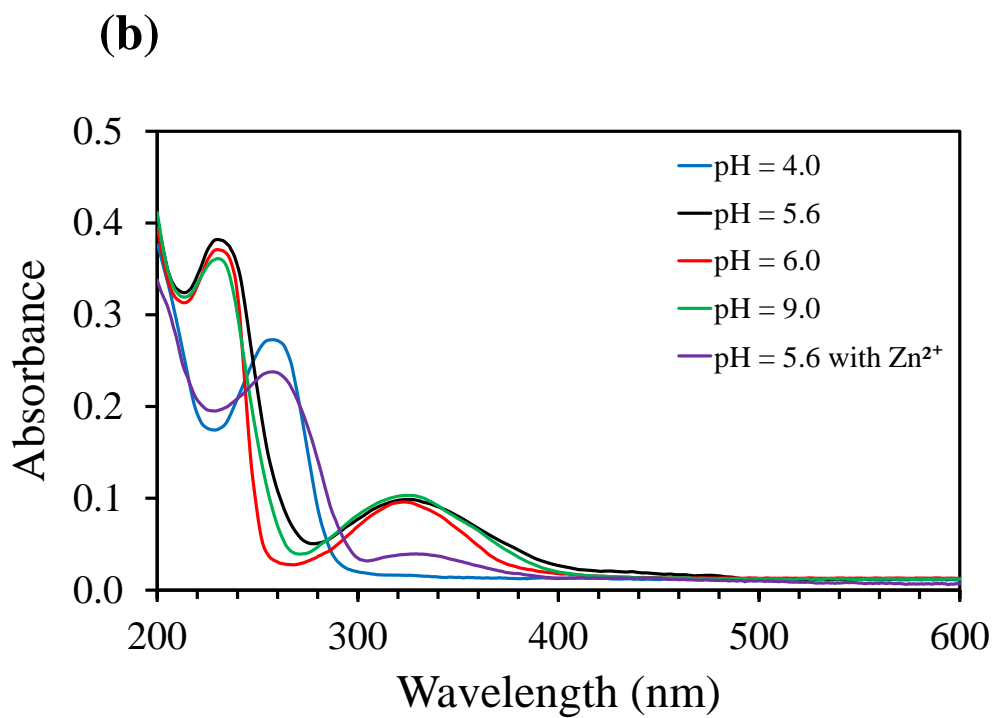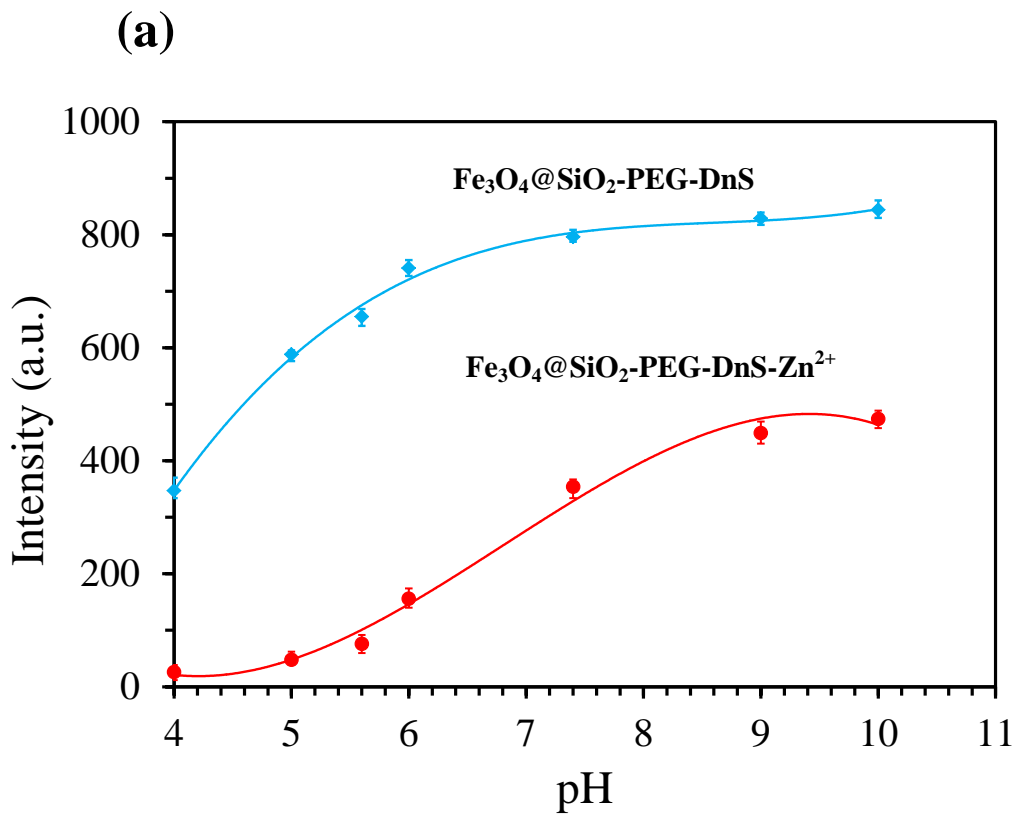
Fig. 2-6. (a) Fluorescent intensity of $Fe_3O_4@SiO_2$-PEG-DnS at different pH values and (b) absorption spectra of $Fe_3O_4@SiO_2$-PEG-DnS under various conditions, (Both are contrasted with results upon the addition of 3.0 equiv. of Zn^{2+})

It should be noted that fluorescent quenching by Cu^{2+} and Fe^{3+} also was shown in Figure 2-5(a) and (b), however by a much smaller amount. This can be attributed to the redox activity of these cations, owing to their partially filled 3d shells, which allows an electron exchange between the fluorophore and the cation via nonradiative energy transfer (Fabbrizzi, Licchelli et al. 1996, Valeur and Leray 2000). There was no significant change in the emission intensity after the addition of other metal ions, indicating a lack of interaction between those cations and the dansylated chemosensors. Moreover, both chemosensors could selectively distinguish between Zn^{2+} and Cd^{2+}, which is an extra benefit of the produced chemosensors. Cd^{2+} often demonstrates coordination properties similar to those of Zn^{2+} due to both having a d^{10} electron configuration (Hanaoka, Kikuchi et al. 2004).

The fluorescent quantum yield was also determined using quinine sulfate in 0.1 M H_2SO_4 (Φ = 0.57) (Lakowicz and Masters 2008) as a reference standard. The results obtained from Equation 2-1 show the highest emission quantum yield for $Fe_3O_4@SiO_2$-PEG-DnS (Φ = 0.39), when compared to those of $Fe_3O_4@SiO_2$-DnS (Φ = 0.28) and free DnCl (Φ = 0.07).

A Job plot was obtained to demonstrate the stoichiometry of the complexation between the nanosensors and Zn^{2+} (Fig. 2-7(a)). A 2:1 stoichiometry ratio was confirmed between the nanosensors and Zn^{2+}.

To further investigate sensing properties quantitatively, fluorescence titration was performed on both nanochemosensors (0.3 μM) by varying the concentration of Zn^{2+} (0 to 5 μM) in aqueous solution. Briefly, 2.5 ml of each of the Zn^{2+} concentrations was added to 2.5 ml of nano-chemosensor solution to make a 5 ml total solution of each. The fluorescent responses of $Fe_3O_4@SiO_2$-DnS and $Fe_3O_4@SiO_2$-PEG-DnS are shown in Figures 2-7(b) and (c), respectively. A gradual decrease is seen in the fluorescent intensity of both chemosensors upon the addition of Zn^{2+}, until saturated, indicating that Zn^{2+} is quantitatively bonded to the dansyl units. A detection limit was determined by comparing the fluorescent intensities of the

produced nanochemosensors with those of a quenched solution. The minimum Zn^{2+} concentration that resulted in a distinguishable intensity difference (confirmed by using a t-test with p < 5%) was taken as the detection limit. This is equivalent to 12.5 nM for $Fe_3O_4@SiO_2$-DnS and 6.25 nM for $Fe_3O_4@SiO_2$-PEG-DnS, which are both much lower than the reported value for Zn^{2+} detection (18.2 nM) in the open literature (Park, Na et al. 2014, Song, Kim et al. 2014).
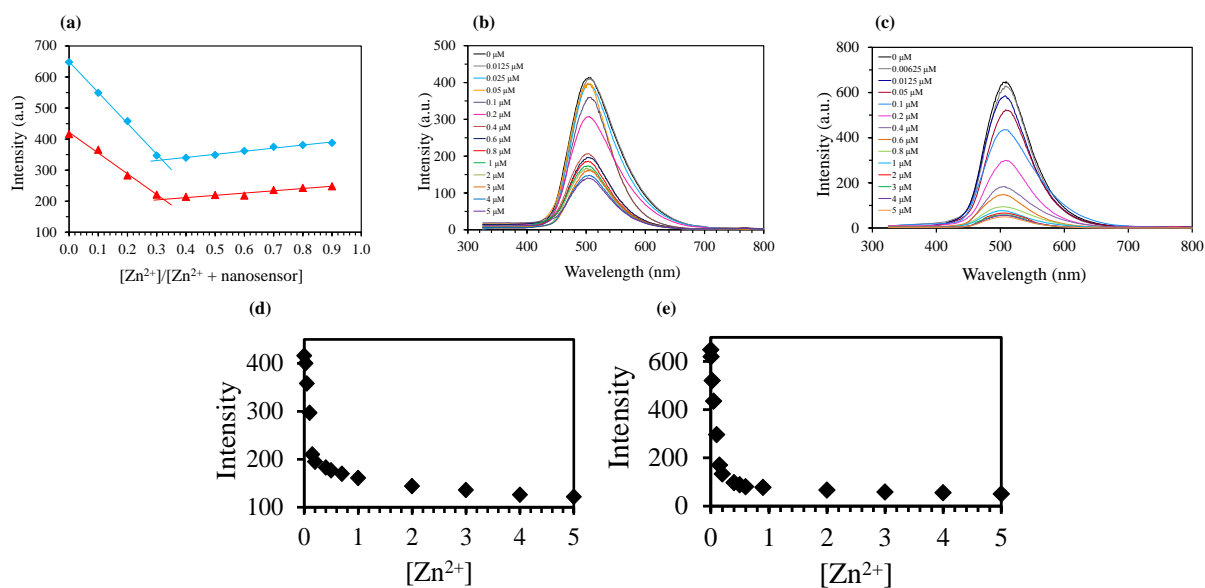
Figure 2-7. (a) The Job plot of $Fe_3O_4@SiO_2$-DnS and $Fe_3O_4@SiO_2$-PEG-DnS, and fluorescence spectra of (b) $Fe_3O_4@SiO_2$-DnS, (c) $Fe_3O_4@SiO_2$-PEG-DnS, (d) and (e) calibration curves of $Fe_3O_4@SiO_2$-DnS and $Fe_3O_4@SiO_2$-PEG-DnS, all upon the addition of Zn^{2+} (0-5 μM) in aqueous solution. Sensor concentration is 0.3 μM

Competition studies also were carried out by treating the nanochemosensor with 3.0 eq. of Zn^{2+} in the presence of identical amounts of other metal ions (listed earlier) at the same concentration. As shown in Figures 2-8(a) and (b), most background metal ions demonstrated little or no obvious interference with the detection of Zn^{2+} ions. An apparent interference by Fe^{3+} and Cu^{2+} was shown to be due to the previously explained quenching nature of the two metal ions, indicating a more favourable interaction of the nanofluorophore with Fe^{3+} and

Cu^{2+} and, therefore, a reduced quenching effect by the Zn^{2+}. The interference by Fe^{3+} and Cu^{2+} was less effective when the pegylated nanochemosensor was used, which is attributable to its more sensitive nature.

(a)

(b)
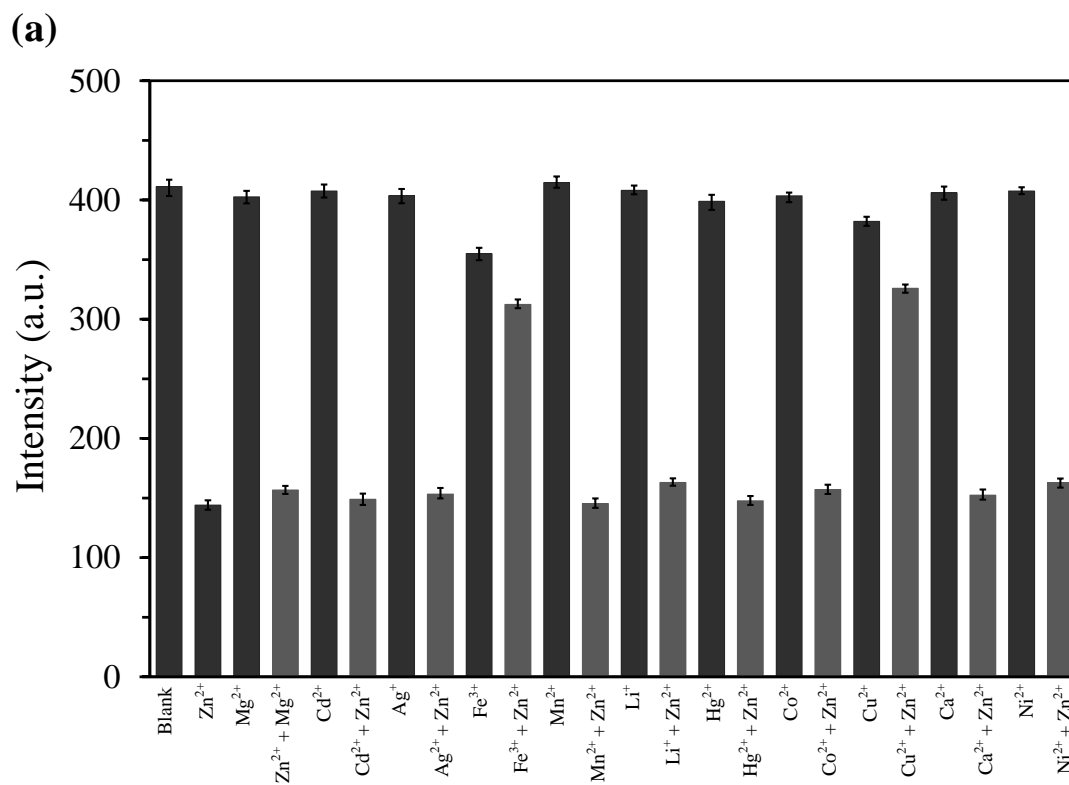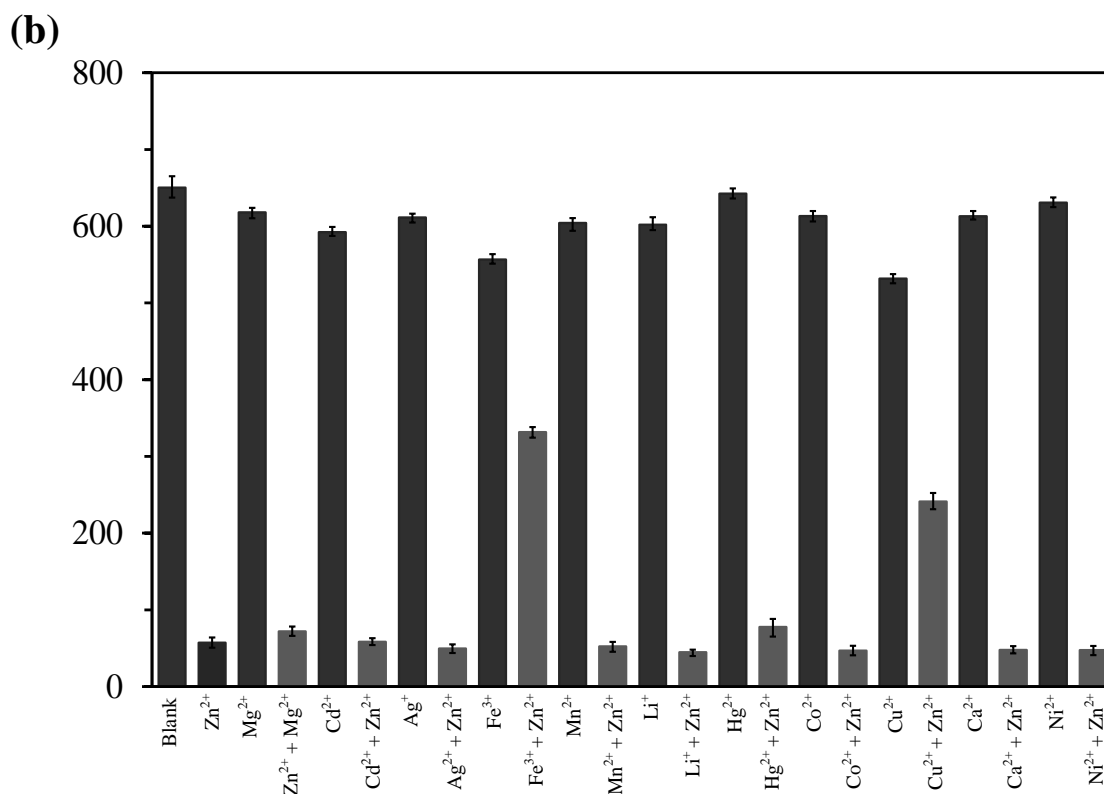
Figure 2-8. Fluorescent emission changes of (a) $Fe_3O_4@SiO_2$-DnS and (b) $Fe_3O_4@SiO_2$-PEG-DnS at 0.3 μM upon the addition of various metal cations (3.0 equivalents)

Reusability and regeneration is one the most key factors in designing nanosensors for practical applications. The recovery of $Fe_3O_4@SiO_2$-PEG-DnS was examined through five cycles. For each cycle, the nanosensor was freed from the Zn^{2+} ions by treating with EDTA in base (pH = 8) condition and equivalent moles towards Zn^{2+}. The fluorescent intensity was examined and a 98.3% recovery was observed after five cycles (Figure 9). The mass recoverability also was examined. A recovery was found to be 94.0 %, 88.8 % and 76.4 % after the 1st , 3rd, and 5th cycle respectively. The results demonstrated an excellent stability of nanochemosensor and its recyclability for the practical applications.
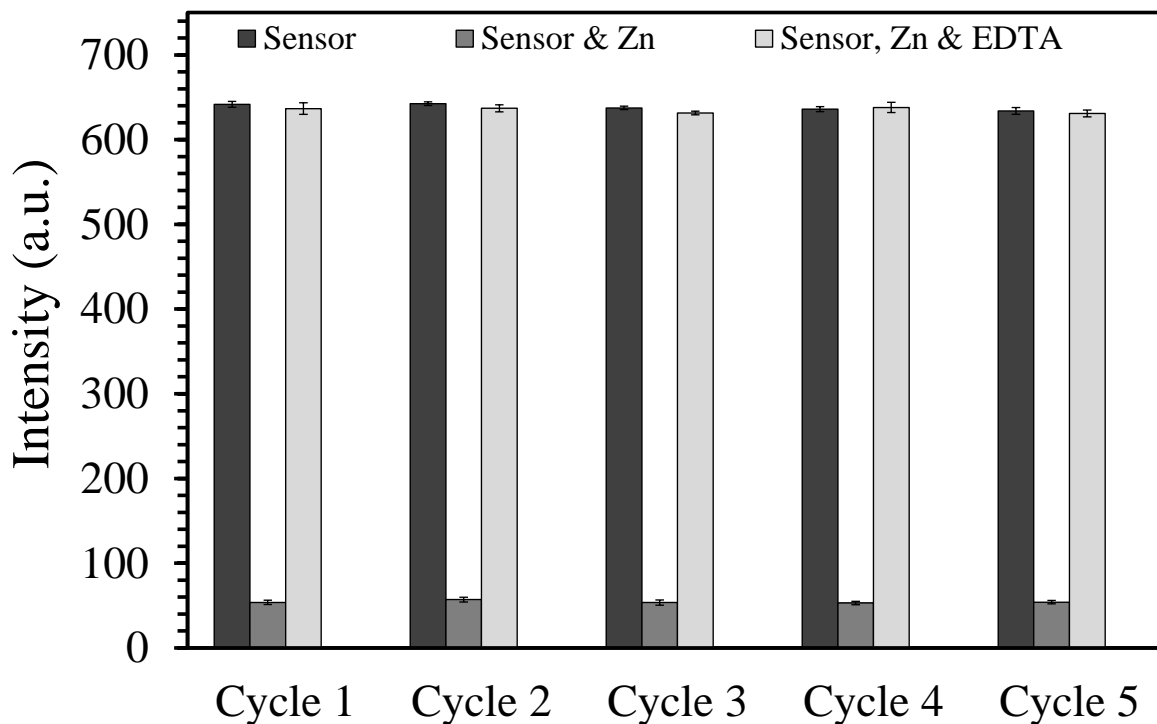
Figure 2-9. The recoverability of Fe_3O_4@SiO_2-PEG-DnS with Zn^{2+}

2.4. Conclusions

In summary, this communication reports the successful fabrication and characterisation of a novel magnetic nanochemosensor, namely Fe_3O_4@SiO_2-PEG-DnS, and includes the investigation results in regard to its sensitivity, selectivity detection limit, and the pH dependence as well as the stability and the reusability in relation to a series of metal ions. A strong and selective fluorescent quenching was obtained towards Zn^{2+} in aqueous solutions. The contributions from both zinc-complexation and/or protonation of the dimethylamine group in the dansyl fluorophore have been hypothesised, both of which are pH dependent. In comparison with Fe_3O_4@SiO_2-DnS, which contains no PEG spacer, Fe_3O_4@SiO_2-PEG-DnS showed a significantly improved sensitivity and selectivity towards zinc ions (Zn^{2+}). Fe_3O_4@SiO_2-PEG-DnS also displayed a noticeably higher value for the quantum yield (0.39)

than that of the non-spacer chemosensor ($\Phi = 0.28$), and a very sensitive detection limit of 6.00 nM towards zinc ions, which is lower than the lowest reported value of 18.2 nM. In addition, the nanochemosensors displayed very good selectivity in competition with other cations, except for Cu^{2+} and Fe^{3+}. Furthermore, the novel $Fe_3O_4@SiO_2$-PEG-DnS nanosensor is proved to be very stable and highly recoverable. Both chemosensors selectively distinguished Zn^{2+} from Cd^{2+}, which is an additional benefit.

2.5.   References

Chen, Q.-Y. and C.-F. Chen (2005). "A new Hg^{2+}-selective fluorescent sensor based on a dansyl amide-armed calix [4]-aza-crown." <u>Tetrahedron Letters</u> **46**(1): 165-168.

Crosby, G. A. and J. N. Demas (1971). "Measurement of photoluminescence quantum yields. Review." <u>The Journal of Physical Chemistry</u> **75**(8): 991-1024.

Fabbrizzi, L., M. Licchelli, et al. (1996). "Sensing of transition metals through fluorescence quenching or enhancement. A review." <u>Analyst</u> **121**(12): 1763-1768.

Feng, J., J. Mao, et al. (2011). "Ultrasonic-assisted in situ synthesis and characterization of superparamagnetic Fe 3 O 4 nanoparticles." <u>Journal of Alloys and Compounds</u> **509**(37): 9093-9097.

Feng, X., S. Zhang, et al. (2013). "Controlling silica coating thickness on TiO_2 nanoparticles for effective photodynamic therapy." <u>Colloids and Surfaces B: Biointerfaces</u> **107**: 220-226.

Feng, X., S. Zhang, et al. (2015). "A novel folic acid-conjugated TiO_2–SiO_2 photosensitizer for cancer targeting in photodynamic therapy." <u>Colloids and Surfaces B: Biointerfaces</u> **125**: 197-205.

Hanaoka, K., K. Kikuchi, et al. (2004). "Development of a zinc ion-selective luminescent lanthanide chemosensor for biological applications." <u>Journal of the American Chemical Society</u> **126**(39): 12470-12476.

Huang, C. Y. (1982). "[27] Determination of binding stoichiometry by the continuous variation method: The job plot." <u>Methods in enzymology</u> **87**: 509-525.

Job, P. (1928). "Formation and stability of inorganic complexes in solution."

Lakowicz, J. R. and B. R. Masters (2008). "Principles of fluorescence spectroscopy." <u>Journal of Biomedical Optics</u> **13**(2): 029901.

Liu, G., H. Wu, et al. (2011). "Synthesis and applications of fluorescent-magnetic-bifunctional dansylated $Fe_3O_4@$ SiO_2 nanoparticles." <u>Journal of materials science</u> **46**(18): 5959-5968.

Maeda, H., T. Maeda, et al. (2012). "Absorption and fluorescence spectroscopic properties of 1-and 1, 4-silyl-substituted naphthalene derivatives." <u>Molecules</u> **17**(5): 5108-5125.

Montalti, M., L. Prodi, et al. (2002). "Solvent-induced modulation of collective photophysical processes in fluorescent silica nanoparticles." <u>Journal of the American Chemical Society</u> **124**(45): 13540-13546.

Park, G. J., Y. J. Na, et al. (2014). "A single chemosensor for multiple analytes: fluorogenic detection of Zn 2+ and OAc− ions in aqueous solution, and an application to bioimaging." New Journal of Chemistry **38**(6): 2587-2594.

Prodi, L., F. Bolletta, et al. (1999). "Searching for new luminescent sensors: synthesis and photophysical properties of a tripodal ligand incorporating the dansyl chromophore and of its metal complexes." European journal of inorganic chemistry **1999**(3): 455-460.

Prodi, L., F. Bolletta, et al. (2000). "Luminescent chemosensors for transition metal ions." Coordination Chemistry Reviews **205**(1): 59-83.

Sauer, M., J. Hofkens, et al. (2011). "Basic principles of fluorescence spectroscopy." Handbook of Fluorescence Spectroscopy and Imaging: From Single Molecules to Ensembles: 1-30.

Schuster, M. and M. Šandor (1996). "N-Dansyl-N′-ethylthiourea for the fluorometric detection of heavy metal ions." Fresenius' journal of analytical chemistry **356**(5): 326-330.

Shankar, B. H. and D. Ramaiah (2011). "Dansyl Naphthalimide Dyads As Molecular Probes: Effect of Spacer Group on Metal Ion Binding Properties." The Journal of Physical Chemistry B **115**(45): 13292-13299.

Song, E. J., H. Kim, et al. (2014). "A single fluorescent chemosensor for multiple target ions: recognition of Zn^{2+} in 100% aqueous solution and F− in organic solvent." Sensors and Actuators B: Chemical **195**: 36-43.

Tharmaraj, V. and K. Pitchumani (2012). "An acyclic, dansyl based colorimetric and fluorescent chemosensor for Hg (II) via twisted intramolecular charge transfer (TICT)." Analytica chimica acta **751**: 171-175.

Valeur, B. and I. Leray (2000). "Design principles of fluorescent molecular sensors for cation recognition." Coordination Chemistry Reviews **205**(1): 3-40.

Weber, G. (1952). "Polarization of the fluorescence of macromolecules. 1. Theory and experimental method." Biochemical Journal **51**(2): 145.

Weber, G. and F. J. Farris (1979). "Synthesis and spectral properties of a hydrophobic fluorescent probe: 6-propionyl-2-(dimethylamino) naphthalene." Biochemistry **18**(14): 3075-3078.

Chapter 3

The Synthesis and Investigation of Quinoline Functionalized Magnetic Nanostructure for Selective Detection of Zn^{2+} in Aqueous Solutions

3.1. Introduction

Fluorescent chemosensors have attracted enormous attention in the recent decades due to their low cost, high sensitivity and technical simplicity. Among many of the reported chemosensors for Zn^{2+}, some suffer from poor water solubility and low selectivity especially when the ions of zinc, cadmium and mercury co-exist (Li, Lu et al. 2012, Choi, You et al. 2016), some show reduced fluorescence as a consequence of quenching, limiting the sensors' applicability (Wu, Wang et al. 2010, Ding, Xie et al. 2011). The development and discovery of highly selective and sensitive fluorophores and fluorescent chemosensors for Zn^{2+} has been an ongoing topic of research. Quinoline based chemosensors have been extensively used as fluoroscopic agents for detection of zinc ion, Zn^{2+}, in aqueous solutions (Nolan, Jaworski et al. 2005, Dong, Guo et al. 2013, Ma, Wang et al. 2013). The quinoline chemosensor relies largely on the photo-induced electron transfer (PET), intermolecular charge transfer (ICT) and fluorescence resonance energy transfer (FRET) for the fluorescent signal transduction in its design (Banthia and Samanta 2006, Sarkar, Banthia et al. 2006). Among the reported studies on chemosensors, 8-aminoquinoline (8AQ) and its derivatives are the most commonly used due to their ability to chelate Zn^{2+} ion by the heterocyclic nitrogen atom and exocyclic amino group forming a chelated complex (Han, Lee et al. 2009, Zhu, Yuan et al. 2010, Rastogi, Pal et al. 2011, Tian, Lou et al. 2013). The 4-isomer of aminoquinoline (4AQ),

however, has attracted less attention despite many studies of the luminescent properties of 8AQ, which was reportedly due to the controversy over the chemical properties of the 4AQ relative to its 8-isomer. Several researchers (Kovi, Capomacchia et al. 1972, Nord, Karlsen et al. 1994, de Souza Santos, de Morais Del et al. 2014) have shown that the chemistry of 4AQ is atypical to normal arylamine while other aminoquinoline isomers are well behaved in this respect. In fact, 4-isomer is more similar to a cyclic amidine than to an aminoquinolines. The chemical structures of the two isomers are displayed in Scheme 3-1.
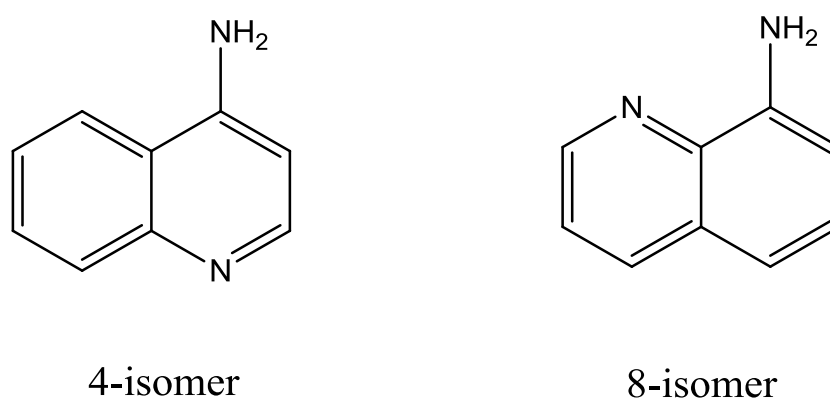
4-isomer   8-isomer

Scheme 3-1: The structure of 4-isomer and 8-isomer of aminoquinoline

An early report indicated that the 4-isomer is a pH-sensitive and non-emissive probe that shows enhanced fluorescence intensity upon protonation due to enhanced ICT (Gunnlaugsson, Mac Dónaill et al. 2001). In recent years, the development of 4AQ derivatives for luminescent sensing of transition metals has attracted increasing interests. However, understanding of the sensing mechanism is limited. For instance, Kaur and co-workers (Kaur, Kaur et al. 2013), synthesised a quinoline-derivative cation sensor based on 4-aminoquinoline. They reported on sensing application of their chemosensor through quenching of fluorescence in the presence of Hg^{2+}, Fe^{3+} and Cu^{2+}. In a similar study, Singh et al. (Singh, Sindhu et al. 2015) fabricated pH-sensitive benzo-xanthene-4-aminoquinoline conjugates for sensing thorium (Th^{4+}). The fluorescent intensity was quenched due to

chelation-enhanced fluorescence quenching caused by specific interaction of Th^{4+} with two nitrogen atoms of linker of xanthene-aminoquinoline conjugate. More recently, Wang et al. (Wang, Jin et al. 2016) synthesised Hg^{2+} selective fluorescent sensor by grafting 4-aminoquinoline to glycosyl pyridyl-triazole. The mechanism of the behaviour of the probe has been attributed to a binding mode of triazolyl quinoline with Hg^{2+}.

This chapter aims to create a novel 4AQ-based nano-magnetic structure and further to investigate its selectivity and sensitivity towards zinc ions in aqueous solutions. Magnetic core-shell structures are widely considered in the design of recyclable and reusable nanochemosensors (Feng, Mao et al. 2011, Feng, Zhang et al. 2013, Feng, Guo et al. 2014) in which the magnetite (Fe_3O_4) nanoparticles are used as a core and various silicon precursors are used to 'shell' the core and to conjugate a selected fluorophore to the surface of the magnetic nanoparticles. The silica shell is capable not only to prevent the aggregation of magnetic nanoparticle, but also to protect the sensor from the interference of other spieces (Lu, Yang et al. 2012). A recent study reported that the presence of polyethylene glycol (PEG) as a spacer between the core nanostructure and the fluorophore moiety has a strong positive impact on the fluorescent properties of the magnetic nanochemosensor.

In this chapter, 4AQ was introduced onto the surface of nano-magnetic core through the silica shell using a facile method, and further investigated on its selectivity and sensitivity towards a series of metal ions in the aqueous solution. The nano-magnetic core-shell structure containing functional precursors of 3-glycidyloxypropyl siloxane was first synthesised using previously reported method (Pourfallah and Lou 2016). Through the functional precursors, polyethylene glycol (NH_2-PEG-COOH, $M_w = 3000$) was conjugated to the surface of the nanoparticles. The free carboxylic acid groups of the PEG spacer were further grafted with 4-amino-2-methyl-8-(trifluoromethyl)quinoline (4AQ) to form a novel nanostructure of $Fe_3O_4@SiO_2$-PEG-4AQ. The chemical synthesis route is illustrated in Scheme 3-2. Using a

similar chemistry, $Fe_3O_4@SiO_2$-4AQ was also prepared containing no PEG spacer. Both nanosensors were fully characterised and investigated as a potential sensor for Zn^{2+} detection in aqueous solutions.
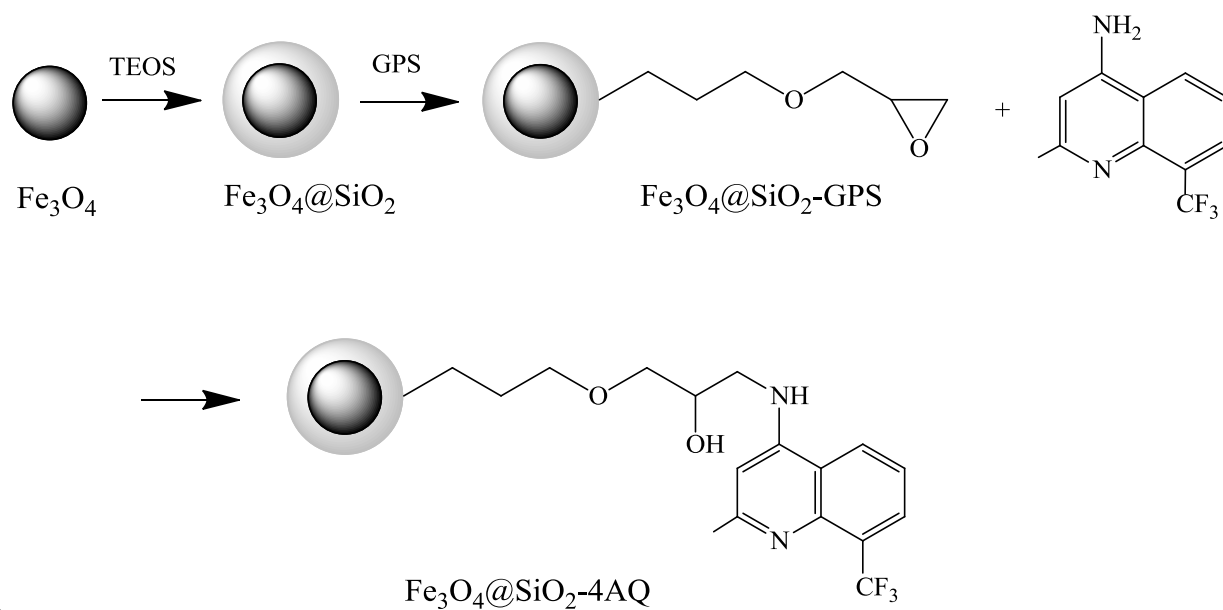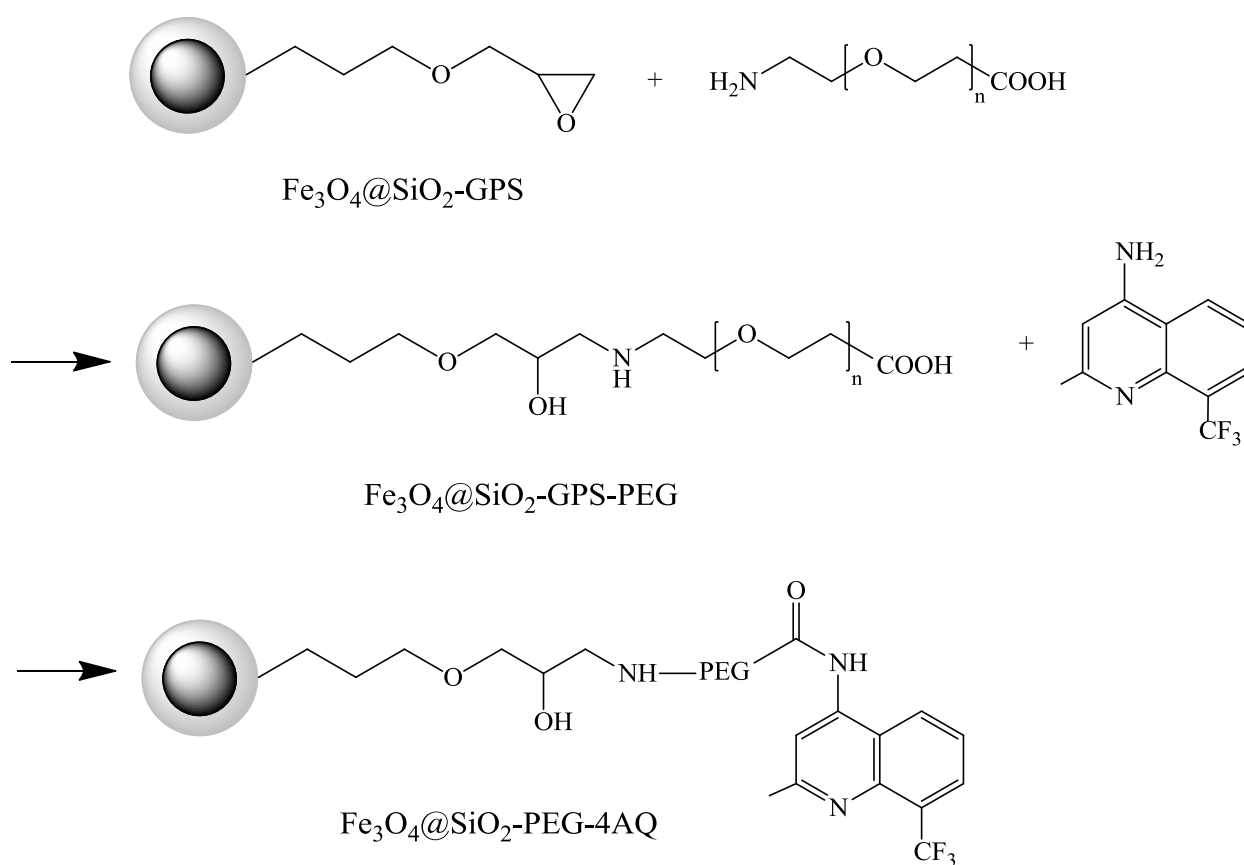
Scheme 3-2. Synthetic procedure of (a) Fe$_3$O$_4$@SiO$_2$-4AQ and (b) Fe$_3$O$_4$@SiO$_2$-PEG-4AQ

3.2. Materials and Methods

3.2.1. Materials

Tetraethoxysilane (TEOS) (99.99%), (3-glycidyloxypropyl) trimethoxylsilane (GPS) (98%), 4-amino-2-methyl-8-(trifluoromethyl)quinoline (4-AQ), N-(3-dimethylaminopropyl)-N′-ethylcarbodiimide hydrochloride (EDC) (98%), N-hydroxysuccinimide (NHS) (98%) were obtained from Sigma–Aldrich. Amino PEG acid NH_2-PEG-COOH (90%, $M_w = 3000$) was purchased from Nanocs (USA).

3.2.2. Synthesis of the 3-glycidyloxypropyl siloxane containing magnetic core-shell nanostructure $Fe_3O_4@SiO_2$-GPS

Fe_3O_4 nanoparticles were prepared according using the same method described in Chapter 2 (Pourfallah and Lou 2016). Similarly, the produced magnetic nanoparticles were functionalised with TEOS and GPS as illustrated in Scheme 3-2. The produced $Fe_3O_4@SiO_2$-GPS contains 2.22×10^{-3} mmol 3-glycidyloxypropyl per mg nanoparticles, which was determined using the UV-vis spectroscope and the thermogravimetric analysis (TGA) (details ccan be found in Chapter 2).

3.2.3. Synthesis of $Fe_3O_4@SiO_2$-4AQ

$Fe_3O_4@SiO_2$-4AQ was synthesised by mixing 100mg of $Fe_3O_4@SiO_2$-GPS (0.222 mmol GPS) with 50.2 mg (0.222 mmol) of 4-amino-2-methyl-8-(trifluoromethyl)quinoline in 20 ml D.I water. The mixture was stirred at 65 ºC for 6 hrs in the dark. After the completion of the reaction, the product $Fe_3O_4@SiO_2$-4AQ was collected by external magnet and washed by ethanol and D.I water each (4×20 ml), in sequence.

3.2.4. Synthesis of Fe_3O_4@SiO_2-PEG-4AQ

The synthesis of Fe_3O_4@SiO_2-PEG-4AQ was carried out through two stages. The first stage was the amination of epoxy ring of GPS by mixing Fe_3O_4@SiO_2-GPS (10 mg, 0.022 mmol) with amino PEG acid (NH_2-PEG-COOH, 66 mg, 0.022 mmol) using a similar procedure described in authors' previous study [20]. This leads to the formation of Fe_3O_4@SiO_2-PEG (Scheme 3-2(b)). The second stage involved the activation of carboxylic acid group by carbodiimide reagent (EDC-NHS) prior to the reaction with 4-Amino-2-methyl-8-(trifluoromethyl)quinoline. For this purpose, EDC (0.162 mg, 1.04×10^{-3} mmol) and NHS (0.06 mg, 5.2×10^{-4} mmol), (EDC: NHS, 2:1 mole ratio) were dissolved in 20 ml ice-cold water. Fe_3O_4@SiO_2-PEG nanoparticles (10 mg containing 2.1×10^{-4} mmol COOH) was then added to the mixture and stirred for 15 min. The 4AQ fluorophore (0.047 mg, 2.1×10^{-4} mmol) was also added to the mixture of nanoparticles and the slurry was kept under stirring for 4 hrs in an ice bath in dark. After 4 hrs, the ice bath was removed and the reaction carried out under stirring at room temperature over the night. Upon finishing the reaction, the produced nanosensors were separated from the mixture by an external magnet and washed by ethanol and D.I water each (4×20 ml), in sequence.

3.2.5. Physicochemical Characterisation

The morphology examination was carried out using a Transmission Electron Microscopy TEM, (JEOL EM-2100). The sample preparation was involved by distributing the ethanol suspension of nanoparticles on a carbon coated copper grid. A Thermo Scientific Nicolet iS50 was used to obtain the Fourier transform infrared (FTIR) spectra of the synthesised nanostructures fitted with a diamond ATR sampling accessory. The spectra were recorded in the range of 400-4000 cm^{-1}. UV absorption spectra were recorded on a Lambda 25 Perkin Elmer UV‑Vis Spectroscopy. Scans were recorded in the wavelength range from

200 to 800 nm with a band width of 1 nm. Thermogravimetric analysis was performed by using TGA/DSC (Mettler-Toledo Star$^\theta$) thermal analysis system. All TGA experiments were carried out under air atmosphere at a heating rate of 5 ºC/min from 35 to 800 ºC. X-ray diffraction (XRD) analysis was performed using a Bruker AXS diffractometer with Co Kα radiation (λ = 1.79 Å). A scan rate of 0.015º/s was used to record the patterns in a 2θ range of 20–80º, and the accelerating voltage and current were 35 kV and 40 mA, respectively.

3.2.6. Fluorescent measurements

The fluorescent emission spectra were obtained from a Perkin Elmer L55 fluorescence spectrometer with an excitation source set at 330 nm and a scanning rate of 5 nm/min. The stock solutions were prepared in D.I waters at the concentration of 1 µM at room temperature. Various metal ion solutions such as Cu^{2+}, Ni^{2+}, Co^{2+}, Ca^{2+}, Cd^{2+}, Hg^{2+}, Mg^{2+}, Fe^{3+}, Mn^{2+}, and Ag^+ were also prepared (10 µM, chloride). The fluorescent solution and metal ion solution mixed together 24 hours before testing. Quantum yield, job's plot and recovery test were obtained by using the exact same method stated in chapter 2.

3.3. Results and Discussions

3.3.1. Characterization of $Fe_3O_4@SiO_2$-4AQ and $Fe_3O_4@SiO_2$-PEG-4AQ

The chemical and physical characterizations of the nanoparticles were carried out using a string of equipment including TEM, FTIR, UV-Vis and TGA. The TEM images of nanoparticles are shown in Figure 3-1. The average size of the original Fe_3O_4 nanoparticles was 6 ± 3 nm by counting thirty particles randomly and taking the average of thirty measurements. Increased sizes of both the magnetic core and the core-shell structure were observed, especially in $Fe_3O_4@SiO_2$-PEG and $Fe_3O_4@SiO_2$-PEG-4AQ, due to the

aggregation of the Fe$_3$O$_4$ nanoparticles and the conjugation of PEG which has an average molecular weight of 3000 Dalton.

The successful synthesis of nanochemosensors was confirmed by FTIR spectra of the plain and functionalized Fe$_3$O$_4$ nanoparticles as demonstrated in Figures 3-2(a) and (b). The band in Figures 3-2(a) and (b) at 561 cm^{-1} is associated with the stretching and vibration of the Fe-O which is seen in all compounds. The FTIR bands at 3422 and 1640 (O−H vibration), 1079 (Si−O−Si vibration), 903 cm^{-1} (C−O−C vibration) and 2927 and 2861 (C−H vibration) are attributed to the nanoparticle core/shell structure (Fe$_3$O$_4$@SiO$_2$-GPS). The additional bands appeared in Fe$_3$O$_4$@SiO$_2$-GPS-4AQ (Fig. 3-2(a)) at 1333, 1537, 1620 and 3248 cm^{-1} are assigned to C−F, C=C, C=N and N−H, respectively which all come from the organic fluorophore molecule. The FTIR bands related to the production of Fe$_3$O$_4$@SiO$_2$-GPS-PEG-4AQ is shown in Fig. 3-2(b). The intense bands at 1426 and 1690 in Fe$_3$O$_4$@SiO$_2$-GPS-PEG are assigned to C−OH and C=O, respectively indicate the presence of functionalised PEG (NH$_2$-PEG-COOH). The additional bands in Fe$_3$O$_4$@SiO$_2$-GPS-PEG-4AQ at 1333, 1537, 1620 and 3248 cm^{-1} are assigned to C−F, C=C, C=N and N−H representing the existence of 4AQ attached to the functionalised PEG.
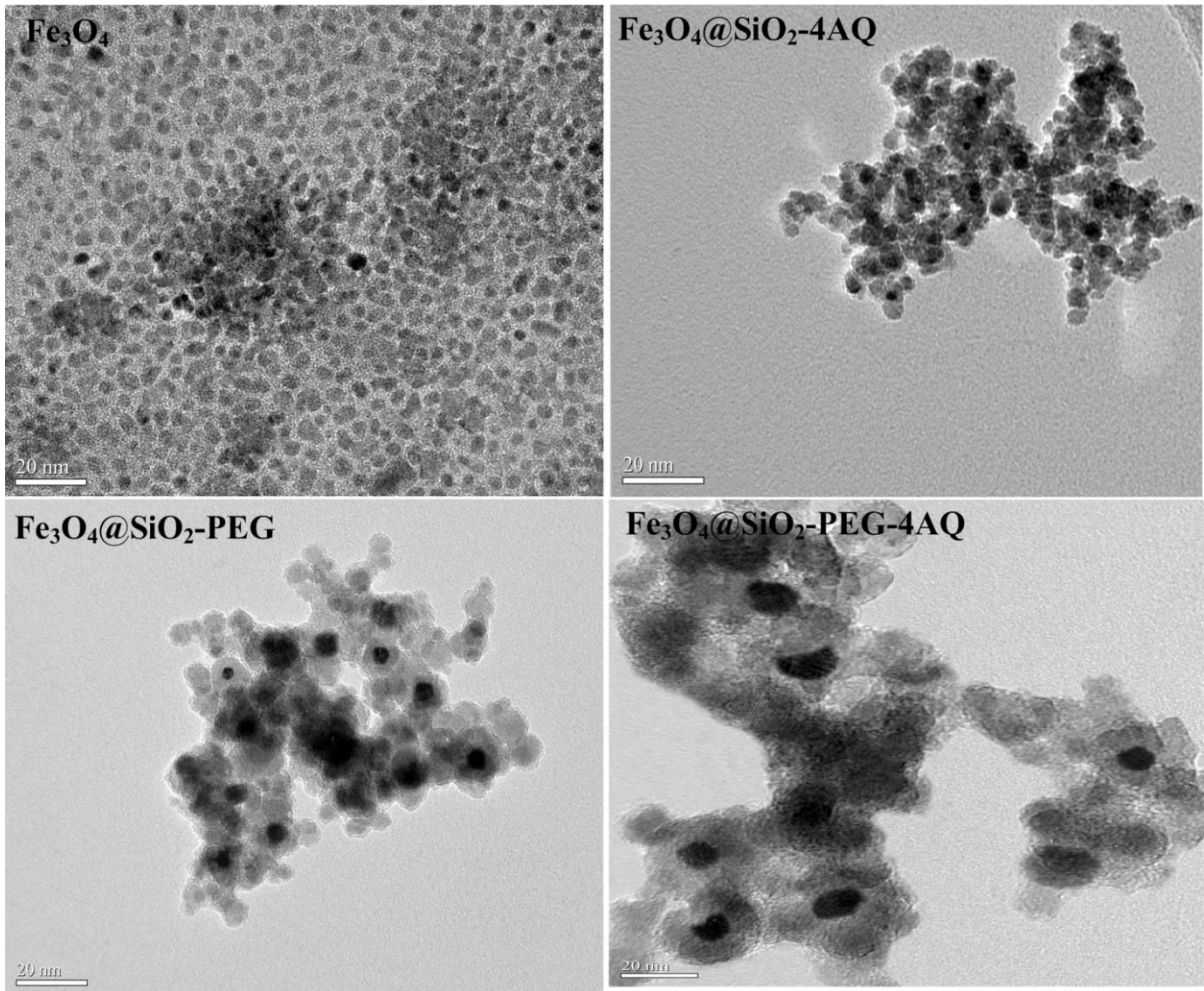
Figure 3-1. TEM images of the produced nanoparticles

(a)

Wavenumber (nm)

(b)

Wavelength (nm)
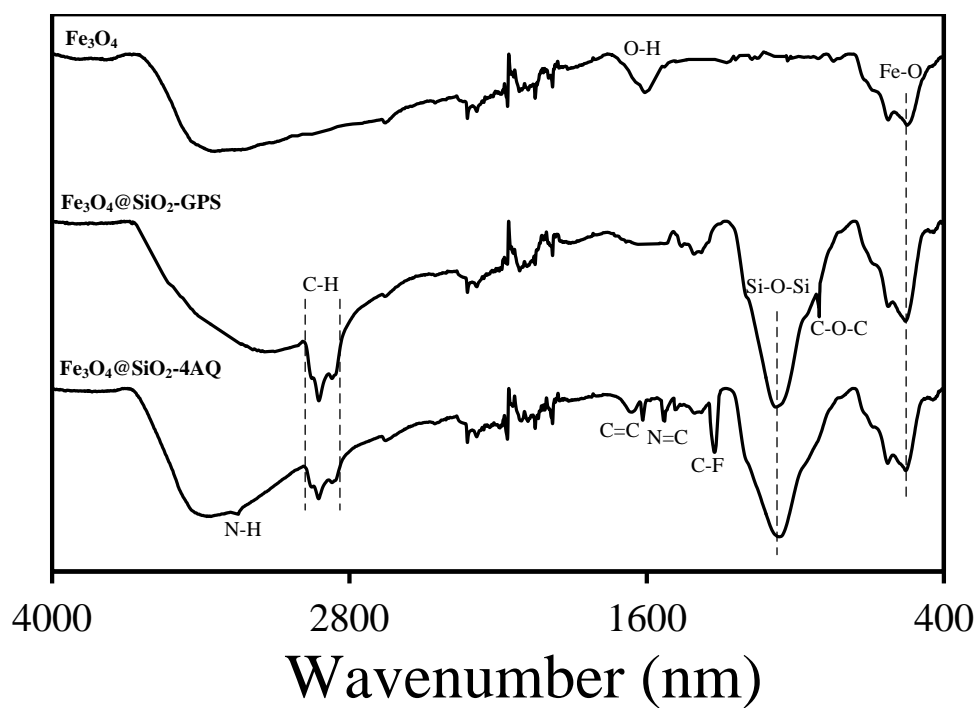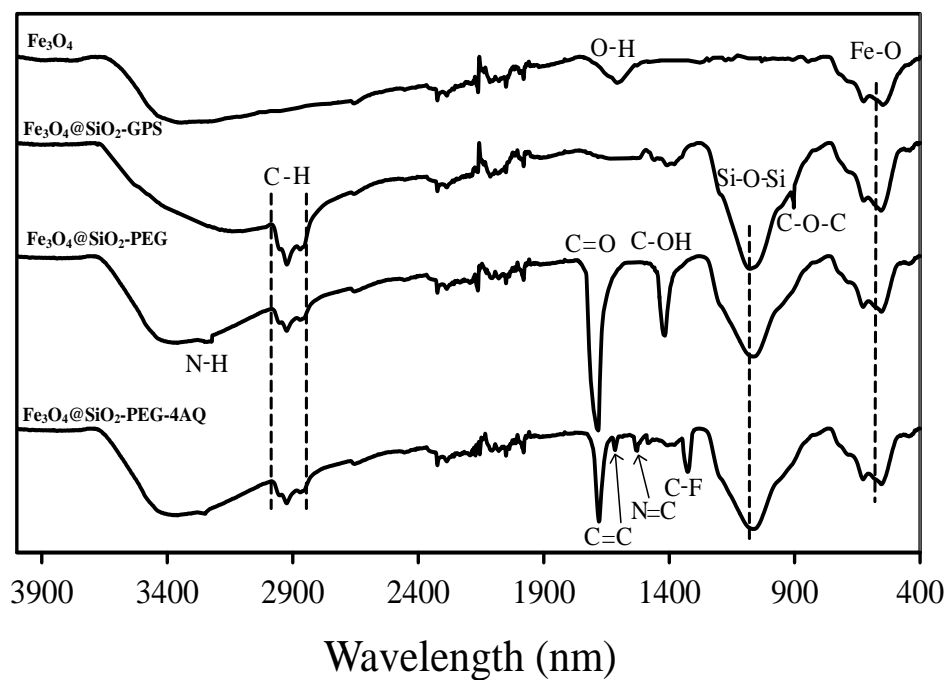
Figure 3-2. FTIR spectra of (a) Fe$_3$O$_4$@SiO$_2$-4AQ and (b) Fe$_3$O$_4$@SiO$_2$-PEG-4AQ and their

deriving compounds

The powder X-ray diffraction patterns of Fe_3O_4 nanoparticles and nanosensors $Fe_3O_4@SiO_2$-4AQ and $Fe_3O_4@SiO_2$-PEG-4AQ are shown in Figure 3-3. All samples possess the characteristic diffraction peaks at (2 2 0), (3 1 1), (4 0 0), (4 2 2), (5 1 1) and (4 4 0), which are in good agreement with pure cubic Fe_3O_4 (Feng, Mao et al. 2011). The broad peak appeared at 20‑$28°$ in the two nanosensors corresponds to the amorphous-state silica layer and the spacer/linker attached to it, which indicates Fe_3O_4 magnetic cores are successfully coated by SiO_2 layer and other functional groups. The XRD patterns of the nanosensors are similar to that of plain Fe_3O_4, demonstrating that no phase change of Fe_3O_4 nanoparticles has been induced by chemical modification.
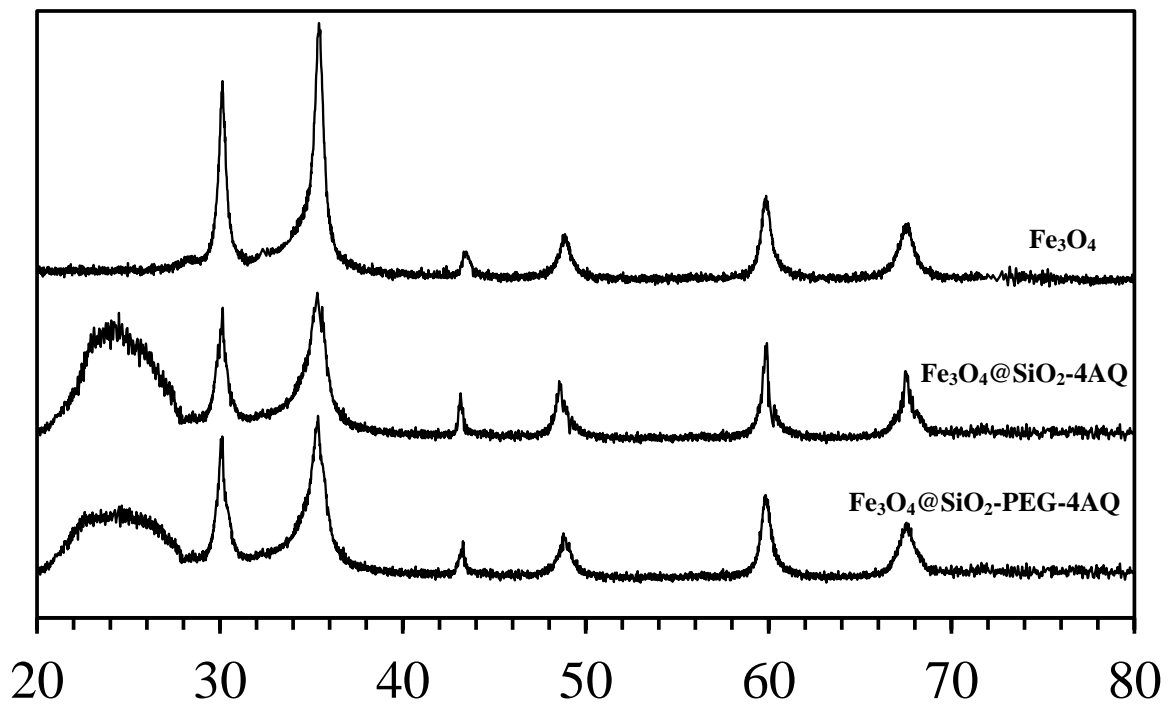
Figure 3-3. XRD patterns of the two nanosensors, $Fe_3O_4@SiO_2$-4AQ and $Fe_3O_4@SiO_2$-PEG-4AQ

The TGA weight loss curves for $Fe_3O_4@SiO_2$-PEG-4AQ are shown in Figure 3-4(a). According to the figure, plain Fe_3O_4 exhibited a slight weight loss in the range of 35-100°C due to the loss of physically absorbed water on the surface of nanoparticles. The amount of weight loss in $Fe_3O_4@SiO_2$-PEG-4AQ TGA is about 39% in the range of 200-800°C which is due to decomposition of organic components. The estimated molar content of 4AQ attached to nanosensor was 1.96 μmol/mg.

Comparative UV-vis absorption spectra are shown in Fig. 3-4(b). As can be seen from the figure, the 4AQ fluorophore exhibits four absorption bands at λ_{max} = 330, 322, 241 and 216 nm. The highest absorption bands at 241 and 216 nm are assigned to the π-π* orbital transitions of the quinoline backbone. The two absorption bands at λ_{max} = 330 and 322 nm of similar intensity are likely due to the intramolecular charge transfer of the heterocyclic rings and is attributed to the n-π* transitions (Otelo, Sant'Ana et al. 2011, Mmonwa, Mphahlele et al. 2014). The UV-vis spectra of $Fe_3O_4@SiO_2$-4AQ and $Fe_3O_4@SiO_2$-PEG-4AQ nanosensors show similar absorption bands to the pristine 4AQ fluorophore at the π-π* orbital transition region and the n-π* transition absorption bands. The $Fe_3O_4@SiO_2$-PEG-4AQ nanoparticles have shown a broader n-π* transition absorption band, likely due to the presence of amide group (-C(O)-NH-) (Scheme 3-2b).

(a)

(b)
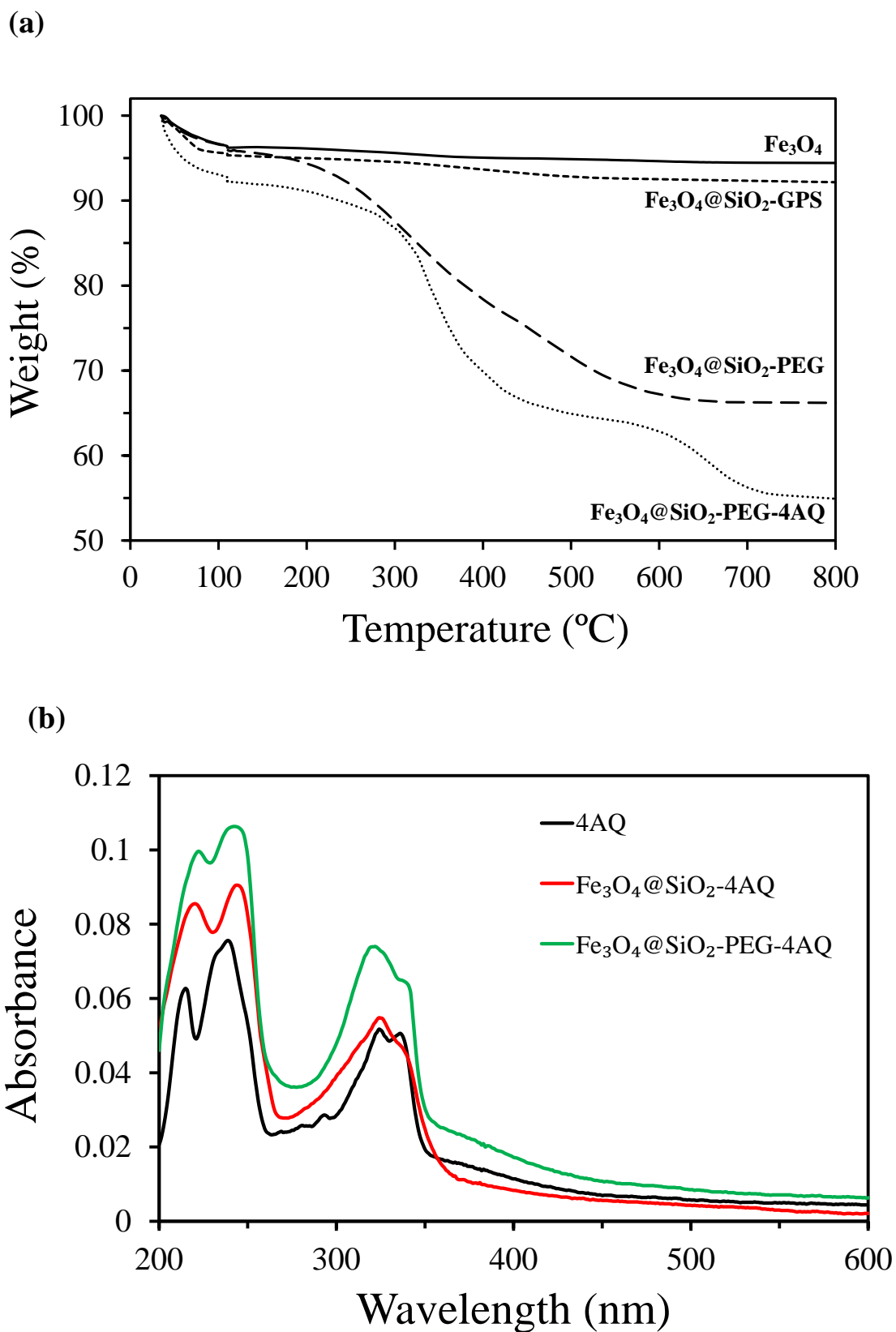
Figure 3-4. (a) TGA weight loss curves of the produced nanoparticles, (b) UV-Vis spectra of

4-AQ, $Fe_3O_4@SiO_2$-4AQ and $Fe_3O_4@SiO_2$-PEG-4AQ

3.3.2. Fluorescent study and metal sensing

Figure 3-5(a) demonstrates the fluorescent response of $Fe_3O_4@SiO_2$-4AQ and $Fe_3O_4@SiO_2$-PEG-4AQ and 4AQ at the same concentration (1.00 μM) in aqueous solutions. As shown in the figure, they all exhibit low fluorescent intensity at the λ_{max} = 406 nm. To investigate the sensing properties of two synthesised nanosensors, 10 equivalent of each metal cations such as Cu^{2+}, Ni^{2+}, Co^{2+}, Ca^{2+}, Cd^{2+}, Hg^{2+}, Mg^{2+}, Fe^{3+}, Mn^{2+} Zn^{2+} and Ag^+ were added to $Fe_3O_4@SiO_2$-4AQ and $Fe_3O_4@SiO_2$-PEG-4AQ aqueous solution (1.00 μM) respectively. As shown in Figure 3-5(b) and (c), the addition of Zn^{2+} has resulted in an 8.6-fold increase of the fluorescent intensity by $Fe_3O_4@SiO_2$-4AQ and a 13.5-fold increase by $Fe_3O_4@SiO_2$-PEG-4AQ, respectively. There was also a red shift of ~ 42 nm (from 407 to 449 nm) observed. A slight quenching effect was observed upon the addition of Cu^{2+}, likely due to the redox activity and energy transfer between the fluorophore and Cu^{2+} cation (Pourfallah and Lou 2016). The addition of other metal cations exhibited no change to nanochemosensors fluorescent intensity. The increased fluorescent intensity upon the addition of Zn^{2+} is likely attributed to an enhanced intermolecular charge transfer (ICT). ICT has been reportedly observed when the protonation of the heterocyclic ring occurs due to the unusual chemistry of the 4-AQ compare to other aminoquinoline isomers, as illustrated in Scheme 3-3 (Kovi and Capomacchia, et al. 1972). Any condition that results in the rearrangement of the aromaticity of heterocyclic ring brought by the loss of the lone pair of the exocyclic amino group can lead to an enhanced ICT (Gunnlaugsson and Mac Dónaill, 2001). In this work, the added Zn^{2+} ions complex with the heterocyclic nitrogen atom (Scheme 3-3), which reduces the electron density from the ring resulting in a delocalization of the n-electrons on the amino group bounded to the ring (Nord, Karlsen et al. 1994). The coordination of Zn^{2+} strengthens the push‑pull effect in ICT mechanism, therefore, a red shift in emission observed. The quantum yield obtained for $Fe_3O_4@SiO_2$-4AQ to be 0.057 and 0.067 for $Fe_3O_4@SiO_2$-PEG-4AQ

before the addition of Zn^{2+}. The method for the quantum yield measurement was reported elsewhere (Pourfallah and Lou 2016). However, after binding with Zn^{2+} the quantum yield values increased significantly to 0.41 and 0.56 for $Fe_3O_4@SiO_2$-4AQ and $Fe_3O_4@SiO_2$-PEG-4AQ, respectively. This further demonstrates the strong coordination of Zn^{2+} with chemosensors.
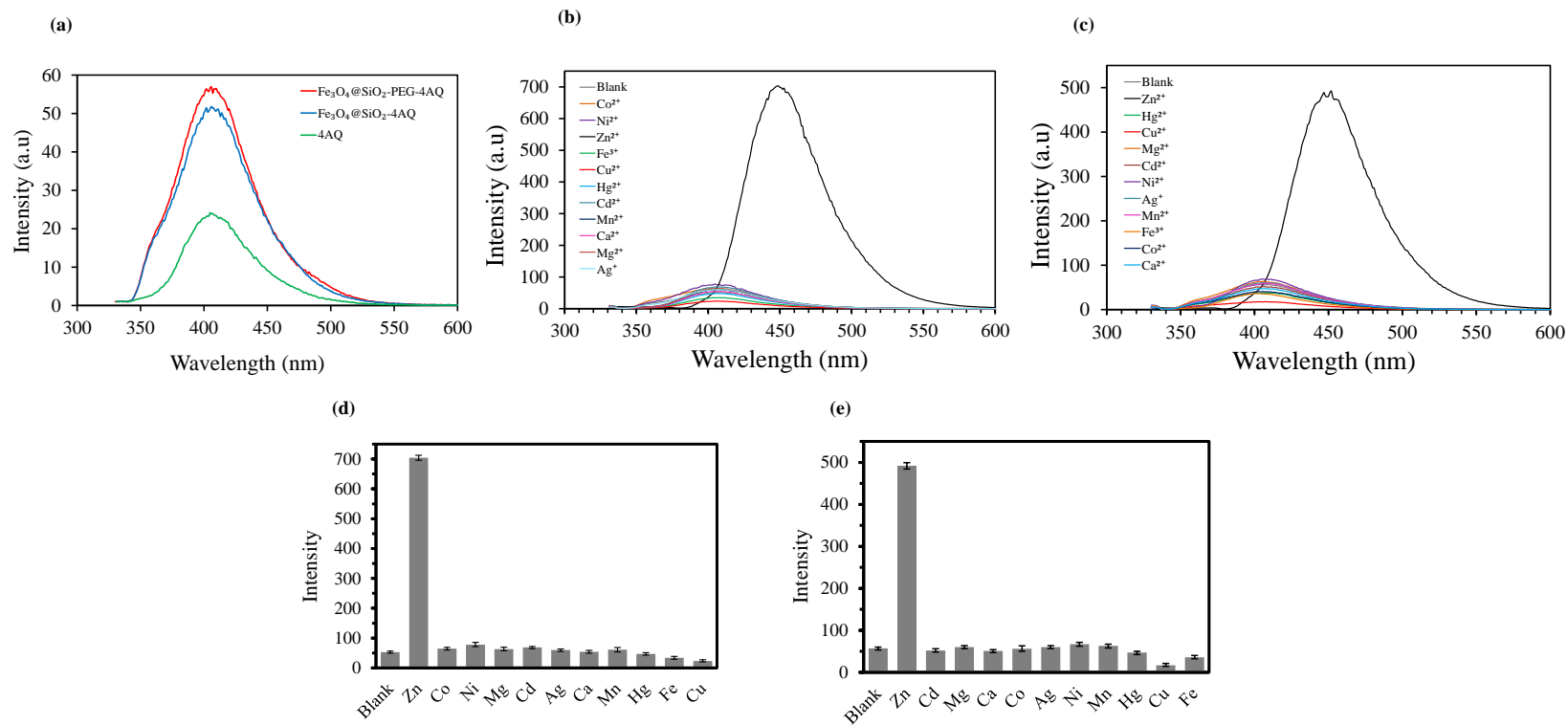
Figure 3-5. Fluorescent emission spectra of (a) 4AQ, Fe_3O_4@SiO_2-4AQ and Fe_3O_4@SiO_2-PEG-4AQ, at 1.00 μM (b) Fe_3O_4@SiO_2-PEG-4AQ, (c) Fe_3O_4@SiO_2-4AQ towards different metal cations (10 μM), (d) and (e) bar graph of Fe_3O_4@SiO_2-PEG-4AQ Fe_3O_4@SiO_2-4AQ towards different metal cations. P value from student t test between Zn^{2+} and blank is 0.0334 and 0.0401 in (d) and (e), respectively.
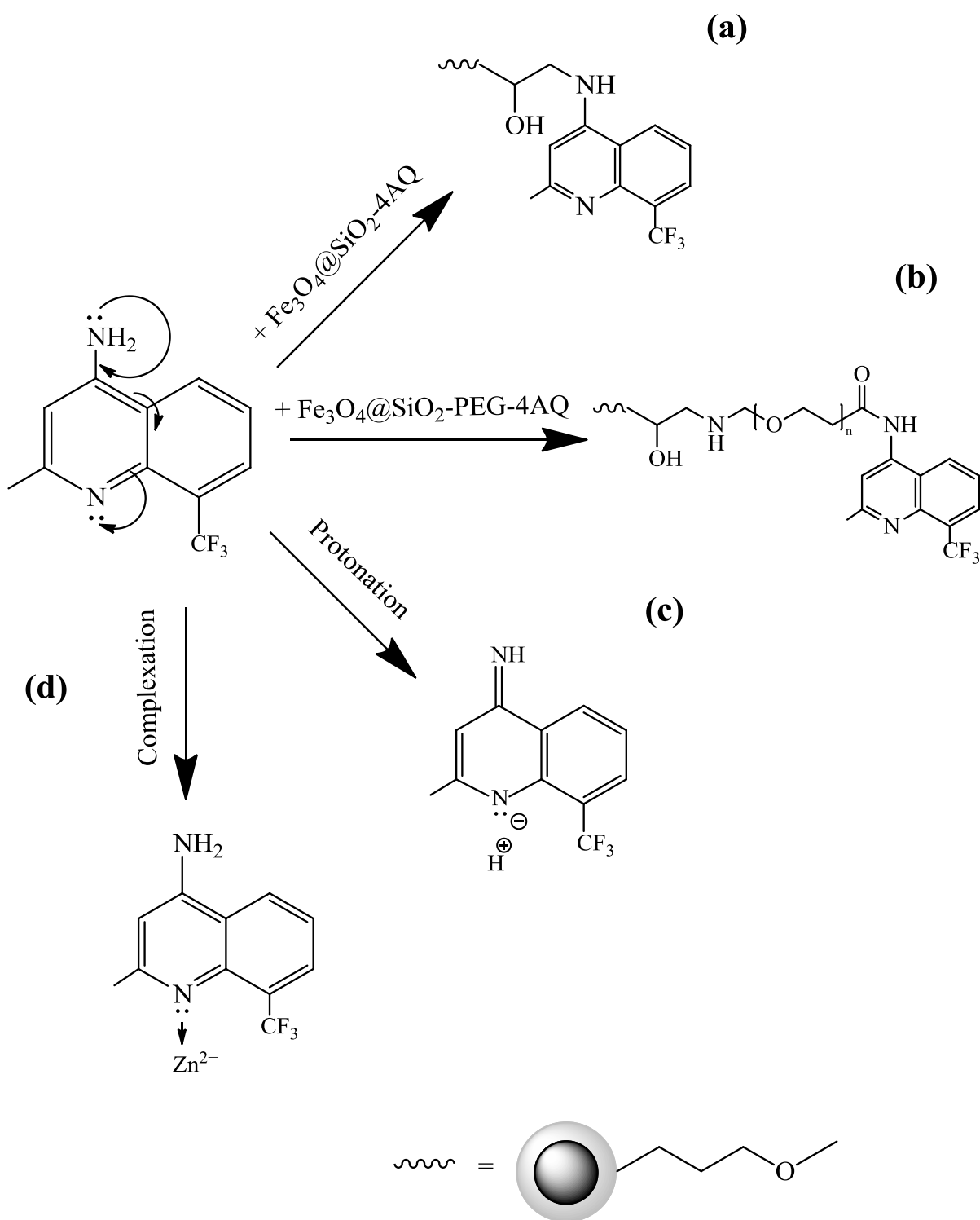
Scheme 3-3. Schematic illustration of ICT occurrence upon protonation, and further enhanced by the complexation of $Fe_3O_4@SiO_2$-4AQ with Zn^{2+}

The pH dependence of the sensing ability of $Fe_3O_4@SiO_2$-PEG-4AQ was investigated and the results are shown in Figure 3-6(a). The fluorescent intensity of $Fe_3O_4@SiO_2$-PEG-4AQ and its complex with Zn^{2+} increased with the reduced pH value (concentration of H^+). For $Fe_3O_4@SiO_2$-PEG-4AQ alone, the increase in the fluorescent intensity is demonstrated at pH below 6, when protonation of heterocyclic nitrogen could have occurred, resulting in tuned ICT. For the sensor-Zn complex, the high sensitivity remained at a greater range of pH (4.0 − 8.0). A significant decrease in intensity was observed when pH was between 7.4 and 12. This could be a result of the deprotonation of exocyclic amine and the changing stability of Zn^{2+}. It was reported that the pKa value of 4-AQ is 7.5 ± 0.02 (Kaschula, Egan et al. 2002), indicating that the 'AQ' moiety may deprotonate when pH approaches 7.5. It is known that zinc ions form $[Zn(OH)_n]^{2-n}$ (n=0-4) at various pH conditions. Below pH = 6.0, Zn^{2+} is dominant. By increasing pH value, the fraction of Zn^{2+} decreases rapidly. A study by Reichle et al (Reichle, McCurdy et al. 1975) indicated that the fraction of Zn^{2+} reduced to approximately 70%, 50% and 0% at pH = 7.5, 8, and 9.5 respectively. This coincides with the range of pH values at which the decreased fluorescent intensity was observed.

The absorption spectra of the nano-chemosensors upon the addition of Zn^{2+} as well as in different pHs were obtained for $Fe_3O_4@SiO_2$-PEG-4AQ to support the photophysical behaviour of 4AQ nanosensors in the presence of Zn^{2+}. As can be seen from Figure 3-6(b), in comparison with the $Fe_3O_4@SiO_2$-PEG-4AQ, the n-π* absorption band has red-shifted from 330 to 370 nm (40 nm) after the addition of the Zn^{2+}, which indicates binding between the nanosensor and Zn^{2+} (Lee, Lee et al. 2011, Kim, You et al. 2015). The protonation of heterocyclic amine at pH = 4 resulted a similar shift of the n-π* absorption band. Aromatic compounds like 4AQ having n-electrons on atoms participating in the aromatic system will show n-π* absorption band at lower frequencies than the π-π* band. This can explain the red

shift of the absorption maximum that observed in the absorption spectra of 4AQ interacted

with Zn^{2+} (Nord, Karlsen et al. 1994, Lee, Lee et al. 2011).
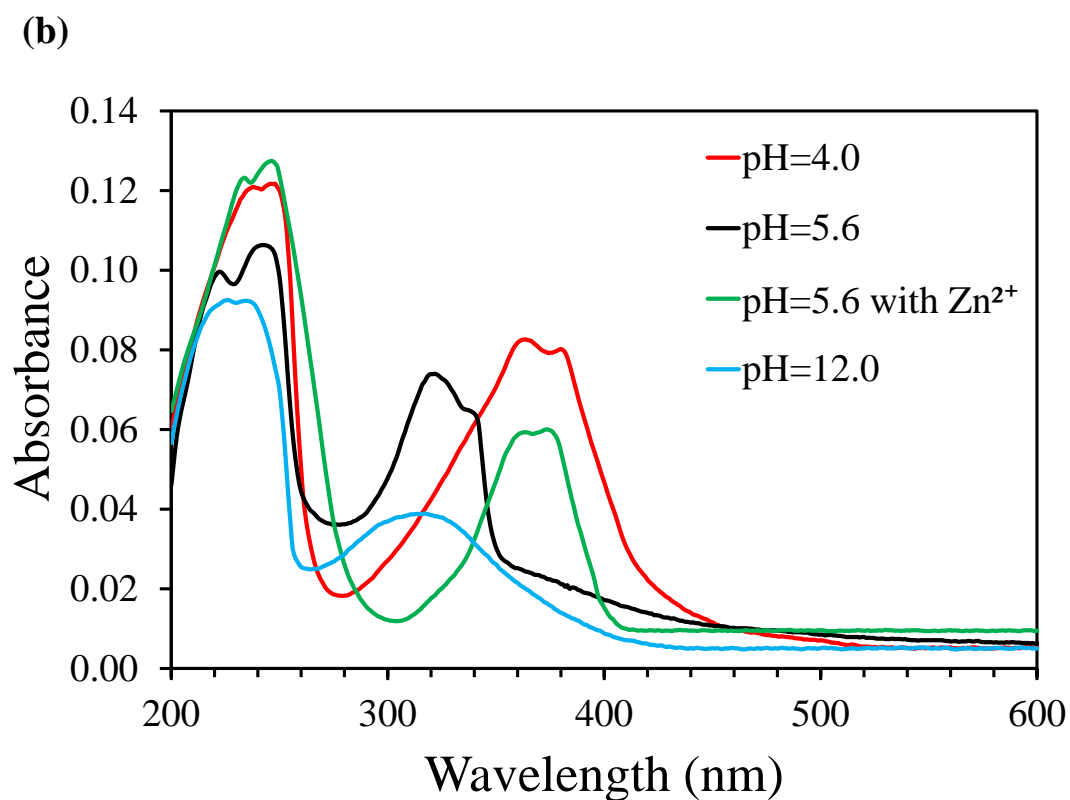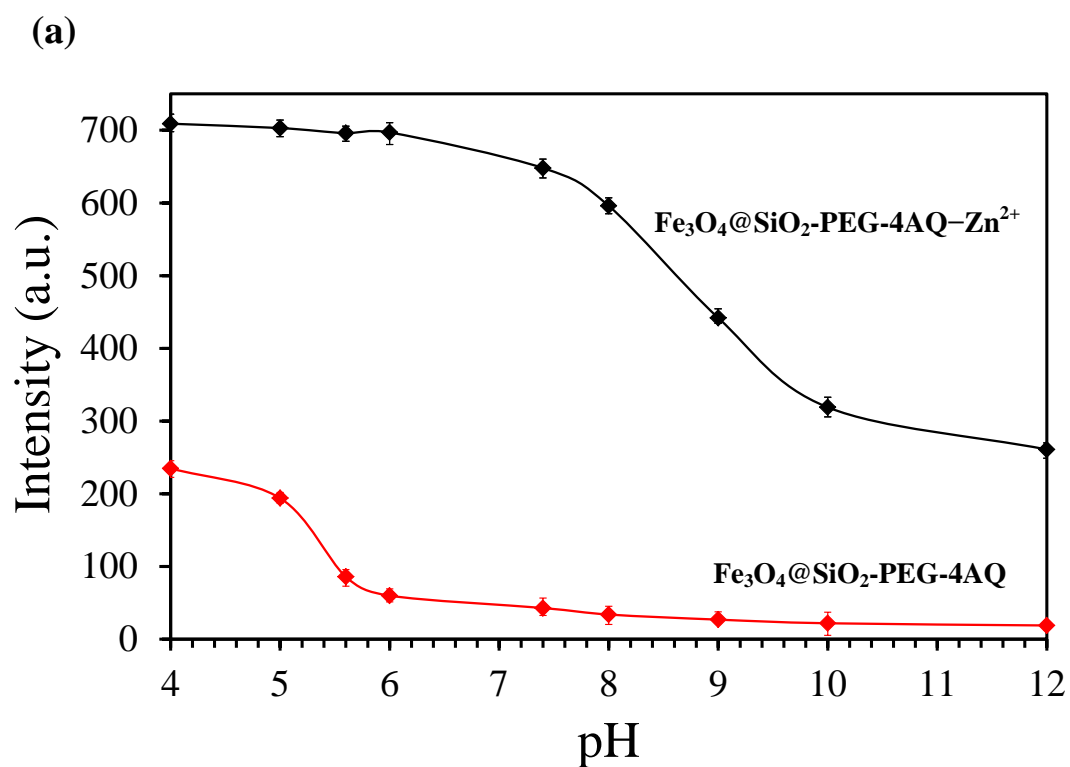
Figure 3-6: (a) Fluorescent intensity of $Fe_3O_4@SiO_2$-PEG-4AQ at different pH values from 4 to 12 (b) Absorption spectra of $Fe_3O_4@SiO_2$-PEG-4AQ, upon the addition of 3 μM of Zn^{2+} in D.I water (pH = 5.6) and in pH = 4 and 12

To further investigate the chemosensing properties of nanosensors, fluorescent titration was conducted in the presence of various concentration of Zn^{2+} solution. An increase in the fluorescent intensity can be seen from Figures 3-7(a) and (b) by varying Zn^{2+} concentration from 0 to 10 μM in $Fe_3O_4@SiO_2$-PEG-4AQ and $Fe_3O_4@SiO_2$-4AQ nanosensors, respectively. A rapid increase is noticeable in fluorescent intensity by increasing the Zn^{2+} concentration from 0 to 4 μM (Figures 3-7(a) and (b)) and a slow increase followed until saturation at 10 μM. The gradual shift in wavelength is attributed to the push‑pull effect in ICT mechanism as was also seen in figures 3-5(a) and (b). The detection limit was calculated to be 3.13 for $Fe_3O_4@SiO_2$-PEG-4AQ and 6.25 nM for $Fe_3O_4@SiO_2$-4AQ nanosensor. The complex formation was of a 1:2 molar ratio between Zn^{2+} and fluorophore, as indicated in job's plot analysis (Figure 3-7(c)).
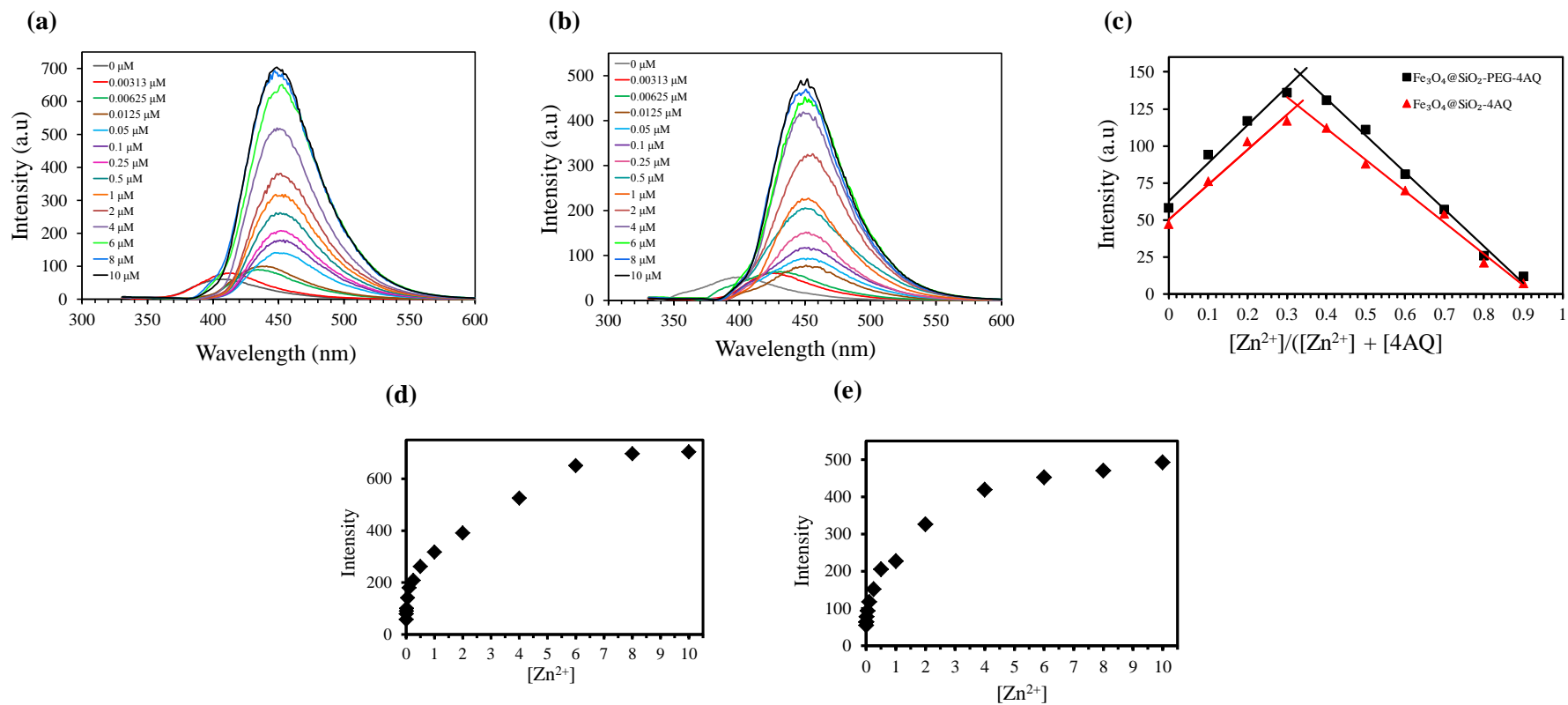
Figure 3-7: Fluorescent titration curves of (a) $Fe_3O_4@SiO_2$-PEG-4AQ, (b) $Fe_3O_4@SiO_2$-4AQ (1 μM) in the presence of Zn^{2+} from 0 to 10 μM, (c) The Job's plot of $Fe_3O_4@SiO_2$-4AQ and $Fe_3O_4@SiO_2$-PEG-4AQ, (d) and (e) calibration curves of $Fe_3O_4@SiO_2$-PEG-4AQ, (b) $Fe_3O_4@SiO_2$-4AQ

Competition experiments were conducted in the presence of Zn^{2+} and other metal ions in the aqueous solution. Figure 3-8(a) and (b) exhibit the fluorescent intensity of Fe_3O_4@SiO_2-PEG-4AQ and Fe_3O_4@SiO_2-4AQ nanosensors, respectively upon binding to Zn^{2+} which did not significantly change in the presence of other metal ions. An exception is the transition metal Cu^{2+} and Fe^{3+} which quenched the fluorescent emission to some extent.

To examine the reversibility of Fe_3O_4@SiO_2-PEG-4AQ toward Zn^{2+} in aqueous solution, EDTA was added to Zn^{2+}-complexed nanosensor. As shown in Figure 3-9, the fluorescence signal upon the addition of Zn^{2+} was reversible with the addition of EDTA. The reversibility has remained the same after five treatment cycles. Each cycle was performed in triplicated for comparison. High reversibility and regeneration is important for sensing Zn^{2+} in practical applications.

(a)
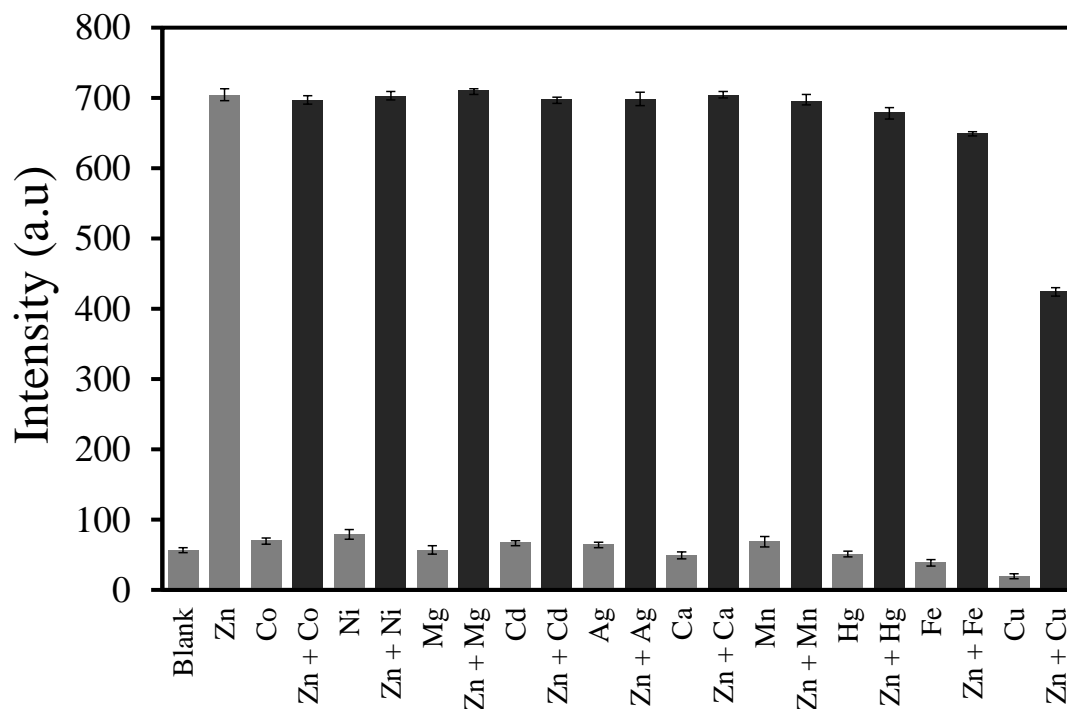
(b)
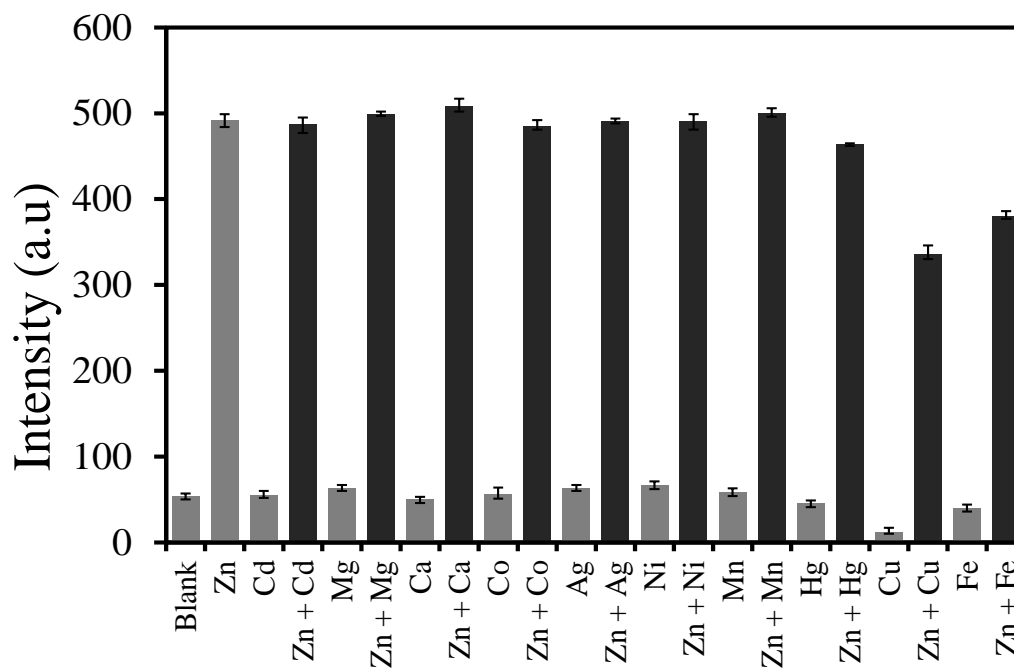
Figure 3-8: Fluorescent emission changes of (a) $Fe_3O_4@SiO_2$-PEG-AQ and (b) $Fe_3O_4@SiO_2$-

AQ at 1 μM aqueous upon the addition of various metal cations with Zn^{2+} (3.0 μM)
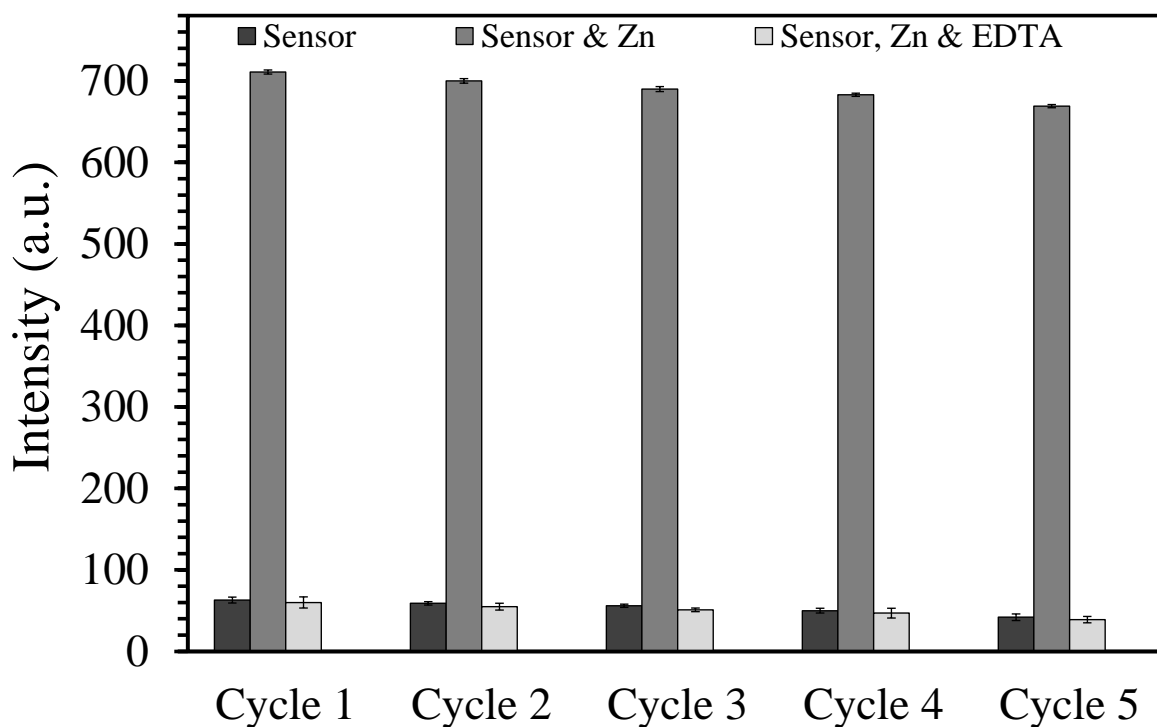
Fig. 3-9: Fluorescent spectra of $Fe_3O_4@SiO_2$-PEG-4AQ in aqueous solution, with Zn^{2+} and after treatment with EDTA (EDTA: Zn^{2+} 1:1 molar ratio) in 5 cycles and triplicated

3.4. Conclusion

Novel magnetic nano-chemosensor $Fe_3O_4@SiO_2$-PEG-4AQ were successfully fabricated for sensitive and selective detection of Zn^{2+} in aqueous solutions. A 4-isomer of aminoquinoline (4-AQ) was used in this study as the fluorophore which is more a cyclic amidine rather than an aminoquinoline. The pH dependence and protonation of the chemosensor were investigated among with its selectivity and sensitivity towards Zn^{2+}. The results of fluorescence experiments demonstrated a 13.5-fold enhancement upon the addition of Zn^{2+} along with a 42 nm red shift. Photophysical properties of the nano-chemosensor were compared with the similar structure $Fe_3O_4@SiO_2$-4AQ and exhibited improved luminescence properties in respect to selectivity and sensitivity of the chemosensor towards Zn^{2+} ion. A 2:1 stoichiometric ratio was obtained for the chemosensor toward Zn^{2+}. The detection limit was

obtained as low as possible for $Fe_3O_4@SiO_2$-PEG-4AQ to be 3.13 nM. The selectivity towards Zn^{2+} ion is reflected in Figure 3-5 as well as in competition study, Figure 3-8 and discussed in section 3.3.2 on page 77. The reported results are the average value of three measurements indicating high reproducibility. The chemosensory process is instantaneously following the addition of the sensor and the ions. The sensitivity and binding kinetics is beyond the scope of this development.

The binding of chemosensor with Zn^{2+} was reversible by the addition of EDTA which demonstrates an excellent capability for the practical applications. The main application can be considered in mining industry. Developing selective, sensitive, fast, and cost-effective detection techniques can overcome all the shortcomings came along with current procedures. There are also some other fields that developing nanochemosensors are very useful such as cell imaging, protein detection and labelling.

3.5. References

Banthia, S. and A. Samanta (2006). "A new strategy for ratiometric fluorescence detection of transition metal ions." The Journal of Physical Chemistry B **110**(13): 6437-6440.

de Souza Santos, M., M. P. F. de Morais Del, et al. (2014). "Binding of chloroquine to ionic micelles: Effect of pH and micellar surface charge." Journal of Luminescence **147**: 49-58.

Dong, Z., Y. Guo, et al. (2013). "Quinoline group based fluorescent sensor for detecting zinc ions in aqueous media and its logic gate behaviour." Journal of Luminescence **134**: 635-639.

Feng, J., J. Mao, et al. (2011). "Ultrasonic-assisted in situ synthesis and characterization of superparamagnetic Fe_3O_4 nanoparticles." Journal of Alloys and Compounds **509**(37): 9093-9097.

Gunnlaugsson, T., D. A. Mac Dónaill, et al. (2001). "Lanthanide macrocyclic quinolyl conjugates as luminescent molecular-level devices." Journal of the American Chemical Society **123**(51): 12866-12876.

Han, W. S., H. Y. Lee, et al. (2009). "Silica-based chromogenic and fluorogenic hybrid chemosensor materials." Chemical Society Reviews **38**(7): 1904-1915.

J.-F. Zhu, H. Yuan, W.-H. Chan, A.W. Lee, A FRET fluorescent chemosensor SPAQ for Zn^{2+} based on a dyad bearing spiropyran and 8-aminoquinoline unit, Tetrahedron Lett 51 (2010) 3550-3554.

Kaschula, C. H., T. J. Egan, et al. (2002). "Structure− activity relationships in 4-aminoquinoline antiplasmodials. The role of the group at the 7-position." Journal of medicinal chemistry **45**(16): 3531-3539.

Kaur, P., H. Kaur, et al. (2013). "A quinoline-based turn-off fluorescent cation sensor." RSC Advances **3**(1): 64-67.

Kim, H., G. R. You, et al. (2015). "Selective zinc sensor based on pyrazoles and quinoline used to image cells." Dyes and Pigments **113**: 723-729.

Kovi, P. J., A. C. Capomacchia, et al. (1972). "Electronic spectra of 2-aminoquinoline and 4-aminoquinaldine. Evidence for the cyclic amidine structures of the singly protonated cations." Analytical Chemistry **44**(9): 1611-1615.

Lee, H. G., J. H. Lee, et al. (2011). "Zinc selective chemosensor based on pyridyl-amide fluorescence." Tetrahedron **67**(42): 8073-8078.

Lu. D, L. Yang, Z. Tian, L. Wang, J. Zhang, Core-shell mesoporous silica nanospheres used as Zn 2+ ratiometric fluorescent sensor and adsorbent, RSC Adv 2 (2012) 2783-2789.

Ma, Y., F. Wang, et al. (2013). "A quinoline-based fluorescent chemosensor for distinguishing cadmium from zinc ions using cysteine as an auxiliary reagent." Sensors and Actuators B: Chemical **188**: 1116-1122.

M. Li, H.Y. Lu, R.L. Liu, J.D. Chen and C.F. Chen, Turn-on fluorescent sensor for selective detection of Zn^{2+}, Cd^{2+}, and Hg^{2+} in water, J Org Chem 77 (2012) 3670-3673.

Mmonwa, M. M., M. J. Mphahlele, et al. (2014). "Synthesis and Photophysical Properties of the 2-(3-(2-Alkyl-6, 8-diaryl-4-oxo-1, 2, 3, 4-tetrahydroquinazolin-2-yl) propyl)-6, 8-diarylquinazolin-4 (3H)-ones." Molecules **19**(7): 9712-9735.

Nolan, E. M., J. Jaworski, et al. (2005). "QZ1 and QZ2: rapid, reversible quinoline-derivatized fluoresceins for sensing biological Zn (II)." Journal of the American Chemical Society **127**(48): 16812-16823.

Nord, K., J. Karlsen, et al. (1994). "Photochemical stability of biologically active compounds." Photochemistry and photobiology **60**(5): 427-431.

Otelo, V. A., A. C. Sant'Ana, et al. (2011). "Molecular modeling and UV–vis spectroscopic studies on the mechanism of action of reversed chloroquine (RCQ)." Bioorganic & medicinal chemistry letters **21**(1): 250-254.

Pourfallah, G. and X. Lou (2016). "A novel recyclable magnetic nanostructure for highly sensitive, selective and reversible detection of zinc ions in aqueous solutions." Sensors and Actuators B: Chemical **233**: 379-387.

Reichle, R. A., K. G. McCurdy, et al. (1975). "Zinc hydroxide: solubility product and hydroxy-complex stability constants from 12.5–75 C." Canadian Journal of Chemistry **53**(24): 3841-3845.

Sarkar, M., S. Banthia, et al. (2006). "pH-Regulated "Off–On" fluorescence signalling of d-block metal ions in aqueous media and realization of molecular IMP logic function." New Journal of Chemistry **30**(11): 1557-1560.

S.K. Rastogi, P. Pal, D.E. Aston, T.E. Bitterwolf, A.L. Branen, 8-Aminoquinoline functionalized silica nanoparticles: a fluorescent nanosensor for detection of divalent zinc in aqueous and in yeast cell suspension, ACS Appl Mater Interfaces 3 (2011) 1731-1739

Singh, H., J. Sindhu, et al. (2015). "Synthesis of novel fluorescence xanthene–aminoquinoline conjugates, determination of dipole moment and selective fluorescence chemosensor for Th^{4+} ions." Optical Materials **42**: 449-457.

Tian, L., X. Lou, et al. (2013). "Synthesis, characterisation and catalase-like activity of silica-coated magnetite nanoparticles modified by a Schiff base Mn complex." Micro & Nano Letters **8**(3): 159-162.

Wang, L., J. Jin, et al. (2016). "Synthesis of C-glycosyl triazolyl quinoline-based fluorescent sensors for the detection of mercury ions." <u>Carbohydrate research</u> **433**: 41-46.

X. Feng, H. Guo, K. Patel, H. Zhou, X. Lou, High performance, recoverable Fe_3O_4 ZnO nanoparticles for enhanced photocatalytic degradation of phenol, Chem Eng J 244 (2014) 327-334.

X. Feng, S. Zhang, X. Lou, Controlling silica coating thickness on TiO_2 nanoparticles for effective photodynamic therapy, Colloids Surf B 107 (2013) 220-226.

Y. W. Choi, G. R. You, J. J. Lee and C. Kim, Turn-on fluorescent chemosensor for selective detection of Zn^{2+} in an aqueous solution: Experimental and theoretical studies, Inorg Chem Commun 63 (2016) 35-38.

Chapter 4

Synthesis, Characterization and Crystallography of PEG Conjugated Dansyl Fluorophore

4.1. Introduction

This chapter focuses on the effect of applying PEG spacer on luminescence properties of the produced chemosensors. It is been revealed in Chapter 2 that the presence of PEG spacer in the nanosensor has resulted in enhanced fluorescent intensity and improved the sensitivity and selectivity of the sensor towards Zn^{2+} ion. It was hypothesised that O-dansyl ligands of $Fe_3O_4@SiO_2$-PEG-DnS have provided increased electron withdrawal capacity of the sulfonate group by having the more electronegative oxygen atom, therefore resulting in an enhancement of the push-pull effect and consequently, an increase in fluorescent intensity. The coordination of the obtained chemosensors towards Zn^{2+} through the exocycle nitrogen was also hypothesized and rationalised. The significant quenching effect of 12.5 folds was seen to be a result of the reduced electron donating nature of the sulfonate group to the naphthalene ring in $Fe_3O_4@SiO_2$-PEG-DnS.

Dansyl chloride is a fluorescent probe that has been widely used in biochemical researches including protein structural studies since the earlier works of Gregorio Weber (Weber and Farris 1979). Dansyl probe is also well-known for sensing metal ions. This widely usage is due to its early introduction as a fluorophore and its favourable lifetime (~ 10 ns) (Higuchi, Narita et al. 2000, Zheng, Cao et al. 2003). Dansyl groups absorb near 320-350 nm and the emission maxima are typically near 500-520 nm. This fluorophore is able to produce a

significant fluorescence which arises by transferring charges between the amine group of the dansyl and the naphthalene ring (Lakowicz and Masters 2008).

Primitive researches on metal sensing application of dansyl fluorophore was by the employment of calixarene-based ligands such as calix[4]arenes, calix[4]-crowns and thiacalix[4]arenes (Bügler, Engbersen et al. 1998). Basically, the level of metal sensing of dansyl containing fluorophores varies by the type of attachment to the receptor moiety which can be either HN-dansyl, obtaining amino-naphthalensulfonamide or O-dansyl ligands, obtaining amino-naphthalensulfonate derivatives. Nonetheless, fluorescence characteristics of both types of dansyl-containing fluorophores are sensitive to the environment (Montalti, Prodi et al. 2005). Particularly, the emission spectra and intensity can be changed with the polarity and hydrophobicity of the solvent and has considerable charge-transfer character (Lee, Kim et al. 2008). The charge transfer is caused by mixing of the ^1L_a and ^1L_b states of naphthalene with a charge-transfer state arising from the promotion of a lone pair electron on the amino group into a π antibonding orbital of the naphthalene ring (Liu, Wu et al. 2011).

HN-dansyl and O-dansyl groups also have some uniqueness properties in metal coordinations as well. HN-dansyl moiety often called a softer electron donor because the charge delocalisation is negative upon the HN-proton dissociation. However, O-dansyl behaves as a harder electron donor and show higher propensity for coordination in transition metals including Cu^{2+} and Zn^{2+} (Talanova and Talanov 2010).

Schuster et al. (Schuster and Šandor 1996) synthesised N-dansyl-N'-ethylthiourea (DET) fluorophore. Complexation of Ni(II) and Cu(II) produced a fluorescence quenching of about 60%. The quenching mechanism was due to the basic nitrogen atom in the dimethylamino group. The protonation of the dimethylamino group causes a strong quenching of the fluorescence. In general, protonation and deprotonation of the ligand should therefore influence the fluorescence properties. The emission maximum is observed at 520 nm,

whereas the excitation maximum can be detected at 325 nm. Koike et al. (Koike, Watanabe et al. 1996) developed a dansyl-containing chemosensor employing cyclen units. Their designed chemosensor was based on the strong affinity towards aromatic sulphonamides of the Zn–cyclen complex, and the good luminescence properties of the dansyl chromophore. The complexation was occurred by the chelating of amine groups of cyclen units with an increase in emission intensity. They also investigated the pH dependence of dansyl units upon protonation. The result showed a complete quenching after protonation (pH=3.6). Prodi et al. (Prodi, Bolletta et al. 1999) also used the dansyl chloride as a well-known chromophore which gives an intense fluorescence arising from a charge transfer state from the amine group of the dansyl to the naphthalene ring. They observed a blue shift and an enhancement in fluorescence by the addition of Cu^{2+}, Co^{2+} and Zn^{2+}. They described the complexation mode through deprotonation of sulphonamide moieties. An increase in the electronic density on the naphthalene ring was the main reason of the blue shift which leads to the charge transfer between the amine to naphthalene group.

This chapter investigates up on the crystal structure of the PEGylated dansyl fluorophore and its interaction with Zn^{2+} ion to evidence the influence of PEG conjugation on luminescence properties as well as the complexation mode of dansyl moieties with Zn^{2+} ion. Methoxy polyethylene glycol (mPEG-160), an analogue to PEG with smaller molecular weight was introduced to the dansyl fluorophore, through the chemical synthesis pathway displayed in Scheme 4-1. The produced compound represents the PEG-DnS moiety of the $Fe_3O_4@SiO_2$-PEG-DnS. The chemical and crystal structure of the compound was confirmed by FTIR, ^{1}H NMR, UV-Vis spectroscopy and XRD analysis. Complexation with zinc ions was carried out by adding Zn^{2+} solution (almost 3 equivalents) to the PEG-DnS solution followed by growing single crystals at room temperature. Crystallographic structure of the PEG-DnS-Zn^{2+} complex

was examined using XRD. The fluorescent studies indicated that PEG-DnS is sensitive to Zn^{2+} by quenching the fluorescent intensity.

4.2. Material and Method

4.2.1. Material

Dansyl chlorides (DnCl), Triethylamine (99.5%), ethanol (99.5%), diethyl ether (99%) were purchased from Sigma Aldrich Australia. Methoxy polyethylene glycol (mPEG-160) (90%, M_w=160) was obtained from Nanocs (USA).

4.2.2. Synthesis of pegylated dansyl fluorophore (PEG-DnS)

mPEG (50 mg, 0.3125 mmol) and DnCl (84.3 mg, 0.3125 mmol) were mixed in 20 ml dry acetone (The dry acetone was prepared through distillation of acetone after drying with calcium chloride overnight). Triethylamine (0.5 ml, 3.58 mmol) was then added to the reaction mixture. The reaction took place in a 50 ml round bottom flask at room temperature in dark for 24 hrs. The solvent was evaporated to yield a yellow-orange oily product. The product was repeatedly washed with diethyl ether and acetone (4 × 10 ml) to remove by-products and then was filtered. The clear filtrate was kept at room temperature and colourless crystals were grown by slow evaporation. Pure crystals were yielded by recrystallization of crystal samples in ethanol (10 ml) followed by slow evaporation at room temperature and were finally kept under vacuum. The synthesis procedure is demonstrated in Scheme 4-1.

Scheme 4-1. Synthetic pathway of PEGlated dansyl fluorophore

The complex crystal of PEG-DnS-Zn^{2+} was also prepared by dissolving 5 mg of PEG-DnS in 10 ml ethanol (1.2 μM) and mixing with 3 μM Zn^{2+} solutions in ethanol. The solution was kept at room temperature for the crystal growth by slow evaporation (Scheme 4-2).
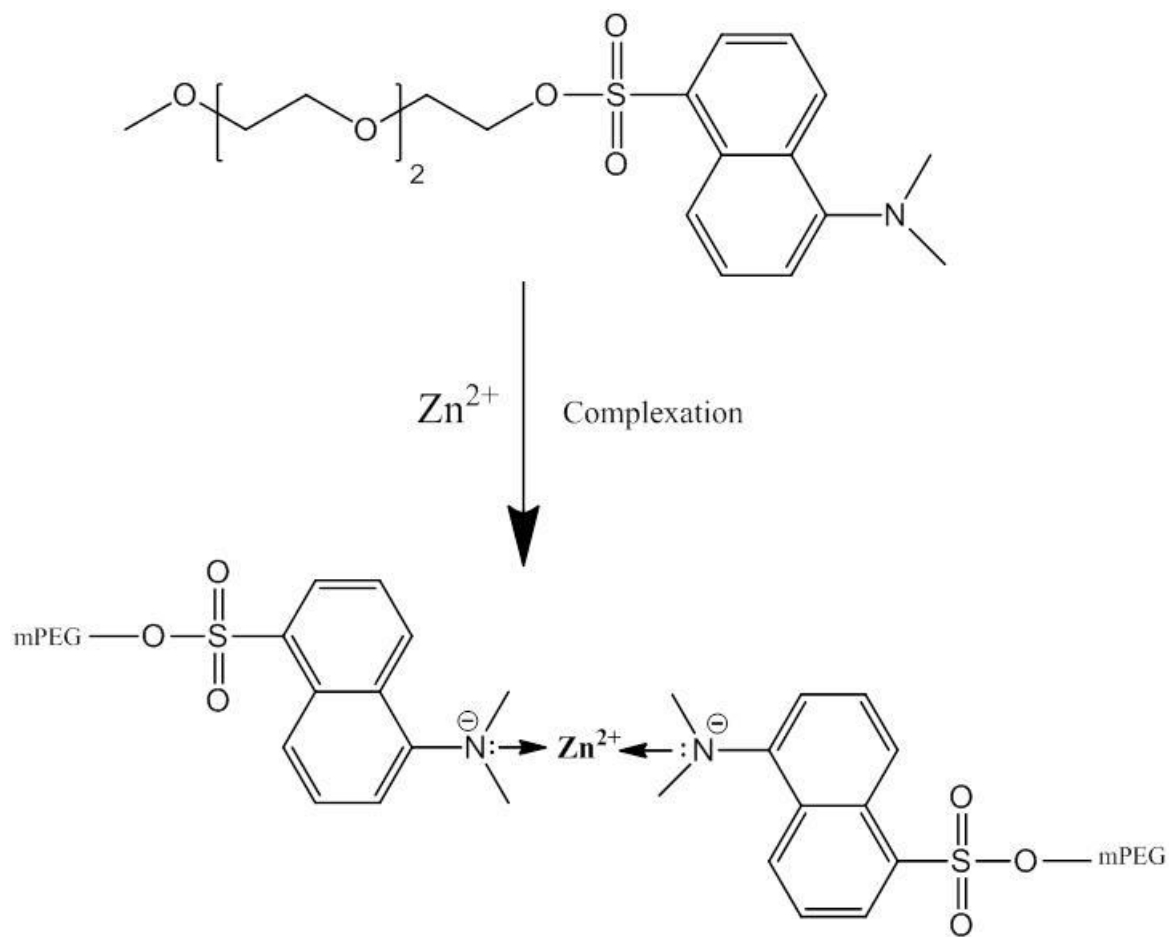
Scheme 4-2. Proposed complexation mode of crystal PEG-DnS with Zn^{2+} ion

4.2.3. Physicochemical Characterisation

The chemical structure of the product was confirmed by ^{1}H NMR, FTIR, UV-VIS and single crystal X-ray Diffraction (XRD).

A Thermo Scientific Nicolet iS50 built-in a diamond ATR sampling accessory was used to obtain the Fourier transform infrared (FTIR) spectra of the synthesised nanostructures. UV absorption spectra were recorded on a Lambda 25 Perkin Elmer UV‑Vis Spectroscopy. Scans were recorded in the wavelength range from 200 to 800 nm with a band width of 1 nm. Nuclear magnetic resonance (^{1}H NMR) was performed on a Bruker Advance III NMR spectrometer (400 MHz), using solvent CDCl$_3$. Sample preparation for ^{1}H NMR was by

dissolving crystal samples (5 mg) in CDCl$_3$ (0.5 ml) and adding the mixture into the dry NMR tube. Crystallographic data for the obtained structure were collected at 100(2) K on a Gemini diffractometer fitted with Mo Kα radiation (λ = 0.71073 Å) and $2\theta_{max} = 65.2°$.

4.2.4. Photophysical measurements

The fluorescent emission spectra were obtained from a Perkin Elmer L55 fluorescence spectrometer with an excitation source set at 325 nm and a scanning rate of 5 nm/min.

4.3. Results and Discussions

4.3.1. Characterization of PEG-DnS

The successful synthesis of PEG-Dns sample was confirmed by FTIR spectra in comparison with plain PEG and DnCl samples. As shown in Figure 4-1, the FTIR bands at 3451 cm^{-1} (O−H vibration) is attributed to the PEG sample which is disappeared in both DnCl and PEG-DnS spectra. The conjugation of PEG segments to DnCl fluorophore is resulted in stretching vibrations of S-O at 1397 cm^{-1} and C-N at 1056 cm^{-1} as well as C–H stretching at 2791 and 2944 cm^{-1} can also be seen in the spectra, denoting the attachment of dansyl groups to PEG moieties.
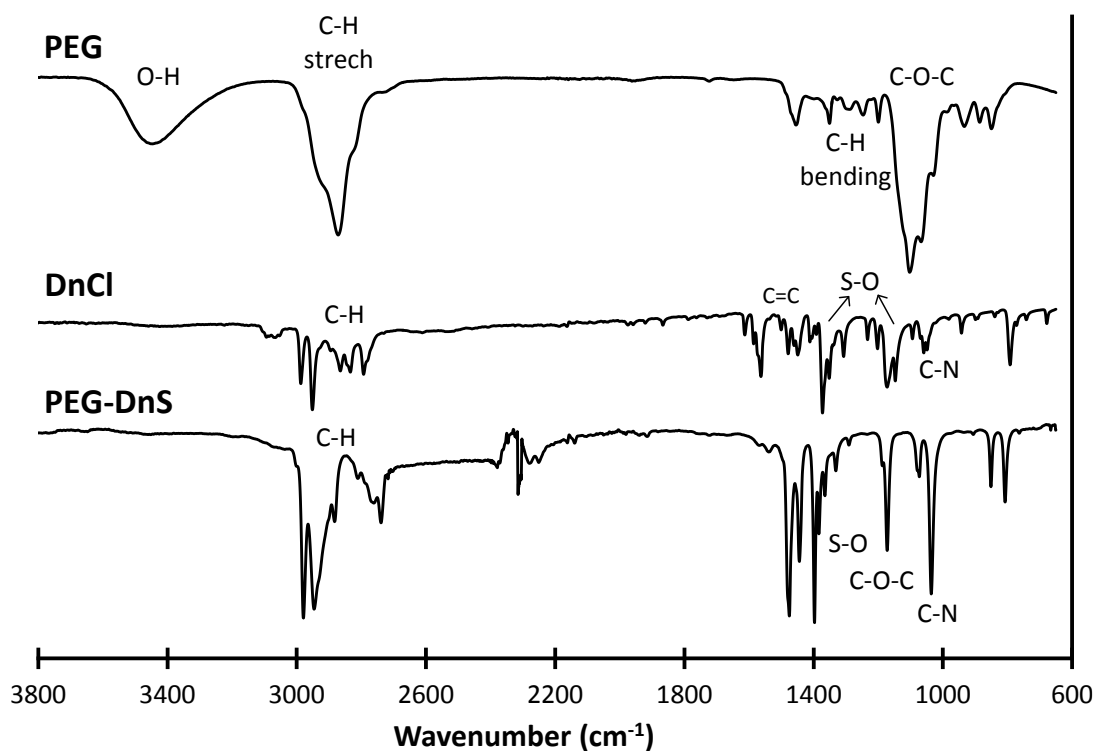
Figure 4-1. FTIR spectra of PEG, DnCl and PEG-DnCl

Figure 4-2 represents the ^{1}H NMR spectrum (400 MHz, CDCl$_3$) of mPEG, DnCl and PEG-DnS, respectively. As can be seen in Figure 4-2, the protons at 3.25 and 3.39 ppm resonates signals of methoxy (CH$_3$-O) and CH$_2$-CH$_2$, respectively. Whereas, the prominent peak of the oxyethylene protons (CH$_2$CH$_2$-O) are centered at 3.46 ppm. Signal displayed at 2.92 ppm in DnCl spectrum corresponds to (CH$_3$)$_2$-N-. The protons of the aromatic dansyl naphthalene group are also resonated at 7.28, 7.61, 7.73, 8.36, 8.46 and 8.74 as shown in Figure 4-2 DnCl spectrum. The ^{1}H NMR spectrum of synthesised PEG-DnS however, is also shown in Figure 4-2. As displayed in the figure, signals at 2.48, 3.45, 3.48 and 3.61 ppm represent the protons of dansyl (CH$_3$)$_2$-N-, PEG CH$_2$-CH$_2$, PEG CH$_3$-O and PEG CH$_2$CH$_2$-O, respectively. Signals also shown at 7.23, 7.26, 7.40, 8.35, 8.44 and 8.78 are attributed to the dansyl naphthalene structure.

PEG

Dansyl chloride

98
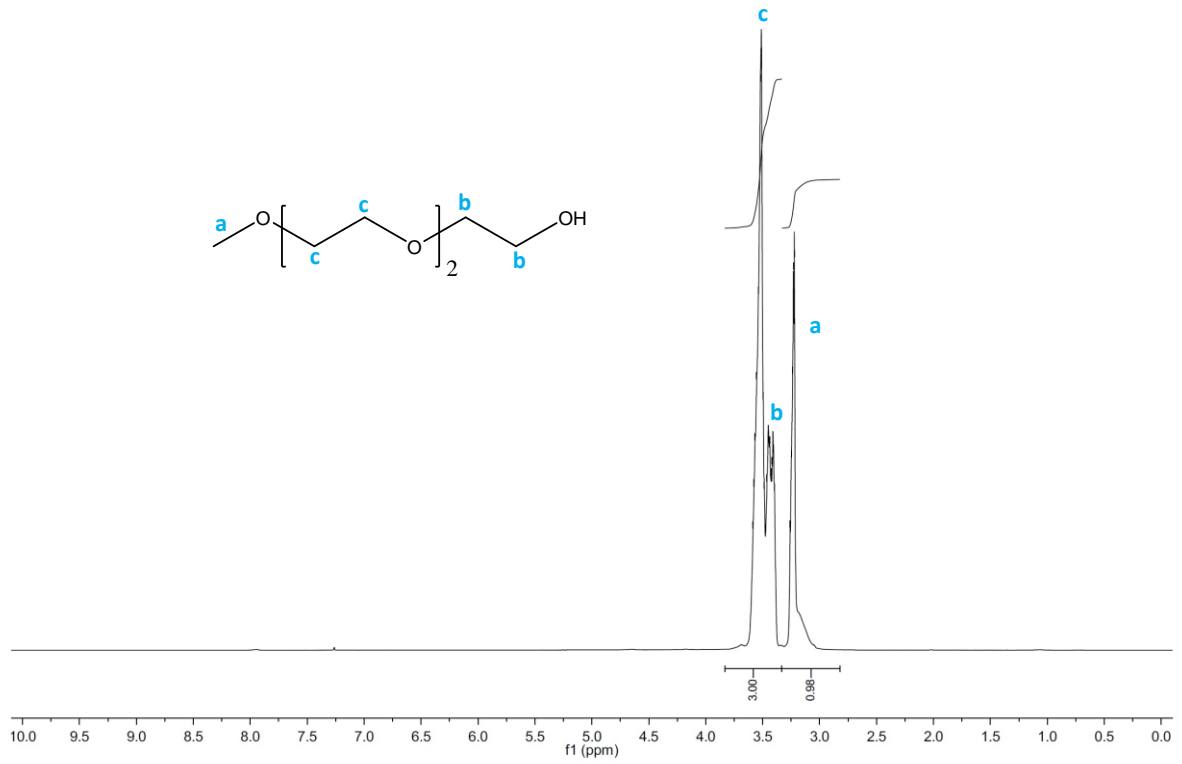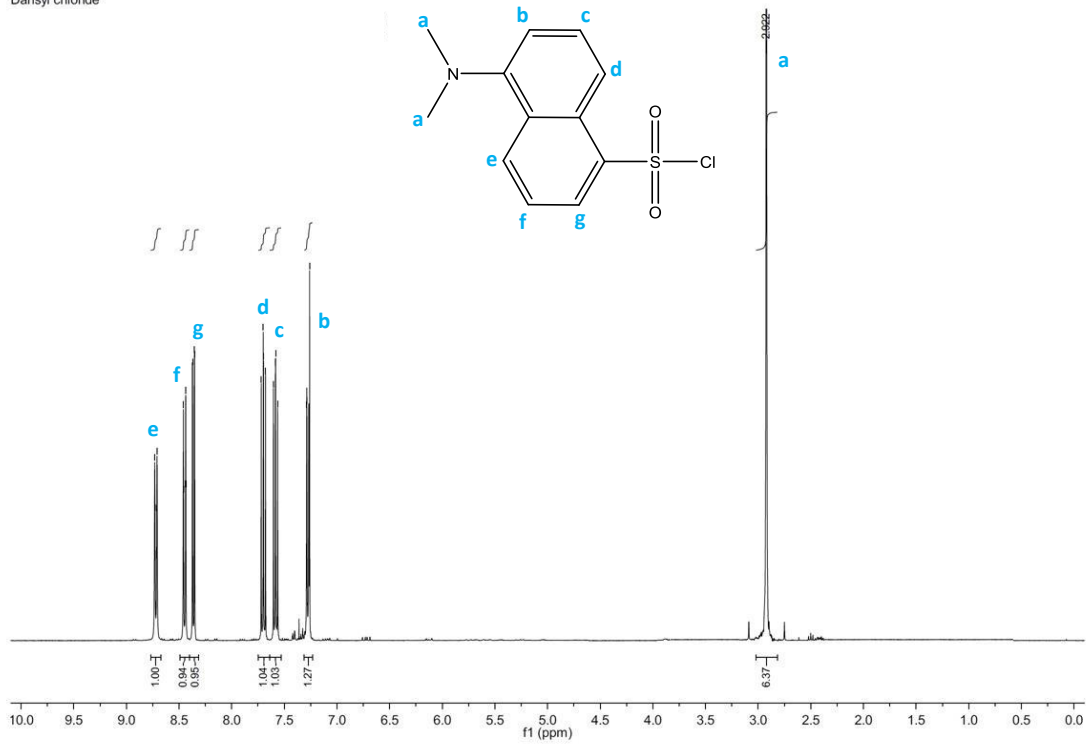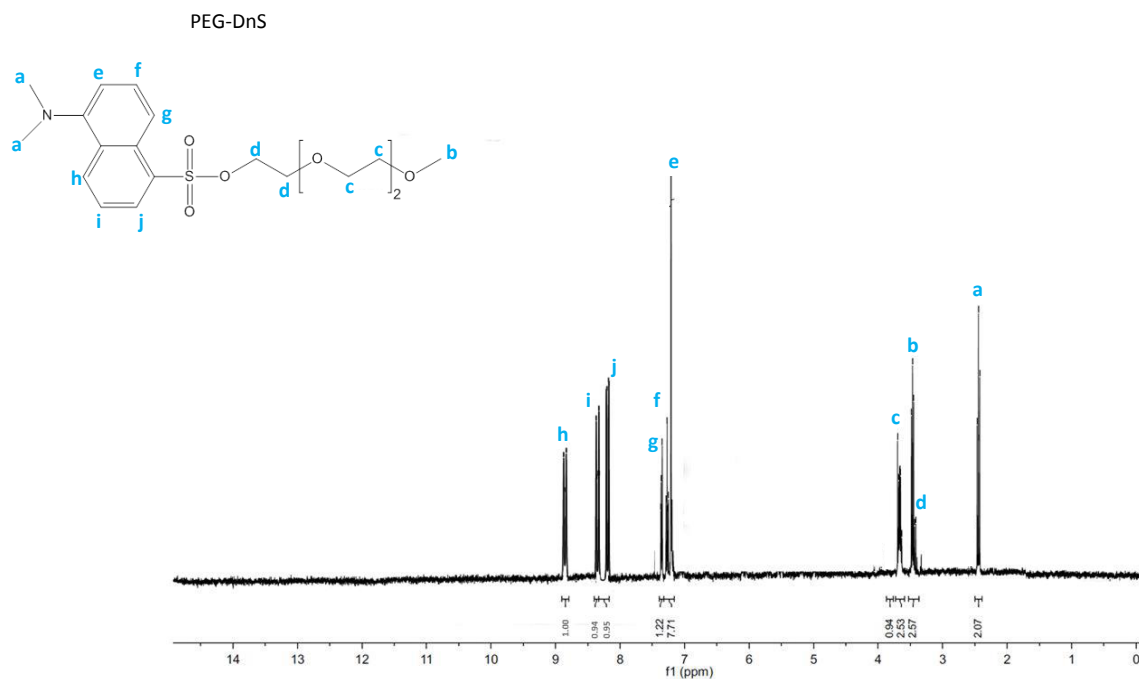
Figure 4-2. NMR spectra of m-PEG, DnCl and PEG-DnS

4.3.2. Photophysical studies

The successful synthesis of PEG-DnS as well as the complexation of Zn^{2+} with PEG-DnS was evident also in the absorption spectra of the chemosensor (Figure 4-3). As shown in the figure, dansyl chloride exhibits absorption bands at $\lambda_{max} = 229$ and 325 nm that correspond to π-π* and n-π* orbital transitions, respectively (Liu, Wu et al. 2011). Both bands appear in PEG-DnS absorption spectra attributing the formation of dansylated PEG. The figure also presents the absorption spectra of PEG-DnS with Zn^{2+}. As shown, the main n-π* absorption band at 325 nm in PEG-DnS is almost diminished due to the complexation of dimethylamine with Zn^{2+} as was also discussed in chapter 2.
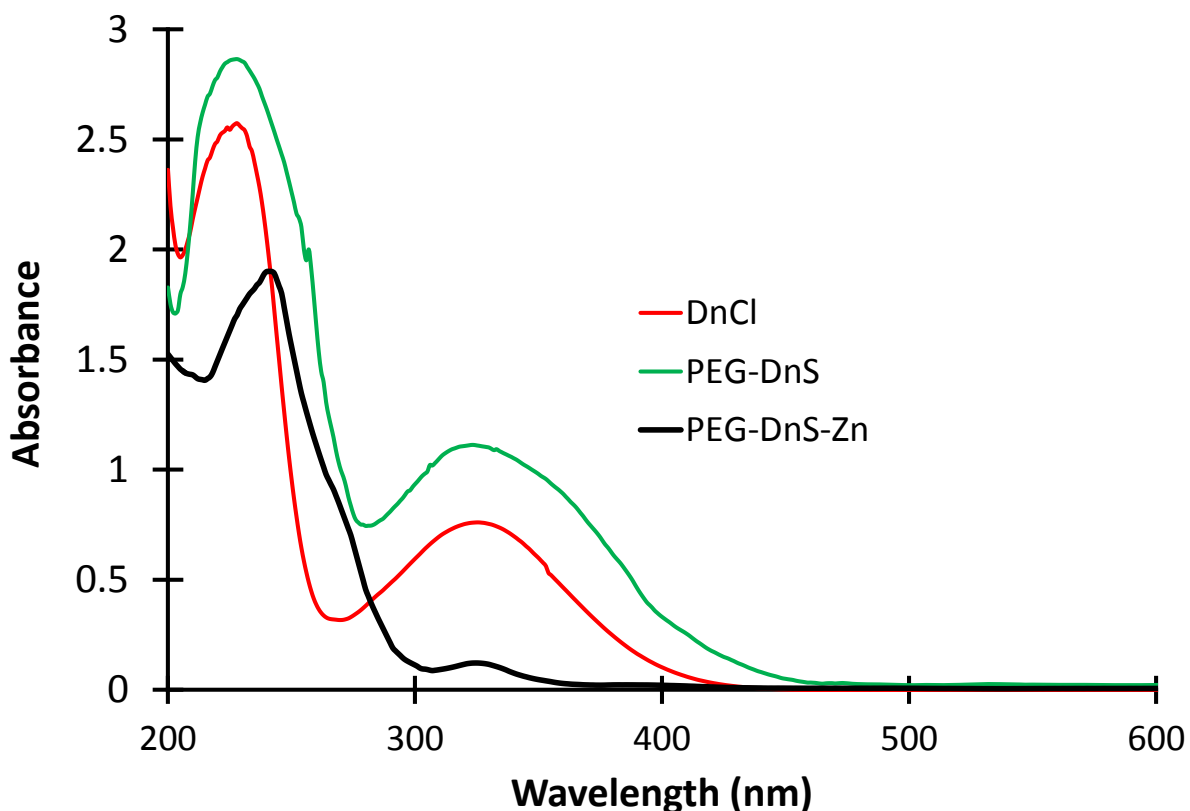
Figure 4-3. Absorption spectra of DnCl, PEG-DnS and PEG-DnS-Zn^{2+} complex. The DnS

concentrations were kept at 1.2 μM for all.

Figure 4-4 illustrates the fluorescent responses of DnCl, PEG-DnS and its complex with Zn^{2+} in aqueous solutions. As can be seen from the figure, an emission at λ_{max} = 502 nm was observed for DnCl, originating from a charge transfer state from the amine group of the dansyl to the naphthalene ring. An enhanced fluorescence was observed for PEG-DNS (λ_{max} = 509 nm) which is likely to be due to intermolecular charge transfer (ICT) from the electron donor dimethylamino group to the electron withdrawal sulfonate group (Prodi, Bolletta et al. 2000, Tharmaraj and Pitchumani 2012). The bonding of PEG with the dansyl group is through the electronegative oxygen atom, thereby increasing the electron withdrawal capacity of the -SO_2- group. This results in enhancement of the push-pull effect and, therefore, increased fluorescence. The increased charge transfer also decreases the energy gap between

the highest occupied molecular orbital (HOMO) and the lowest unoccupied molecular orbital (LUMO), leading to red shifting of the emission wavelength.

Figure 4-4 also contains the emission spectra of PEG-DnS after the addition of Zn^{2+} ion. A quenching (~ 4.9 fold) can be seen from the figure as it was expected from the interaction of Zn^{2+} with the dansyl moiety through complexation with the electron pair-containing nitrogen in the dimethylamine group. This results in a reduction in the electron donating nature of this group to the naphthalene ring. In fact, the large fluorescent intensity before the addition of Zn^{2+} would have been due to the high electron density caused by the injection of electrons from the electron donor dimethylamine group into the π anti-bonding orbital of the naphthalene ring. So, the complexation between dimethylamine and Zn^{2+} resulted in diminishment of electron injection, leading to the observed quenching of fluorescent intensity.

Comparing the level of quenching obtained for PEG-DnS (4.9 fold) in this chapter with that of achieved in chapter 2 for $Fe_3O_4@SiO_2$-PEG-DnS (12.5-fold) emphasises on the significance of the presence of long chain of PEG spacers in improving the photophysical properties. As discussed before, PEG provides more hydrophilicity and consequently more flexibility for the DnS moieties to interact with Zn^{2+} ions and response as a fluorophore.
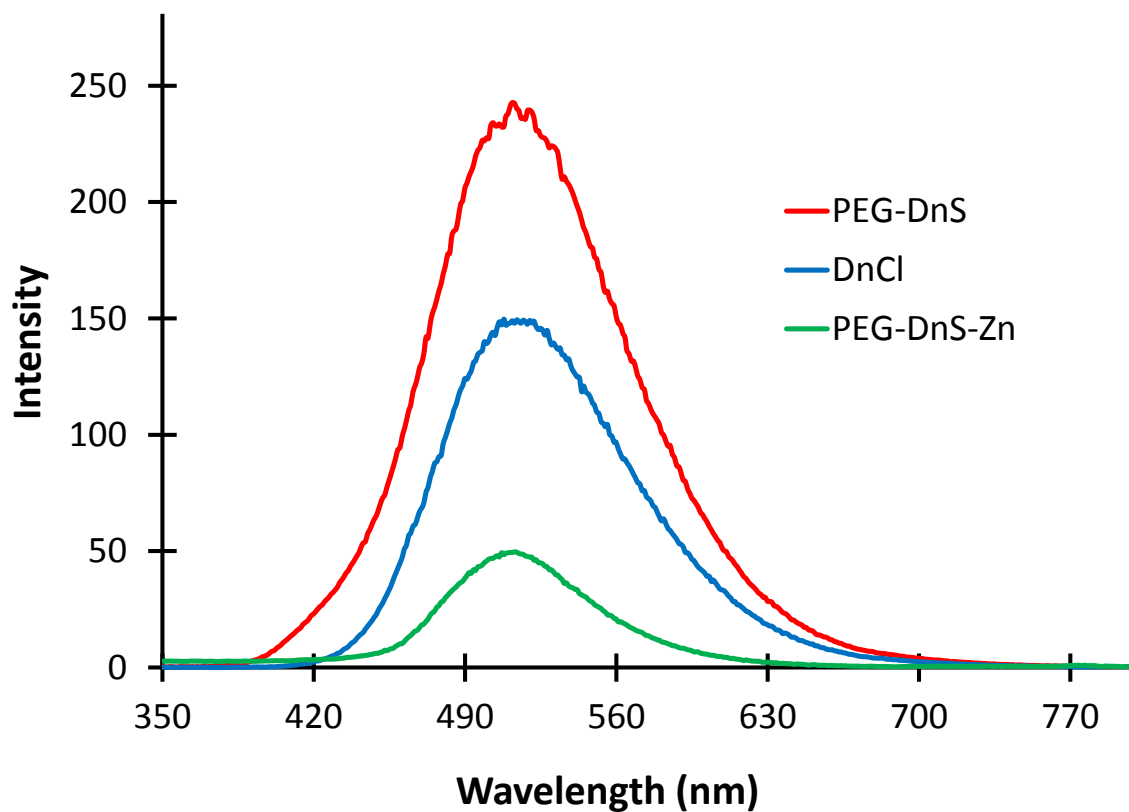
Figure 4-4. Fluorescent emission spectra of DnCl, PEG-DnS and its complexation with Zn^{2+}. The DnS concentrations were kept at 1.2 μM for all.

A Job plot was obtained to demonstrate the stoichiometry of the complexation between PEG-DnS and Zn^{2+} (Figure 4-5). A 2:1 stoichiometry ratio was confirmed between the nanosensor and Zn^{2+} which evident similar achievements from chapter two.
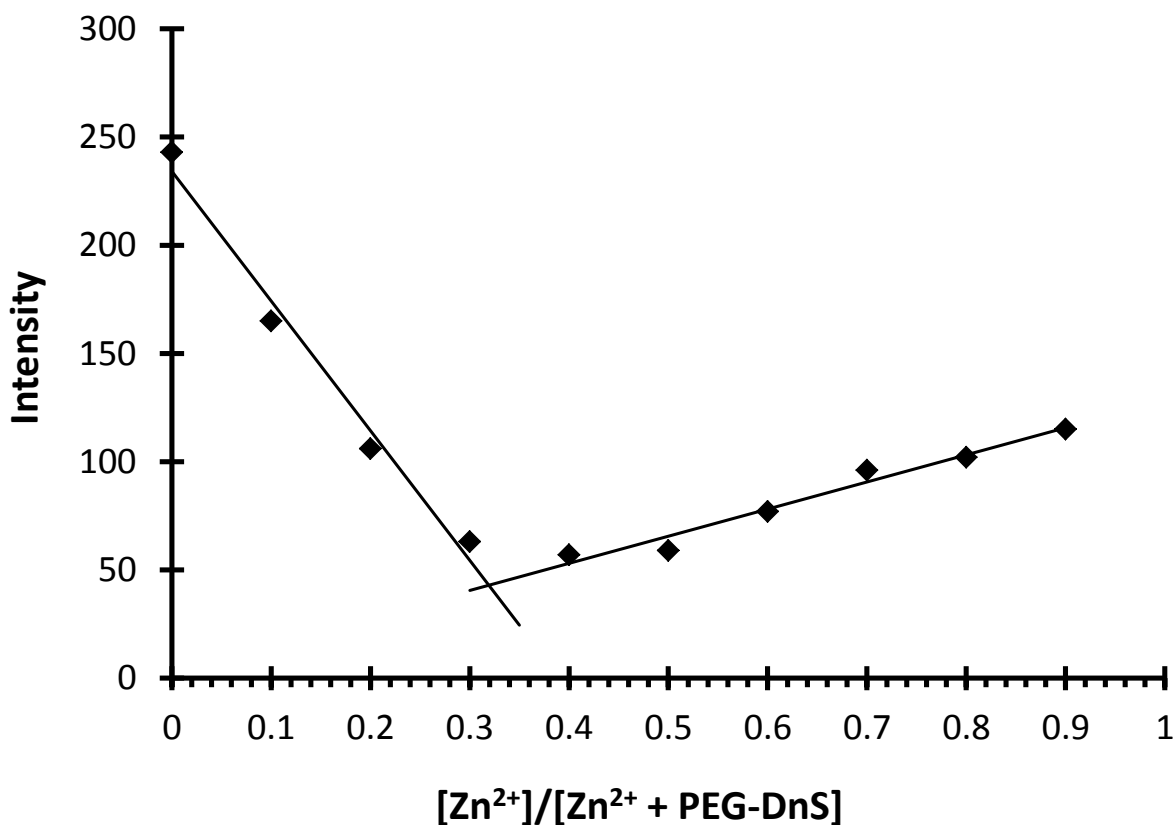
Figure 4-5. The Job plot of PEG-DnS with Zn^{2+}

4.3.3. Crystallography

Crystal structure of PEG-DnS chemosensor before and after complexation with Zn^{2+} is shown in Figure 4-6(a) and (b) which was obtained from X-ray crystallographic analysis. The structural analysis of PEG-DnS was carried out to understand the fluorescent behaviour and complexation mode of the chemosensor with Zn^{2+} as was hypothesised in Chapter Two. As shown in Figure 4-6(a), PEG-DnS adopts conformation similar to other N-aryl sulfonates with two aryl rings almost perpendicular to the chain (Kimber, Geue et al. 2003). The crystal structure PEG-DnS-Zn^{2+} is also displayed in Figure 4-6(b) which demonstrates the coordination of Zn with the N-aryl from two molecules of PEG-DnS as was demonstrated by Job plot. The crystallographic data and structural analysis data for PEG-DnS fluorophore and its complex with Zn^{2+} are tabulated in Table 4-1 and 4-2, respectively.

The variation in bond lengths and angles in PEG-DnS before and after complexation with Zn^{2+} is shown in Table 4-2. Before complexation with Zn^{2+} the electron charge transfer was from the electron donor dimethylamino group to the electron withdrawal sulfonate group. However, after complexation, a reduction in the electron donating nature of this group to the naphthalene ring occurs which leads to the quenching of fluorescent. As can be found in Table 4-2, the N_1-C_{11} bond length is increased in PEG-DnS-Zn^{2+} complex since N_1 is more attracted to the Zn^{2+} ion and there is less electron injection from dimethylamino group to the naphthalene ring. On the other hand, the S_1-C_6 bond length is decreased after complexation due to the less electron withdrawal capacity of the -SO_2- group which is resulted from less electron density on the naphthalene ring. Consequently, less push-pull effect between the electron donor dimethylamino and electron withdrawal sulfonate group causing the suppression of fluorescent intensity. The S_1-O_2 bond length is also decreased which is attributed to the less electron withdrawal by -SO_2- group from the naphthalene ring.

Table 4-1. Crystallographic data

	PEG-DnS	PEG-DnS-Zn
Molecular formula	$C_{19}H_{27}NO_6S$	$C_{38}H_{54}ZnN_2O_{12}S_2$
Molecular weight	397.20	860.24
Crystal system	monoclinic	monoclinic
Space group	$P2_1/c$	$P2_1/c$
Cell volume ($\mathring{A}^3$)	1539.75(2)	2889.2(12)
Cell constants ($\mathring{A}$)	$a = 8.245(4)$ $b = 15.702(2)$ $c = 11.986(2)$	$a = 13.728(4)$ $b = 23.431(2)$ $c = 9.157(2)$
Z	2	2
D_c (g/cm^3)	1.411	1.259
μ (MoKα) (mm^{-1})	0.378	0.643
GooF (Goodness-of-fit)	1.028	1.036
R [$I > 2\sigma(I)$]	0.0380	0.057
R_w	0.1065	0.1135

(a)
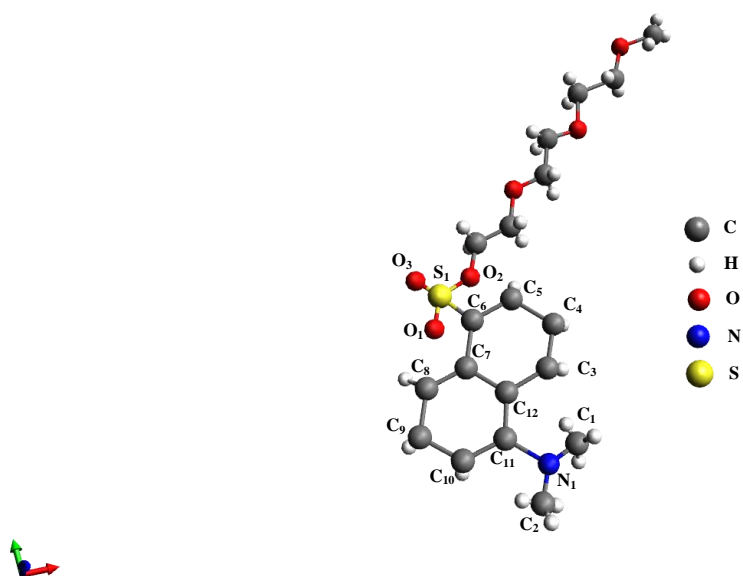
(b)
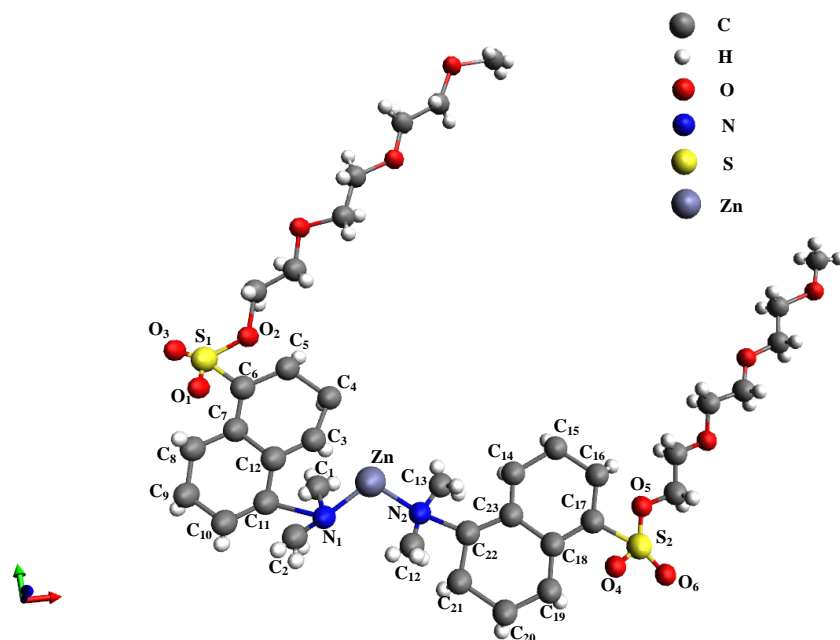
Figure 4-6. Crystal structure of (a) PEG-DnS and (b) PEG-DnS-Zn^{2+}

Table 4-2. Selected bond lengths (in Å) and angles (degree) of PEG-DnS and PEG-DnS-Zn^{2+}

PEG-DnS	
$N_1 - C_{11}$	1.604(3)
$S_1 - C_6$	1.373(2)
$S_1 - O_2$	1.578(3)
$C_1 - N_1 - C_{11}$	107.9(1)
$C_1 - N_1 - C_2$	136.3(2)
PEG-DnS-Zn^{2+}	
$N_1 - C_{11}$	1.741(2)
$Zn - N_1$	1.939(3)
$Zn - N_2$	1.917(2)
$S_1 - C_6$	1.139(2)
$S_1 - O_2$	1.406(4)
$N_1 - Zn - N_2$	139.4(1)
$C_{11} - N_1 - Zn$	143.8(1)
$C_{22} - N_2 - Zn$	166.5(1)

4.4. Conclusion

The successful fabrication of PEGlated dansyl fluorophore was described in this chapter. A deep characterization was performed by FTIR, UV-Vis and ^{1}H NMR to confirm the accurate structure of the chemosensor. Single crystals were also obtained by slow evaporation of solvent at room temperature. The fluorescent study of the chemosensor towards Zn^{2+} ion showed interactions with Zn^{2+} and demonstrates a similar trend to that of achieved in chapter two for Fe_3O_4@SiO_2-PEG-DnS.

X-ray single crystal diffraction revealed the formation of stable complex between PEG-Dns sensor and Zn^{2+} ion and also used to investigate the complexation mode of the PEG-DnS chemosensor with Zn^{2+}. The result was well in agreement with hypotheses made in chapter two and exposed a 2:1 stoichiometry for the complexation of PEG-DnS with Zn^{2+} which was evident by Job plot. The analysis of bond lengths and angles of PEG-DnS before and after complexation with Zn^{2+} ion also indicates the interaction of the fluorophore with Zn^{2+} ion and the existence of push-pull effect due to the presence of PEG spacer.

Comparing the quenching effect of PEG-DnS in this chapter (4.9-fold) with Fe_3O_4@SiO_2-PEG-DnS in chapter 2 (12.5-fold) illustrates that the presence of long chain PEG moieties can significantly improve the photophysical properties of DnS fluorophore.

Finally, the achievements of this chapter including the synthesis of PEG-DnS, its complexation with Zn^{2+} and its crystallography study are entirely new to the author's best of knowledge.

4.5. References

Bügler, J., J. F. Engbersen, et al. (1998). "Novel Water-Soluble β-Cyclodextrin− Calix [4] arene Couples as Fluorescent Sensor Molecules for the Detection of Neutral Analytes." The Journal of Organic Chemistry 63(16): 5339-5344.

Higuchi, Y., M. Narita, et al. (2000). "Fluorescent chemo-sensor for metal cations based on thiacalix [4] arenes modified with dansyl moieties at the lower rim." Tetrahedron 56(27): 4659-4666.

Kimber, M. C., J. P. Geue, et al. (2003). "A preparative and preliminary spectroscopic study of analogues of a zinquin-related fluorophore." Australian journal of chemistry 56(1): 39-44.

Koike, T., T. Watanabe, et al. (1996). "A novel biomimetic zinc (ii)− fluorophore, dansylamidoethyl− pendant macrocyclic tetraamine 1, 4, 7, 10-tetraazacyclododecane (cyclen)." Journal of the American Chemical Society 118(50): 12696-12703.

Lakowicz, J. R. and B. R. Masters (2008). "Principles of fluorescence spectroscopy." Journal of Biomedical Optics 13(2): 029901.

Lee, M. H., H. J. Kim, et al. (2008). "Metal ion induced FRET OFF− ON in Tren/Dansyl-appended rhodamine." Organic letters 10(2): 213-216.

Liu, G., H. Wu, et al. (2011). "Synthesis and applications of fluorescent-magnetic-bifunctional dansylated Fe_3O_4@ SiO_2 nanoparticles." Journal of materials science 46(18): 5959-5968.

Montalti, M., L. Prodi, et al. (2005). "Fluorescence quenching amplification in silica nanosensors for metal ions." Journal of Materials Chemistry 15(27-28): 2810-2814.

Prodi, L., F. Bolletta, et al. (1999). "Searching for new luminescent sensors: synthesis and photophysical properties of a tripodal ligand incorporating the dansyl chromophore and of its metal complexes." European journal of inorganic chemistry 1999(3): 455-460.

Prodi, L., F. Bolletta, et al. (2000). "Luminescent chemosensors for transition metal ions." Coordination Chemistry Reviews 205(1): 59-83.

Schuster, M. and M. Šandor (1996). "N-Dansyl-N′-ethylthiourea for the fluorometric detection of heavy metal ions." Fresenius' journal of analytical chemistry 356(5): 326-330.

Talanova, G. G. and V. S. Talanov (2010). "Dansyl-containing fluorogenic calixarenes as optical chemosensors of hazardous metal ions: a mini-review." Supramolecular Chemistry 22(11-12): 838-852.

Tharmaraj, V. and K. Pitchumani (2012). "An acyclic, dansyl based colorimetric and fluorescent chemosensor for Hg (II) via twisted intramolecular charge transfer (TICT)." Analytica chimica acta 751: 171-175.

Weber, G. and F. J. Farris (1979). "Synthesis and spectral properties of a hydrophobic fluorescent probe: 6-propionyl-2-(dimethylamino) naphthalene." Biochemistry 18(14): 3075-3078.

Zheng, Y., X. Cao, et al. (2003). "Peptidyl fluorescent chemosensors for the detection of divalent copper." Analytical Chemistry 75(7): 1706-1712.

Chapter 5

Conclusion and Future Considerations

This dissertation presents a significant effort on the synthesis, characterisation and investigation of two novel nanochemosensors, $Fe_3O_4@SiO_2$-PEG-DnS and $Fe_3O_4@SiO_2$-PEG-4AQ, upon their detection of zinc ion $(Zn^{2+)}$ in aqueous envirnments. The novel fluorescent nanochemosensors were carefully designed and synthesised by taking advantages of the significant properties of the two flurofores, $Fe_3O_4@SiO_2$-PEG-DnS and $Fe_3O_4@SiO_2$-PEG-4AQ, the Fe_3O_4 core nanoparticles and the polymer segments. The organic flruorfore moieties in particular, the 4 isomer of AQ offers significant impact in this design due to its contraversary structural properties. The magnetic Fe_3O_4 provides the benefit of high dispersion and high surface area and more importantly the ability of recyclability and reusability by means of an external magnetic field. The polymer spacer not only provides water solubilityand flexibility to the nanostructure, preventing theaggregation the stability of the nanochemosensor, it also has enhanced the sensitivity of the respective sensors.

The major achievements in this research work included the successful fabrication and comprehensive characterisation and evluation of the new nanochemosensors. The results have demonstrated that $Fe_3O_4@SiO_2$-PEG-DnS and $Fe_3O_4@SiO_2$-PEG-4AQ are able to detect heavy metal cation (Zn^{2+}) at a concentration as low as of 6.25 and 3.13 nM, respectively. The detection of Zn^{2+} was not interfered when other cations including Cu^{2+}, Ni^{2+}, Co^{2+}, Ca^{2+}, Cd^{2+}, Hg^{2+}, Mg^{2+}, Fe^{3+}, Mn^{2+} Zn^{2+} and Ag^+, was present, indicating an excellent selectivity of the nanosensors.

Table 5-1 has summarised the detection limit of some reported fluorescent chemosensors either small molecules or magnetic nanosensors towards Zn^{2+} ion. The detection limits are sorted from the highest value to the lowest. As can be seen from the table the detection limits achieved in this study for Fe_3O_4@SiO_2-PEG-DnS and Fe_3O_4@SiO_2-PEG-4AQ nanochemosensors are almost the lowest among others and is comparable to that of obtained for R6G/8-AQ co-functionalized Fe_3O_4@SiO_2 (Gu, Meng et al. 2015).

Table 5-1. A summary of detection limits of different chemosnsors from literatures vs. current study (Fe_3O_4@SiO_2-PEG-DnS and Fe_3O_4@SiO_2-PEG-4AQ)

Chemosensor	Detection limit	Ref.
di(2-picolyl)amine functionalized Fe_3O_4@SiO_2	10^{-5} M	(Zeng, Zhou et al. 2014)
Julolidine 2-(aminomethyl)benzenamine	10.9 μM	(Choi, You et al. 2016)
2-((1-hydroxynaphthalene-2-yl)methyleneamino)acetic acid	1.80 μM	(Song, Kim et al. 2014)
Porphyrin derivative	1.80 μM	(Lv, Cao et al. 2013)
Rhodamine derivative	0.664 μM	(Tang, Han et al. 2017)
Salicylaldehyde derivative	0.32 μM	(Lee, Bok et al. 2017)
1-(2-hydroxy-3-(2-hydroxybenzylidene)amino)phenyl)ethanone methyl oxime	0.144 μM	(Dong, Akogun et al. 2017)
AQ-Fe_3O_4@SiO_2@KCC-1	0.108 μM	(Sun, Li et al. 2015)
4-(4-hydroxy-3-methoxybenzylideneamino)-2,3-dimethyl-1-phenyl-1,2- dihydropyrazol-5-one	0.10 μM	(Gupta, Singh et al. 2014)
Fe_3O_4@SiO_2- NQTP	0.10 μM	(Liu, Geng et al. 2011)
(2-(N-(2-hydroxyethyl)-N-((pyridin-2-yl) methyl)amino)-N-(quinolin-8-yl)acetamide)	0.02 μM	(Park, Kim et al. 2015)
4-(5-Chloro-2-hydroxybenzylideneamino)-1H-1,2,4-triazole-5(4H)-thione	51.00 nM	(Yuan, Liu et al. 2016)
(4Z)-4-(4-diethylamino)-2-hydroxybenzylidene amino)-1,2dihydro-1,5- dimethyl-2-phenylpyrazol-3-one	15.00 nM	(Fegade, Sahoo et al. 2015)
Quinolone derivative pyridylaminophenol	8.14 nM	(Song, Park et al. 2015)
Quinoline derivative carbon dots	6.40 nM	(Zhang, Shi et al. 2014)

Fe$_3$O$_4$@SiO$_2$-PEG-DnS	6.25 nM	Current study
Fe$_3$O$_4$@SiO$_2$-PEG-4AQ	3.13 nM	Current study
R6G/8-AQ co-functionalized Fe$_3$O$_4$@SiO$_2$	3.00 nM	(Gu, Meng et al. 2015)

It should be noted that such metal cations as Cd^{2+} and Hg^{2+} often interfere with the detection of Zn^{2+}. However, the sensors developed in this work showed no interference by these metals. Moreover, through EDTA titration, both nanochemosensors have demonstated excellent stability and reusability for the practical applications.

The investigation also showed that the two sensors work differently when the zinc ion was added in. Quenching of fluorescent intensity (12.5-fold) was found in the case of Fe$_3$O$_4$@SiO$_2$-PEG-DnS, whilst an enhancement by 13.5-fold was observed in the case of Fe$_3$O$_4$@SiO$_2$-PEG-4AQ nanosensor. The observations were hypothetically due to the complexation of Zn^{2+} with the electron pair-containing nitrogen in the dimethylamine for Fe$_3$O$_4$@SiO$_2$-PEG-DnS and heterocyclic amine group for Fe$_3$O$_4$@SiO$_2$-PEG-4AQ. The presence of the PEG spacer has resulted in improved photophysical properties. We speculated the enhanced sensitivity is due to the hydrophilicity of PEG moieties and increased mobilities of nanochemosensors.

Further study was required by the author to confirm the mechanisms. One approach is to use small molecules mimicking the structure of PEG cojugates with the two flourophores: dansyl chloride and 4-aminoquinoline derivative. Growing single crystals is critical to perform deep investigation of crystalline structure and understanding the complexation mechanism. Chapter 4 already demonstrated the investigation of PEGylated dansyl fluorophore and its interaction with Zn^{2+} ion to evidence the influence of PEG conjugation on luminescence properties as well as understanding the complexation mode of dansyl moieties with Zn^{2+} ion. Extended research is needed to synthesis and to exmine the structure of small molecular chemosensors mimicking the conjugating moied between the PEG and the fluorescent

moiety. Determination of charge/electron or energy transfer between the sensor and the metal cation also is needed.

Although both $Fe_3O_4@SiO_2$-PEG-DnS and $Fe_3O_4@SiO_2$-PEG-4AQ nanochemosensors have performed well in selective detection of Zn^{2+} ion, there was limited time to investigate their applications in other fields. Further work focusing on cell imaging and sensing in biological environments is a continuous topic of research in this research group. Developing dual functional theroanostics using the sening components developed in this work is is also a research topic of the group.

Finally, the achievements of this study can be considered as a practical setting for investigation of the amount of heavy metals and their separations with high sensitivity and selectivity. It can also provide a viable, cost effective and environmentally friendly procedure for the detection of metal cations, simultaneously.

5.1. References

Albani, J. R. (2008). Principles and applications of fluorescence spectroscopy, John Wiley & Sons.

Arfsten, N. J., S. Armes, P. J. P. Buskens, J. C. Thies and P. W. A. Vrijaldenhoven (2007). Core-shell nanoparticles, Google Patents.

Banthia, S. and A. Samanta (2006). "A new strategy for ratiometric fluorescence detection of transition metal ions." The Journal of Physical Chemistry B **110**(13): 6437-6440.

Basabe-Desmonts, L., D. N. Reinhoudt and M. Crego-Calama (2007). "Design of fluorescent materials for chemical sensing." Chemical Society Reviews **36**(6): 993-1017.

Bazrafshan, A., S. Hajati and M. Ghaedi (2015). "Improvement in the performance of a zinc ion-selective potentiometric sensor using modified core/shell $Fe_3O_4@SiO_2$ nanoparticles." RSC Advances **5**(128): 105925-105933.

Buck, S. M., H. Xu, M. Brasuel, M. A. Philbert and R. Kopelman (2004). "Nanoscale probes encapsulated by biologically localized embedding (PEBBLEs) for ion sensing and imaging in live cells." Talanta **63**(1): 41-59.

Bügler, J., J. F. Engbersen and D. N. Reinhoudt (1998). "Novel Water-Soluble β-Cyclodextrin− Calix [4] arene Couples as Fluorescent Sensor Molecules for the Detection of Neutral Analytes." The Journal of Organic Chemistry **63**(16): 5339-5344.

Chen, L., D. W. McBranch, H.-L. Wang, R. Helgeson, F. Wudl and D. G. Whitten (1999). "Highly sensitive biological and chemical sensors based on reversible fluorescence quenching in a conjugated polymer." Proceedings of the National Academy of Sciences **96**(22): 12287-12292.

Chen, Q.-Y. and C.-F. Chen (2005). "A new Hg 2+-selective fluorescent sensor based on a dansyl amide-armed calix [4]-aza-crown." Tetrahedron Letters **46**(1): 165-168.

Cho, Y., S. S. Lee and J. H. Jung (2010). "Recyclable fluorimetric and colorimetric mercury-specific sensor using porphyrin-functionalized $Au@SiO_2$ core/shell nanoparticles." Analyst **135**(7): 1551-1555.

Choi, Y. W., G. R. You, J. J. Lee and C. Kim (2016). "Turn-on fluorescent chemosensor for selective detection of Zn 2+ in an aqueous solution: experimental and theoretical studies." Inorganic Chemistry Communications **63**: 35-38.

Crosby, G. A. and J. N. Demas (1971). "Measurement of photoluminescence quantum yields. Review." The Journal of Physical Chemistry **75**(8): 991-1024.

Czarnik, A. W. (1993). Fluorescent chemosensors for ion and molecule recognition, ACS Publications.

De Leon-Rodriguez, L., A. J. M. Lubag and A. D. Sherry (2012). "Imaging free zinc levels in vivo–What can be learned?" Inorganica chimica acta **393**: 12-23.

De Silva, A. P., H. N. Gunaratne, T. Gunnlaugsson, A. J. Huxley, C. P. McCoy, J. T. Rademacher and T. E. Rice (1997). "Signaling recognition events with fluorescent sensors and switches." Chemical Reviews **97**(5): 1515-1566.

de Souza Santos, M., M. P. F. de Morais Del, A. S. Ito and R. M. Z. G. Naal (2014). "Binding of chloroquine to ionic micelles: Effect of pH and micellar surface charge." Journal of Luminescence **147**: 49-58.

Delgado-Pinar, E., N. Montoya, M. Galiana, M. T. Albelda, J. C. Frías, H. R. Jiménez, E. García-España and J. Alarcón (2010). "Preparation of Hg^{2+} selective fluorescent chemosensors based on surface modified core–shell aluminosilicate nanoparticles." New Journal of Chemistry **34**(3): 567-570.

Demchenko, A. P. (2008). Introduction to fluorescence sensing, Springer Science & Business Media.

Deng, Y.-H., C.-C. Wang, J.-H. Hu, W.-L. Yang and S.-K. Fu (2005). "Investigation of formation of silica-coated magnetite nanoparticles via sol–gel approach." Colloids and Surfaces A: Physicochemical and Engineering Aspects **262**(1): 87-93.

Desvergne, J.-P. and A. W. Czarnik (1997). Chemosensors of ion and molecule recognition, Springer Science & Business Media.

Desvergne, J.-P. and A. W. Czarnik (2012). Chemosensors of ion and molecule recognition, Springer Science & Business Media.

Dong, W.-K., S. F. Akogun, Y. Zhang, Y.-X. Sun and X.-Y. Dong (2017). "A reversible "turn-on" fluorescent sensor for selective detection of Zn 2+." Sensors and Actuators B: Chemical **238**: 723-734.

Dong, Z., Y. Guo, X. Tian and J. Ma (2013). "Quinoline group based fluorescent sensor for detecting zinc ions in aqueous media and its logic gate behaviour." Journal of Luminescence **134**: 635-639.

Endre, L., F. Beck and A. Prasad (1990). "The role of zinc in human health." The Journal of trace elements in experimental medicine **3**(4): 337-375.

Fabbrizzi, L., M. Licchelli, P. Pallavicini, A. Perotti, A. Taglietti and D. Sacchi (1996). "Fluorescent Sensors for Transition Metals Based on Electron- Transfer and Energy- Transfer Mechanisms." Chemistry–A European Journal **2**(1): 75-82.

Fabbrizzi, L., M. Licchelli, P. Pallavicini, D. Sacchi and A. Taglietti (1996). "Sensing of transition metals through fluorescence quenching or enhancement. A review." Analyst **121**(12): 1763-1768.

Fan, L.-J., Y. Zhang, C. B. Murphy, S. E. Angell, M. F. Parker, B. R. Flynn and W. E. Jones (2009). "Fluorescent conjugated polymer molecular wire chemosensors for transition metal ion recognition and signaling." Coordination Chemistry Reviews **253**(3): 410-422.

Fegade, U. A., S. K. Sahoo, A. Singh, N. Singh, S. B. Attarde and A. S. Kuwar (2015). "A chemosensor showing discriminating fluorescent response for highly selective and nanomolar detection of Cu 2+ and Zn 2+ and its application in molecular logic gate." Analytica chimica acta **872**: 63-69.

Feng, J., J. Mao, X. Wen and M. Tu (2011). "Ultrasonic-assisted in situ synthesis and characterization of superparamagnetic Fe3O4 nanoparticles." Journal of Alloys and Compounds **509**(37): 9093-9097.

Feng, J., J. Mao, X. Wen and M. Tu (2011). "Ultrasonic-assisted in situ synthesis and characterization of superparamagnetic Fe 3 O 4 nanoparticles." Journal of Alloys and Compounds **509**(37): 9093-9097.

Feng, X., H. Guo, K. Patel, H. Zhou and X. Lou (2014). "High performance, recoverable Fe3O4ZnO nanoparticles for enhanced photocatalytic degradation of phenol." Chemical Engineering Journal **244**: 327-334.

Feng, X., S. Zhang and X. Lou (2013). "Controlling silica coating thickness on TiO2 nanoparticles for effective photodynamic therapy." Colloids and Surfaces B: Biointerfaces **107**: 220-226.

Feng, X., S. Zhang and X. Lou (2013). "Controlling silica coating thickness on TiO 2 nanoparticles for effective photodynamic therapy." Colloids and Surfaces B: Biointerfaces **107**: 220-226.

Feng, X., S. Zhang, H. Wu and X. Lou (2015). "A novel folic acid-conjugated TiO 2–SiO 2 photosensitizer for cancer targeting in photodynamic therapy." Colloids and Surfaces B: Biointerfaces **125**: 197-205.

Frackowiak, D. (1988). "The jablonski diagram." Journal of Photochemistry and Photobiology B: Biology **2**(3): 399.

Frey, N. A., S. Peng, K. Cheng and S. Sun (2009). "Magnetic nanoparticles: synthesis, functionalization, and applications in bioimaging and magnetic energy storage." Chemical Society Reviews **38**(9): 2532-2542.

Ghosh Chaudhuri, R. and S. Paria (2011). "Core/shell nanoparticles: classes, properties, synthesis mechanisms, characterization, and applications." Chemical Reviews **112**(4): 2373-2433.

Gu, Y., G. Meng, M. Wang, Q. Huang, C. Zhu and Z. Huang (2015). "R6G/8-AQ co-functionalized Fe3O4@ SiO2 nanoparticles for fluorescence detection of trace Hg2+ and Zn2+ in aqueous solution." Science China Materials **58**(7): 550-558.

Gunnlaugsson, T., D. A. Mac Dónaill and D. Parker (2001). "Lanthanide macrocyclic quinolyl conjugates as luminescent molecular-level devices." Journal of the American Chemical Society **123**(51): 12866-12876.

Guo, Z., W. Zhu and H. Tian (2009). "Hydrophilic copolymer bearing dicyanomethylene-4 H-pyran moiety as fluorescent film sensor for Cu^{2+} and pyrophosphate anion." Macromolecules **43**(2): 739-744.

Gupta, V. K., A. K. Singh and L. K. Kumawat (2014). "A turn-on fluorescent chemosensor for Zn 2+ ions based on antipyrine schiff base." Sensors and Actuators B: Chemical **204**: 507-514.

Han, W. S., H. Y. Lee, S. H. Jung, S. J. Lee and J. H. Jung (2009). "Silica-based chromogenic and fluorogenic hybrid chemosensor materials." Chemical Society Reviews **38**(7): 1904-1915.

Hanaoka, K., K. Kikuchi, H. Kojima, Y. Urano and T. Nagano (2004). "Development of a zinc ion-selective luminescent lanthanide chemosensor for biological applications." Journal of the American Chemical Society **126**(39): 12470-12476.

Higuchi, Y., M. Narita, T. Niimi, N. Ogawa, F. Hamada, H. Kumagai, N. Iki, S. Miyano and C. Kabuto (2000). "Fluorescent chemo-sensor for metal cations based on thiacalix [4] arenes modified with dansyl moieties at the lower rim." Tetrahedron **56**(27): 4659-4666.

Hu, J., C. Li and S. Liu (2009). "Hg2+-reactive double hydrophilic block copolymer assemblies as novel multifunctional fluorescent probes with improved performance." Langmuir **26**(2): 724-729.

Huang, C. Y. (1982). "[27] Determination of binding stoichiometry by the continuous variation method: The job plot." Methods in enzymology **87**: 509-525.

Jeong, U., H. H. Shin and Y. Kim (2015). "Functionalized magnetic core–shell Fe@SiO$_2$ nanoparticles as recoverable colorimetric sensor for Co^{2+} ion." Chemical Engineering Journal **281**: 428-433.

Job, P. (1928). "Formation and stability of inorganic complexes in solution."

Jokerst, J. V., T. Lobovkina, R. N. Zare and S. S. Gambhir (2011). "Nanoparticle PEGylation for imaging and therapy." Nanomedicine **6**(4): 715-728.

Jung, J. H., J. H. Lee and S. Shinkai (2011). "Functionalized magnetic nanoparticles as chemosensors and adsorbents for toxic metal ions in environmental and biological fields." Chemical Society Reviews **40**(9): 4464-4474.

Kaschula, C. H., T. J. Egan, R. Hunter, N. Basilico, S. Parapini, D. Taramelli, E. Pasini and D. Monti (2002). "Structure− activity relationships in 4-aminoquinoline antiplasmodials. The role of the group at the 7-position." Journal of medicinal chemistry **45**(16): 3531-3539.

Kaur, K., R. Gupta, S. A. Saraf and S. K. Saraf (2014). "Zinc: the metal of life." Comprehensive Reviews in Food Science and Food Safety **13**(4): 358-376.

Kaur, P., H. Kaur and K. Singh (2013). "A quinoline-based turn-off fluorescent cation sensor." RSC Advances **3**(1): 64-67.

Kim, H., G. R. You, G. J. Park, J. Y. Choi, I. Noh, Y. Kim, S.-J. Kim, C. Kim and R. G. Harrison (2015). "Selective zinc sensor based on pyrazoles and quinoline used to image cells." Dyes and Pigments **113**: 723-729.

Kim, K. T., S. A. Yoon, J. Ahn, Y. Choi, M. H. Lee, J. H. Jung and J. Park (2017). "Synthesis of fluorescent naphthalimide-functionalized Fe_3O_4 nanoparticles and their application for the selective detection of Zn^{2+} present in contaminated soil." Sensors and Actuators B: Chemical **243**: 1034-1041.

Kimber, M. C., J. P. Geue, S. F. Lincoln, A. D. Ward and E. R. Tiekink (2003). "A preparative and preliminary spectroscopic study of analogues of a zinquin-related fluorophore." Australian journal of chemistry **56**(1): 39-44.

Kimura, M., T. Horai, K. Hanabusa and H. Shirai (1998). "Fluorescence chemosensor for metal ions using conjugated polymers." Advanced Materials **10**(6): 459-462.

Koike, T., T. Watanabe, S. Aoki, E. Kimura and M. Shiro (1996). "A novel biomimetic zinc (ii)− fluorophore, dansylamidoethyl− pendant macrocyclic tetraamine 1, 4, 7, 10-tetraazacyclododecane (cyclen)." Journal of the American Chemical Society **118**(50): 12696-12703.

Kovi, P. J., A. C. Capomacchia and S. G. Schulman (1972). "Electronic spectra of 2-aminoquinoline and 4-aminoquinaldine. Evidence for the cyclic amidine structures of the singly protonated cations." Analytical Chemistry **44**(9): 1611-1615.

Lakowicz, J. R. and B. R. Masters (2008). "Principles of fluorescence spectroscopy." Journal of Biomedical Optics **13**(2): 029901.

Laws, W. R. and P. B. Contino (1992). "[21] Fluorescence quenching studies: Analysis of nonlinear Stern-Volmer data." Methods in enzymology **210**: 448-463.

Lee, H. G., J. H. Lee, S. P. Jang, H. M. Park, S.-J. Kim, Y. Kim, C. Kim and R. G. Harrison (2011). "Zinc selective chemosensor based on pyridyl-amide fluorescence." Tetrahedron **67**(42): 8073-8078.

Lee, M. H., H. J. Kim, S. Yoon, N. Park and J. S. Kim (2008). "Metal ion induced FRET OFF− ON in Tren/Dansyl-appended rhodamine." Organic letters **10**(2): 213-216.

Lee, S. Y., K. H. Bok, T. G. Jo, S. Y. Kim and C. Kim (2017). "A simple Schiff-base fluorescence probe for the simultaneous detection of Ga 3+ and Zn 2+." Inorganica Chimica Acta **461**: 127-135.

Li, N., Q. Xu, X. Xia, J. Lu and X. Wen (2009). "A polymeric chemosensor for Fe 3+ based on fluorescence quenching of polymer with quinoline derivative in the side chain." Materials Chemistry and Physics **114**(1): 339-343.

Lin, W., X. Cao, Y. Ding, L. Yuan and Q. Yu (2010). "A reversible fluorescent Hg^{2+} chemosensor based on a receptor composed of a thiol atom and an alkene moiety for living cell fluorescence imaging." Organic & biomolecular chemistry **8**(16): 3618-3620.

Liu, G., H. Wu, H. Zheng, L. Tang, H. Hu, H. Yang and S. Yang (2011). "Synthesis and applications of fluorescent-magnetic-bifunctional dansylated Fe3O4@ SiO2 nanoparticles." Journal of materials science **46**(18): 5959-5968.

Liu, G., H. Wu, H. Zheng, L. Tang, H. Hu, H. Yang and S. Yang (2011). "Synthesis and applications of fluorescent-magnetic-bifunctional dansylated $Fe_3O_4@SiO_2$ nanoparticles." Journal of materials science **46**(18): 5959-5968.

Liu, Z., H. Geng, J. Sheng and J. Ma (2011). "Highly selective and sensitive magnetic silica nanoparticles based fluorescent sensor for detection of Zn 2+ ions." Materials Science and Engineering: B **176**(5): 412-416.

Lv, Y., M. Cao, J. Li and J. Wang (2013). "A sensitive ratiometric fluorescent sensor for zinc (II) with high selectivity." Sensors **13**(3): 3131-3141.

Ma, Y., F. Wang, S. Kambam and X. Chen (2013). "A quinoline-based fluorescent chemosensor for distinguishing cadmium from zinc ions using cysteine as an auxiliary reagent." Sensors and Actuators B: Chemical **188**: 1116-1122.

Maeda, H., T. Maeda and K. Mizuno (2012). "Absorption and fluorescence spectroscopic properties of 1-and 1, 4-silyl-substituted naphthalene derivatives." Molecules **17**(5): 5108-5125.

Mao, H. and Z. Liu (2018). "Two emissive-magnetic composite platforms for Hg (II) sensing and removal: The combination of magnetic core, silica molecular sieve and rhodamine chemosensors." Spectrochimica Acta Part A: Molecular and Biomolecular Spectroscopy **189**: 366-373.

Méallet-Renault, R., R. Pansu, S. Amigoni-Gerbier and C. Larpent (2004). "Metal-chelating nanoparticles as selective fluorescent sensor for Cu^{2+}." Chemical communications(20): 2344-2345.

Mmonwa, M. M., M. J. Mphahlele, M. M. El-Hendawy, A. M. El-Nahas and N. Koga (2014). "Synthesis and Photophysical Properties of the 2-(3-(2-Alkyl-6, 8-diaryl-4-oxo-1, 2, 3, 4-tetrahydroquinazolin-2-yl) propyl)-6, 8-diarylquinazolin-4 (3H)-ones." Molecules **19**(7): 9712-9735.

Montalti, M., L. Prodi and N. Zaccheroni (2005). "Fluorescence quenching amplification in silica nanosensors for metal ions." Journal of Materials Chemistry **15**(27-28): 2810-2814.

Montalti, M., L. Prodi, N. Zaccheroni and G. Falini (2002). "Solvent-induced modulation of collective photophysical processes in fluorescent silica nanoparticles." Journal of the American Chemical Society **124**(45): 13540-13546.

Nogués, J., V. Skumryev, J. Sort, S. Stoyanov and D. Givord (2006). "Shell-driven magnetic stability in core-shell nanoparticles." Physical review letters **97**(15): 157203.

Nolan, E. M., J. Jaworski, K.-I. Okamoto, Y. Hayashi, M. Sheng and S. J. Lippard (2005). "QZ1 and QZ2: rapid, reversible quinoline-derivatized fluoresceins for sensing biological Zn (II)." Journal of the American Chemical Society **127**(48): 16812-16823.

Nord, K., J. Karlsen and H. W. Tosnnesen (1994). "PHOTOCHEMICAL STABILITY OF BIOLOGICALLY ACTIVE COMPOUNDS. IX. CHARACTERIZATION OF THE SPECTROSCOPIC PROPERTIES OF THE 4- AMINOQUINOLINES, CHLOROQUINE AND HYDROXYCHLOROQUINE, AND OF SELECTED METABOLITES BY ABSORPTION, FLUORESCENCE AND PHOSPHORESCENCE MEASUREMENTS." Photochemistry and photobiology **60**(5): 427-431.

Otelo, V. A., A. C. Sant'Ana, D. L. de Faria and C. M. Menezes (2011). "Molecular modeling and UV–vis spectroscopic studies on the mechanism of action of reversed chloroquine (RCQ)." Bioorganic & medicinal chemistry letters **21**(1): 250-254.

Otsuka, H., Y. Nagasaki and K. Kataoka (2003). "PEGylated nanoparticles for biological and pharmaceutical applications." Advanced drug delivery reviews **55**(3): 403-419.

Pankhurst, Q. A., J. Connolly, S. K. Jones and J. Dobson (2003). "Applications of magnetic nanoparticles in biomedicine." Journal of physics D: Applied physics **36**(13): R167.

Park, G. J., H. Kim, J. J. Lee, Y. S. Kim, S. Y. Lee, S. Lee, I. Noh and C. Kim (2015). "A highly selective turn-on chemosensor capable of monitoring Zn 2+ concentrations in living cells and aqueous solution." Sensors and Actuators B: Chemical **215**: 568-576.

Park, G. J., Y. J. Na, H. Y. Jo, S. A. Lee, A. R. Kim, I. Noh and C. Kim (2014). "A single chemosensor for multiple analytes: fluorogenic detection of Zn 2+ and OAc− ions in aqueous solution, and an application to bioimaging." New Journal of Chemistry **38**(6): 2587-2594.

Park, M., S. Seo, S. J. Lee and J. H. Jung (2010). "Functionalized Ni@ SiO_2 core/shell magnetic nanoparticles as a chemosensor and adsorbent for Cu^{2+} ion in drinking water and human blood." Analyst **135**(11): 2802-2805.

Parker, D. and J. G. Williams (1995). "Luminescence behaviour of cadmium, lead, zinc, copper, nickel and lanthanide complexes of octadentate macrocyclic ligands bearing naphthyl chromophores." Journal of the Chemical Society, Perkin Transactions 2(7): 1305-1314.

Peng, X., Y. Wang, X. Tang and W. Liu (2011). "Functionalized magnetic core–shell $Fe_3O_4@SiO_2$ nanoparticles as selectivity-enhanced chemosensor for Hg (II)." Dyes and Pigments 91(1): 26-32.

Pourfallah, G. and X. Lou (2016). "A novel recyclable magnetic nanostructure for highly sensitive, selective and reversible detection of zinc ions in aqueous solutions." Sensors and Actuators B: Chemical 233: 379-387.

Prodi, L. (2005). "Luminescent chemosensors: from molecules to nanoparticles." New Journal of Chemistry 29(1): 20-31.

Prodi, L., F. Bolletta, M. Montalti and N. Zaccheroni (1999). "Searching for new luminescent sensors: synthesis and photophysical properties of a tripodal ligand incorporating the dansyl chromophore and of its metal complexes." European journal of inorganic chemistry 1999(3): 455-460.

Prodi, L., F. Bolletta, M. Montalti and N. Zaccheroni (2000). "Luminescent chemosensors for transition metal ions." Coordination Chemistry Reviews 205(1): 59-83.

Prodi, L., M. Montalti, N. Zaccheroni, J. S. Bradshaw, R. M. Izatt and P. B. Savage (2001). "Characterization of 5-chloro-8-methoxyquinoline appended diaza-18-crown-6 as a chemosensor for cadmium." Tetrahedron Letters 42(16): 2941-2944.

Qian, X., Y. Xiao, Y. Xu, X. Guo, J. Qian and W. Zhu (2010). ""Alive" dyes as fluorescent sensors: fluorophore, mechanism, receptor and images in living cells." Chemical communications 46(35): 6418-6436.

Rampazzo, E., E. Brasola, S. Marcuz, F. Mancin, P. Tecilla and U. Tonellato (2005). "Surface modification of silica nanoparticles: a new strategy for the realization of self-organized fluorescence chemosensors." Journal of Materials Chemistry 15(27-28): 2687-2696.

Rastogi, S. K., P. Pal, D. E. Aston, T. E. Bitterwolf and A. L. Branen (2011). "8-Aminoquinoline functionalized silica nanoparticles: a fluorescent nanosensor for detection of divalent zinc in aqueous and in yeast cell suspension." ACS applied materials & interfaces 3(5): 1731-1739.

Rehm, D. and A. Weller (1970). "Kinetics of fluorescence quenching by electron and H-atom transfer." Israel Journal of Chemistry 8(2): 259-271.

Reichle, R. A., K. G. McCurdy and L. G. Hepler (1975). "Zinc hydroxide: solubility product and hydroxy-complex stability constants from 12.5–75 C." Canadian Journal of Chemistry 53(24): 3841-3845.

Roca, A., R. Costo, A. Rebolledo, S. Veintemillas-Verdaguer, P. Tartaj, T. Gonzalez-Carreno, M. Morales and C. Serna (2009). "Progress in the preparation of magnetic nanoparticles for applications in biomedicine." Journal of physics D: Applied physics 42(22): 224002.

Roohani, N., R. Hurrell, R. Kelishadi and R. Schulin (2013). "Zinc and its importance for human health: An integrative review." Journal of Research in Medical Sciences 18(2): 144-157.

Salgueiro, M. J., M. Zubillaga, A. Lysionek, M. I. Sarabia, R. Caro, T. De Paoli, A. Hager, R. Weill and J. Boccio (2000). "Zinc as an essential micronutrient: a review." Nutrition Research 20(5): 737-755.

Sarkar, M., S. Banthia, A. Patil, M. B. Ansari and A. Samanta (2006). "pH-Regulated "Off–On" fluorescence signalling of d-block metal ions in aqueous media and realization of molecular IMP logic function." New Journal of Chemistry 30(11): 1557-1560.

Sauer, M., J. Hofkens and J. Enderlein (2011). "Basic principles of fluorescence spectroscopy." Handbook of Fluorescence Spectroscopy and Imaging: From Single Molecules to Ensembles: 1-30.

Schuster, M. and M. Šandor (1996). "N-Dansyl-N′-ethylthiourea for the fluorometric detection of heavy metal ions." Fresenius' journal of analytical chemistry **356**(5): 326-330.

Shang, G.-Q., X. Gao, M.-X. Chen, H. Zheng and J.-G. Xu (2008). "A novel Hg^{2+} selective ratiometric fluorescent chemodosimeter based on an intramolecular FRET mechanism." Journal of fluorescence **18**(6): 1187.

Shankar, B. H. and D. Ramaiah (2011). "Dansyl□ Naphthalimide Dyads As Molecular Probes: Effect of Spacer Group on Metal Ion Binding Properties." The Journal of Physical Chemistry B **115**(45): 13292-13299.

Shao, M., F. Ning, J. Zhao, M. Wei, D. G. Evans and X. Duan (2012). "Preparation of $Fe_3O_4@SiO_2$ layered double hydroxide core–shell microspheres for magnetic separation of proteins." Journal of the American Chemical Society **134**(2): 1071-1077.

Singh, H., J. Sindhu and J. M. Khurana (2015). "Synthesis of novel fluorescence xanthene–aminoquinoline conjugates, determination of dipole moment and selective fluorescence chemosensor for Th 4+ ions." Optical Materials **42**: 449-457.

Song, E. J., H. Kim, I. H. Hwang, K. B. Kim, A. R. Kim, I. Noh and C. Kim (2014). "A single fluorescent chemosensor for multiple target ions: recognition of Zn 2+ in 100% aqueous solution and F− in organic solvent." Sensors and Actuators B: Chemical **195**: 36-43.

Song, E. J., G. J. Park, J. J. Lee, S. Lee, I. Noh, Y. Kim, S.-J. Kim, C. Kim and R. G. Harrison (2015). "A fluorescence sensor for Zn 2+ that also acts as a visible sensor for Co 2+ and Cu 2+." Sensors and Actuators B: Chemical **213**: 268-275.

Song, Q., M. Li, L. Huang, Q. Wu, Y. Zhou and Y. Wang (2013). "Bifunctional polydopamine@ Fe_3O_4 core–shell nanoparticles for electrochemical determination of lead (II) and cadmium (II)." Analytica chimica acta **787**: 64-70.

Sun, Z., H. Li, D. Guo, J. Sun, G. Cui, Y. Liu, Y. Tian and S. Yan (2015). "A multifunctional magnetic core–shell fibrous silica sensing probe for highly sensitive detection and removal of Zn^{2+} from aqueous solution." Journal of Materials Chemistry C **3**(18): 4713-4722.

Sun, Z., H. Li, D. Guo, J. Sun, G. Cui, Y. Liu, Y. Tian and S. Yan (2015). "A multifunctional magnetic core–shell fibrous silica sensing probe for highly sensitive detection and removal of Zn 2+ from aqueous solution." Journal of Materials Chemistry C **3**(18): 4713-4722.

Talanova, G. G. and V. S. Talanov (2010). "Dansyl-containing fluorogenic calixarenes as optical chemosensors of hazardous metal ions: a mini-review." Supramolecular Chemistry **22**(11-12): 838-852.

Tang, X., J. Han, Y. Wang, L. Ni, X. Bao, L. Wang and W. Zhang (2017). "A multifunctional Schiff base as a fluorescence sensor for Fe 3+ and Zn 2+ ions, and a colorimetric sensor for Cu 2+ and applications." Spectrochimica Acta Part A: Molecular and Biomolecular Spectroscopy **173**: 721-726.

Tartaj, P., S. Veintemillas-Verdaguer and C. J. Serna (2003). "The preparation of magnetic nanoparticles for applications in biomedicine." Journal of physics D: Applied physics **36**(13): R182.

Tharmaraj, V. and K. Pitchumani (2012). "An acyclic, dansyl based colorimetric and fluorescent chemosensor for Hg (II) via twisted intramolecular charge transfer (TICT)." Analytica chimica acta **751**: 171-175.

Thiagarajan, V., P. Ramamurthy, D. Thirumalai and V. T. Ramakrishnan (2005). "A novel colorimetric and fluorescent chemosensor for anions involving PET and ICT pathways." Organic letters **7**(4): 657-660.

Tian, L., X. Lou, Z. Q. Pan, Q. M. Huang and H. Zhou (2013). "Synthesis, characterisation and catalase-like activity of silica-coated magnetite nanoparticles modified by a Schiff base Mn complex." Micro & Nano Letters **8**(3): 159-162.

Tian, X., Z. Dong, R. Wang and J. Ma (2013). "A quinoline group modified $Fe_3O_4@SiO_2$ nanoparticles for sequential detection of Zn^{2+} and hydrogen sulfide in aqueous solution and its logic behavior." Sensors and Actuators B: Chemical **183**: 446-453.

Ueno, T. and T. Nagano (2011). "Fluorescent probes for sensing and imaging." Nature methods **8**(8): 642.

Valeur, B. and M. N. Berberan-Santos (2012). Molecular fluorescence: principles and applications, John Wiley & Sons.

Valeur, B. and J.-C. Brochon (2012). New trends in fluorescence spectroscopy: applications to chemical and life sciences, Springer Science & Business Media.

Valeur, B. and I. Leray (2000). "Design principles of fluorescent molecular sensors for cation recognition." Coordination Chemistry Reviews **205**(1): 3-40.

Wang, B. Y., X. Y. Liu, Y. L. Hu and Z. X. Su (2009). "Synthesis and photophysical behavior of a water- soluble coumarin- bearing polymer for proton and Ni2+ ion sensing." Polymer International **58**(6): 703-709.

Wang, L., J. Jin, L. Zhao, H. Shen, C. Shen and P. Zhang (2016). "Synthesis of C-glycosyl triazolyl quinoline-based fluorescent sensors for the detection of mercury ions." Carbohydrate research **433**: 41-46.

Wang, T., L. Zhang, C. Li, W. Yang, T. Song, C. Tang, Y. Meng, S. Dai, H. Wang and L. Chai (2015). "Synthesis of core–shell magnetic $Fe_3O_4@poly(m-phenylenediamine)$ particles for chromium reduction and adsorption." Environmental science & technology **49**(9): 5654-5662.

Wang, Y., X. Peng, J. Shi, X. Tang, J. Jiang and W. Liu (2012). "Highly selective fluorescent chemosensor for Zn^{2+} derived from inorganic-organic hybrid magnetic core/shell $Fe_3O_4@SiO_2$ nanoparticles." Nanoscale research letters **7**(1): 86.

Weber, G. (1952). "Polarization of the fluorescence of macromolecules. 1. Theory and experimental method." Biochemical Journal **51**(2): 145.

Weber, G. and F. J. Farris (1979). "Synthesis and spectral properties of a hydrophobic fluorescent probe: 6-propionyl-2-(dimethylamino) naphthalene." Biochemistry **18**(14): 3075-3078.

Weiss, S. (1999). "Fluorescence spectroscopy of single biomolecules." Science **283**(5408): 1676-1683.

Xu, Q. and D. Pascoe (1994). "The importance of food and water as sources of zinc during exposure of Gammarus pulex (Amphipoda)." Archives of Environmental Contamination and Toxicology **26**(4): 459-465.

Xu, Y., Y. Zhou, W. Ma and S. Wang (2013). "A fluorescent sensor for zinc detection and removal based on core-shell functionalized $Fe_3O_4@SiO_2$ nanoparticles." Journal of Nanomaterials **2013**.

Xu, Y., Y. Zhou, W. Ma, S. Wang and S. Li (2013). "Highly sensitive and selective OFF-ON fluorescent sensor based on functionalized $Fe_3O_4@SiO_2$ nanoparticles for detection of Zn^{2+} in acetonitrile media." Applied Surface Science **276**: 705-710.

Yoon, T. J., K. N. Yu, E. Kim, J. S. Kim, B. G. Kim, S. H. Yun, B. H. Sohn, M. H. Cho, J. K. Lee and S. B. Park (2006). "Specific targeting, cell sorting, and bioimaging with smart magnetic silica core–shell nanomaterials." small **2**(2): 209-215.

Yuan, C., X. Liu, Y. Wu, L. Lu and M. Zhu (2016). "A triazole Schiff base-based selective and sensitive fluorescent probe for Zn 2+: a combined experimental and theoretical study." Spectrochimica Acta Part A: Molecular and Biomolecular Spectroscopy **154**: 215-219.

Yuan, L., W. Lin, K. Zheng and S. Zhu (2013). "FRET-based small-molecule fluorescent probes: rational design and bioimaging applications." Accounts of chemical research **46**(7): 1462-1473.

Zeng, X., Y. Xu, X. Chen, W. Ma and Y. Zhou (2017). "An inorganic/organic hybrid magnetic network as a colorimetric fluorescent nanosensor and its recognizing behavior toward Hg^{2+}." Applied Surface Science **423**: 1103-1110.

Zeng, X., Y. Zhou, W. Ma, S. Wang, K. Xie, J. Wu and K. Wei (2014). "Selective Zn (II) chemosensor based on di (2-picolyl) amine functionalized inorganic/organic hybrid magnetic network." Chemical Engineering Journal **244**: 75-81.

Zhang, Z., Y. Shi, Y. Pan, X. Cheng, L. Zhang, J. Chen, M.-J. Li and C. Yi (2014). "Quinoline derivative-functionalized carbon dots as a fluorescent nanosensor for sensing and intracellular imaging of Zn 2+." Journal of Materials Chemistry B **2**(31): 5020-5027.

Zheng, Y., X. Cao, J. Orbulescu, V. Konka, F. M. Andreopoulos, S. M. Pham and R. M. Leblanc (2003). "Peptidyl fluorescent chemosensors for the detection of divalent copper." Analytical Chemistry **75**(7): 1706-1712.

Zhu, J.-F., H. Yuan, W.-H. Chan and A. W. Lee (2010). "A FRET fluorescent chemosensor SPAQ for Zn2+ based on a dyad bearing spiropyran and 8-aminoquinoline unit." Tetrahedron Letters **51**(27): 3550-3554.

APPENDIX 1

The following pages contain documents outlining permission granted from copyright owners for use of third party copyright material or published work in which the copyright is held by another party.

Every reasonable effort has been made to acknowledge the owners of copyright material. I would be pleased to hear from any copyright owner who has been omitted or incorrectly acknowledged.

Copyright agreement for Figure 1-6 in Chapter 1

Copyright agreement for Figure 1-8 in Chapter 1

Copyright Clearance Center

RightsLink®

| Home | Account Info | Help | ✉ |

Title: Functionalized magnetic core–shell Fe3O4@SiO2 nanoparticles as selectivity-enhanced chemosensor for Hg(II)

Author: Xiaohong Peng,Yujiao Wang,Xiaoliang Tang,Weisheng Liu

Publication: Dyes and Pigments

Publisher: Elsevier

Date: October 2011

Copyright © 2011 Elsevier Ltd. All rights reserved.

Logged in as:
Ghazaleh Pourfallah
Curtin University
Account #:
3001190092

LOGOUT

Order Completed

Thank you for your order.

This Agreement between Curtin University -- Ghazaleh Pourfallah ("You") and Elsevier ("Elsevier") consists of your license details and the terms and conditions provided by Elsevier and Copyright Clearance Center.

Your confirmation email will contain your order number for future reference.

Printable details.

License Number	4185761117268
License date	Sep 11, 2017
Licensed Content Publisher	Elsevier
Licensed Content Publication	Dyes and Pigments
Licensed Content Title	Functionalized magnetic core–shell Fe3O4@SiO2 nanoparticles as selectivity-enhanced chemosensor for Hg(II)
Licensed Content Author	Xiaohong Peng,Yujiao Wang,Xiaoliang Tang,Weisheng Liu
Licensed Content Date	Oct 1, 2011
Licensed Content Volume	91
Licensed Content Issue	1
Licensed Content Pages	7
Type of Use	reuse in a thesis/dissertation
Portion	figures/tables/illustrations
Number of figures/tables/illustrations	1
Format	both print and electronic
Are you the author of this Elsevier article?	No
Will you be translating?	No
Original figure numbers	Scheme 1
Title of your thesis/dissertation	Magnetic nanochemosensors for selective detection of zinc ions in aqueous solutions.
Expected completion date	Sep 2017
Estimated size (number of pages)	150
Requestor Location	Curtin University Kent Street
	Bentley, WA 6102 Australia Attn: Curtin University
Total	0.00 USD

ORDER MORE   CLOSE WINDOW

Copyright agreement for Figure 1-9 in Chapter 1

Copyright Clearance Center

RightsLink®

| Home | Account Info | Help | ✉ |

Title: Bifunctional polydopamine@Fe3O4 core–shell nanoparticles for electrochemical determination of lead(II) and cadmium(II)

Author: Qian Song,Maoguo Li,Li Huang,Qikang Wu,Yunyou Zhou,Yinling Wang

Publication: Analytica Chimica Acta

Publisher: Elsevier

Date: 17 July 2013

Copyright © 2013 Elsevier B.V. All rights reserved.

Logged in as:
Ghazaleh Pourfallah
Curtin University
Account #:
3001190092

LOGOUT

Order Completed

Thank you for your order.

This Agreement between Curtin University -- Ghazaleh Pourfallah ("You") and Elsevier ("Elsevier") consists of your license details and the terms and conditions provided by Elsevier and Copyright Clearance Center.

Your confirmation email will contain your order number for future reference.

Printable details.

License Number	4185761344658
License date	Sep 11, 2017
Licensed Content Publisher	Elsevier
Licensed Content Publication	Analytica Chimica Acta
Licensed Content Title	Bifunctional polydopamine@Fe3O4 core–shell nanoparticles for electrochemical determination of lead(II) and cadmium(II)
Licensed Content Author	Qian Song,Maoguo Li,Li Huang,Qikang Wu,Yunyou Zhou,Yinling Wang
Licensed Content Date	Jul 17, 2013
Licensed Content Volume	787
Licensed Content Issue	n/a
Licensed Content Pages	7
Type of Use	reuse in a thesis/dissertation
Portion	figures/tables/illustrations
Number of figures/tables/illustrations	1
Format	both print and electronic
Are you the author of this Elsevier article?	No
Will you be translating?	No
Original figure numbers	Figure 2
Title of your thesis/dissertation	Magnetic nanochemosensors for selective detection of zinc ions in aqueous solutions.
Expected completion date	Sep 2017
Estimated size (number of pages)	150
Requestor Location	Curtin University Kent Street
	Bentley, WA 6102 Australia Attn: Curtin University
Total	0.00 USD

ORDER MORE   CLOSE WINDOW

Copyright agreement for Figure 1-10 in Chapter 1

Copyright Clearance Center

RightsLink®

Home   Account Info   Help

Title:	Functionalized magnetic core–shell Fe@SiO2 nanoparticles as recoverable colorimetric sensor for Co2+ ion
Author:	Uiseok Jeong, Hyeon Ho Shin, Younghun Kim
Publication:	Chemical Engineering Journal
Publisher:	Elsevier
Date:	1 December 2015

Copyright © 2015 Elsevier B.V. All rights reserved.

Logged in as:
Ghazaleh Pourfallah
Curtin University
Account #:
3001190092

LOGOUT

Order Completed

Thank you for your order.

This Agreement between Curtin University -- Ghazaleh Pourfallah ("You") and Elsevier ("Elsevier") consists of your license details and the terms and conditions provided by Elsevier and Copyright Clearance Center.

Your confirmation email will contain your order number for future reference.

Printable details.

License Number	4185750847163
License date	Sep 11, 2017
Licensed Content Publisher	Elsevier
Licensed Content Publication	Chemical Engineering Journal
Licensed Content Title	Functionalized magnetic core–shell Fe@SiO2 nanoparticles as recoverable colorimetric sensor for Co2+ ion
Licensed Content Author	Uiseok Jeong, Hyeon Ho Shin, Younghun Kim
Licensed Content Date	Dec 1, 2015
Licensed Content Volume	281
Licensed Content Issue	n/a
Licensed Content Pages	6
Type of Use	reuse in a thesis/dissertation
Portion	figures/tables/illustrations
Number of figures/tables/illustrations	1
Format	both print and electronic
Are you the author of this Elsevier article?	No
Will you be translating?	No
Original figure numbers	Fig.1
Title of your thesis/dissertation	Magnetic nanochemosensors for selective detection of zinc ions in aqueous solutions.
Expected completion date	Sep 2017
Estimated size (number of pages)	150
Requestor Location	Curtin University Kent Street
	Bentley, WA 6102 Australia Attn: Curtin University
Total	0.00 USD

ORDER MORE   CLOSE WINDOW

Copyright agreement for Figure 1-15 in Chapter 1

Copyright Clearance Center

RightsLink®

Home   Account Info   Help

Chemical Engineering Journal

Title: Selective Zn (II) chemosensor based on di(2-picolyl)amine functionalized inorganic/organic hybrid magnetic network

Author: Xianfei Zeng,Yang Zhou,Wenhui Ma,Shixing Wang,Keqiang Xie,Jijun Wu,Kuixian Wei

Publication: Chemical Engineering Journal

Publisher: Elsevier

Date: 15 May 2014

Copyright © 2014 Elsevier B.V. All rights reserved.

Logged in as:
Ghazaleh Pourfallah
Curtin University
Account #:
3001190092

LOGOUT

Order Completed

Thank you for your order.

This Agreement between Curtin University -- Ghazaleh Pourfallah ("You") and Elsevier ("Elsevier") consists of your license details and the terms and conditions provided by Elsevier and Copyright Clearance Center.

Your confirmation email will contain your order number for future reference.

Printable details.

License Number	4186260792144
License date	Sep 11, 2017
Licensed Content Publisher	Elsevier
Licensed Content Publication	Chemical Engineering Journal
Licensed Content Title	Selective Zn (II) chemosensor based on di(2-picolyl)amine functionalized inorganic/organic hybrid magnetic network
Licensed Content Author	Xianfei Zeng,Yang Zhou,Wenhui Ma,Shixing Wang,Keqiang Xie,Jijun Wu,Kuixian Wei
Licensed Content Date	May 15, 2014
Licensed Content Volume	244
Licensed Content Issue	n/a
Licensed Content Pages	7
Type of Use	reuse in a thesis/dissertation
Portion	figures/tables/illustrations
Number of figures/tables/illustrations	1
Format	both print and electronic
Are you the author of this Elsevier article?	No
Will you be translating?	No
Original figure numbers	Scheme 2
Title of your thesis/dissertation	Magnetic nanochemosensors for selective detection of zinc ions in aqueous solutions.
Expected completion date	Sep 2017
Estimated size (number of pages)	150
Requestor Location	Curtin University Kent Street
	Bentley, WA 6102 Australia Attn: Curtin University
Total	0.00 USD

ORDER MORE   CLOSE WINDOW

Copyright agreement for Chapter 2

RightsLink®

Home Account Info Help

Title: A novel recyclable magnetic nanostructure for highly sensitive, selective and reversible detection of zinc ions in aqueous solutions

Author: Ghazaleh Pourfallah, Xia Lou

Publication: Sensors and Actuators B: Chemical

Publisher: Elsevier

Date: 5 October 2016

© 2016 Elsevier B.V. All rights reserved.

Order Completed

Thank you for your order.

This Agreement between Curtin University -- Ghazaleh Pourfallah ("You") and Elsevier ("Elsevier") consists of your license details and the terms and conditions provided by Elsevier and Copyright Clearance Center.

Your confirmation email will contain your order number for future reference.

Printable details.

License Number	4179211489334
License date	Aug 31, 2017
Licensed Content Publisher	Elsevier
Licensed Content Publication	Sensors and Actuators B: Chemical
Licensed Content Title	A novel recyclable magnetic nanostructure for highly sensitive, selective and reversible detection of zinc ions in aqueous solutions
Licensed Content Author	Ghazaleh Pourfallah, Xia Lou
Licensed Content Date	Oct 5, 2016
Licensed Content Volume	233
Licensed Content Issue	n/a
Licensed Content Pages	9
Type of Use	reuse in a thesis/dissertation
Portion	full article
Format	electronic
Are you the author of this Elsevier article?	Yes
Will you be translating?	No
Title of your thesis/dissertation	Magnetic nanochemosensors for selective detection of zinc ions in aqueous solutions.
Expected completion date	Sep 2017
Estimated size (number of pages)	150
Requestor Location	Curtin University Kent Street Bentley, WA 6102 Australia Attn: Curtin University
Total	0.00 USD

ORDER MORE   CLOSE WINDOW

APPENDIX 2

This paper is pubished based on the achievements in chapter 2

A novel recyclable magnetic nanostructure for highly sensitive, selective and reversible detection of zinc ions in aqueous solutions

Ghazaleh Pourfallah, Xia Lou *

Department of Chemical Engineering, Curtin University, Kent Street, Bentley, WA 6102, Australia

ABSTRACT

The synthesis and characterisation of a novel dansylated magnetic nanostructure, namely $Fe_3O_4@SiO_2$-PEG-DnS, is reported here. Investigations of its fluorescent properties showed that the presence of the PEG moiety significantly enhanced the fluorescent intensity of the nanostructure when compared to both the free dansyl fluorophore and a nanostructure that contained no PEG spacer between the core and the attached dansyl group. The addition of zinc (Zn^{2+}) ions to the aqueous suspension of $Fe_3O_4@SiO_2$-PEG-DnS led to a 12.5-fold decrease in intensity. The quenching was selective to only Zn^{2+}. No interference was observed by other examined metal cations, including cadmium (Cd^{2+}). A very low detection limit of 6.00 nM in relation to zinc ions was demonstrated. In addition, the newly developed magnetic nanostructured chemosensor was found to be highly stable, reusable and recoverable.

© 2016 Elsevier B.V. All rights reserved.

1. Introduction

Developing sensors that can selectively detect zinc ions (Zn^{2+}) at low concentrations in aqueous solutions has always been an attractive topic for those who value the significance of zinc to the life sciences, mineral exploration and environmental sustainability [1,2]. Small-molecule fluorescent chemosensors are rather simple to use and have been widely used for cation detection with moderately high selectivity and sensitivity [3]. Many efforts have been focused on the development of smart fluorophores for Zn^{2+} detection, which include BODIPY [4,5], quinolone [6,7] and coumarin [8]. Despite all efforts to date, the development of a cost-effective and highly sensitive and selective chemosensor for Zn^{2+} detection remains a challenge. Magnetic core-shell nanostructures have been reported to offer recyclability/reusability of many nanomaterials, including the chemosensors, via an external magnetic field [9–11]. In many of the studies, a silica shell commonly has been used to provide stability and hydrophilicity to the magnetic nanoparticles, and to prevent possible interactions between the magnetic core and the additional functional moieties that are directly immobilised on the silica surface [12,13]. Various silicane precursors can be covalently bonded to the silica shell, providing sites for further functionalisation via simple methods [12,14,15].

In this paper, the synthesis and characterisation of a novel magnetic core-shell nanostructure, $Fe_3O_4@SiO_2$-PEG-DnS, which contains a dansyl fluorophore via a poly(ethyleneglycol) (PEG) spacer, is reported. Dansyl chloride (DnCl) is a well-established fluorophore that has been widely used for the labelling and detection of amino acids, proteins and drugs [11,16,17]. It offers a large Stokes shift [18], a charge-transfer character [19] with high emission quantum yield [20] and the synthetic flexibility of the sulfonic acid group. Dansyl groups can be excited at around 325 nm, producing emission maxima typically near 510 nm [16,18]. Despite numerous attempts in regard to biological applications, the exploration of interactions between dansyl fluorophores and metal ions has been limited to small organic molecules. An early work by Schuster et al. [21] reported the complexation of Ni(II) and Cu(II) with N-dansyl-N'-ethylthiourea (DET) fluorophore, which resulted in quenching of the fluorescence. Prodi and co-workers [22] reported the synthesis of a tripodal ligand containing dansyl fluorophore, and the observation of a blue shift accompanied by an enhanced fluorescence after the addition of Zn^{2+} into the produced fluorescent molecule. Shankar et al. [23] also developed a number of dansylated chemosensors that demonstrated an effective interaction with Cu(II) by quenching of the emission intensity. PEG is hydrophilic and chemically inert. The purposes of incorporating PEG onto the surfaces of the nanoparticles include: 1) improving the stability of, and offering wettability to, the magnetic core; 2) improving the mobility of the dansyl fluorophore moiety; and 3) spatially separating the dansyl fluorophore from the magnetic core, therefore reducing the probability of core-fluorophore interactions.

---

* Corresponding author.
  E-mail addresses: x.lou@curtin.edu.au, lizilou7854@gmail.com (X. Lou).

A similar structure, $Fe_3O_4@SiO_2$-DnS, which contains no PEG spacer, also was synthesised and investigated alongside $Fe_3O_4@SiO_2$-PEG-DnS. The fluorescence spectra of the produced nanochemosensors and their interactions with various metal cations in aqueous solutions were further investigated. Selective interactions with Zn^{2+} have been observed. Changes in fluorescent intensity as a consequence of protonation and/or selective interaction with Zn^{2+} were investigated. The nanochemosenors, in particular the one containing PEG spacers, have shown a very low detection limit of 6 nM that is selective towards zinc ions, as well as very high reversibility and good recyclability.

2. Experimental

2.1. Materials

Sigma-Aldrich was the supplier of all chemicals used: Ferric chloride hexahydrate ($FeCl_3 \cdot 6H_2O$, 99.99%), ferrous chloride tetrahydrate ($FeCl_2 \cdot 4H_2O$, 99.99%), citric acid (99.5%), dansyl chloride (DnCl) (99.99%), tetraethoxysilane (TEOS) (99.99%), (3-glycidyloxypropyl) trimethoxylsilane (GPS) (98%), (3-aminopropyl) triethoxysilane (APS) (98%), ethanol (99.5%), O-(2-aminoethyl) polyethylene glycol ($M_w = 3000$), ammonium hydroxide (99.99%). All reagents were used, as received, without further purification. Deionised (D.I.) water was used in all experiments.

2.2. Synthesis of magnetic Fe_3O_4 nanoparticles

$FeCl_3 \cdot 6H_2O$ (2.7 g, 10 mmol) and $FeCl_2 \cdot 4H_2O$ (0.99 g, 5 mmol) were dissolved in 10 ml HCl solution (2 M) under vigorous stirring and nitrogen bubbling. The Fe^{2+}/Fe^{3+} solution then was added, dropwise, to 50 ml sodium hydroxide solution (0.5 M) and allowed to proceed for 1 h under mechanical stirring. After completion of the reaction, the black precipitate was isolated via an external magnet and washed sequentially four times, with 20 ml D.I. water then 20 ml ethanol each time. In order to obtain well-dispersed magnetic nanoparticles, particles were added to 2 ml citric acid solution (0.1 M) with ultrasonic treatment for 30 min. Then the mixture was maintained at room temperature for 12 h. Finally, nanoparticles were rinsed with D.I. water (4×20 ml), collected from the reaction mixture by an external magnet and dispersed as a suspension in D.I. water.

2.3. Synthesis of core/shell-structured $Fe_3O_4@SiO_2$-APS and $Fe_3O_4@SiO_2$-GPS

Silanisation of the produced Fe_3O_4 nanoparticles was carried out using a previously reported method [12,24]. Fe_3O_4 nanoparticles (0.5 g, 2.16 mmol) were dispersed in a mixture of ethanol/water (30 ml, 2:1 ratio) and 1 ml ammonium hydroxide solution (25 wt%) under mechanical stirring for 1 h. TEOS (0.5 ml, 2.25 mmol) was mixed with 5 ml ethanol, and the mixture was added, dropwise, to the prepared dispersion of Fe_3O_4 nanoparticles. The reaction then was allowed to proceed for 2 h, under stirring at room temperature, to obtain silica-coated Fe_3O_4 nanoparticles: $Fe_3O_4@SiO_2$. Amino functionalisation of $Fe_3O_4@SiO_2$ was achieved by the dropwise addition of a mixture of APS (1.05 ml, 4.5 mmol) and 5 ml ethanol into the $Fe_3O_4@SiO_2$ solution, and the reaction was carried out for 2 h under stirring. The obtained functionalised magnetic nanoparticles, $Fe_3O_4@SiO_2$-APS, were removed from the reaction mixture by applying an external magnet. They were washed sequentially with 20 ml D.I. water then 20 ml ethanol, four times, and suspended in D.I. water.

Epoxy-functionalised nanoparticles, $Fe_3O_4@SiO_2$-GPS, were prepared by adding a solution of GPS (1.17 ml, 4.5 mmol) to

the mixture, following the same procedure that was used for $Fe_3O_4@SiO_2$-APS. The resultant and purified $Fe_3O_4@SiO_2$-GPS also was suspended in D.I. water for further analyses.

2.4. Synthesis of $Fe_3O_4@SiO_2$-DnS

$Fe_3O_4@SiO_2$-APS (15 mg) was dispersed in 30 ml dry acetone. (The dry acetone was prepared through distillation of acetone after drying with calcium chloride overnight.) Triethylamine (0.5 ml, 3.58 mmol) then was added to the dispersion, and the solution was sonicated for 30 min. DnCl (45 mg, 0.166 mmol) was dissolved in 20 ml dry acetone and then added to the $Fe_3O_4@SiO_2$-APS dispersion. The mixture then was stirred at room temperature, in the dark, for 24 h. The product, $Fe_3O_4@SiO_2$-DnS, was separated from the solution via an external magnet and washed sequentially with 20 ml each of acetone, ethanol and D.I. water in repetition for a total of four times.

2.5. Synthesis of $Fe_3O_4@SiO_2$-PEG-DnS

The synthesis of $Fe_3O_4@SiO_2$-PEG-DnS was carried out in two stages. Firstly, pegylated $Fe_3O_4@SiO_2$-GPS was prepared by dispersing 0.45 g of $Fe_3O_4@SiO_2$-GPS in 10 ml D.I. water, to which O-(2-aminoethyl) polyethylene glycol (0.135 g dissolved in 10 ml D.I. water) was added under stirring at 65 °C and further stirred for 6 h at the same temperature. After collection via external magnet, the resultant $Fe_3O_4@SiO_2$-GPS-PEG was repeatedly washed with fresh D.I. water (4×20 ml). Then the D.I. water was sequentially substituted with acetone and dry acetone prior to the dansylation. Dansylation of the $Fe_3O_4@SiO_2$-GPS-PEG nanoparticles was carried out using the same procedure that was applied to $Fe_3O_4@SiO_2$-APS. The final product, $Fe_3O_4@SiO_2$-PEG-DnS, then was washed and kept as a suspension in D.I. water.

2.6. Physicochemical characterisation

Fourier transform infrared (FTIR) spectra of the products were obtained using a Thermo Scientific Nicolet iS50 for the qualitative analysis of the synthesised nanostructures. All spectra were recorded in the range of 400–4000 cm^{-1}. X-ray diffraction (XRD) analysis was performed using a Bruker AXS diffractometer with Co Kα radiation ($\lambda = 1.79$ Å). A scan rate of 0.015°/s was used to record the patterns in a 2θ range of 20–80°, and the accelerating voltage and current were 35 kV and 40 mA, respectively.

The produced samples also were examined using a Lambda 25 Perkin Elmer UV–vis Spectroscope. Scans were recorded in the wavelength range from 200 to 800 nm, with a band width of 1 nm. The size and morphology of the synthesised nanoparticles were examined using a Transmission Electron Microscope (TEM, (JEOL JSM 2011)) that was equipped with a Gatan Digital Camera. Samples were suspended in ethanol and distributed onto a carbon-coated copper grid. The TEM images were recorded at an accelerating voltage of 200 kV. For nanoparticles size measurement, thirty particles were randomly selected and the average of the thirty measurements was representatively used as the size of nanoparticles.

2.7. Fluorescence measurements

A PerkinElmer L55 fluorescence spectrometer was used, with an excitation source set at 325 nm and a scanning rate of 5 nm/min. The emission intensities of $Fe_3O_4@SiO_2$-DnS at 0.3 μM of the fluorophore (0.1 mg mL^{-1}) and $Fe_3O_4@SiO_2$-PEG-DnS at 0.3 μM of the fluorophore (0.043 mg mL^{-1}) were measured both before and after being mixed with a variety of metal ions, namely Ag^+, Li^+, Cu^{2+}, Ni^{2+}, Co^{2+}, Ca^{2+}, Cd^{2+}, Hg^{2+}, Mg^{2+}, Fe^{2+}, Mn^{2+}, Al^{3+}, Cr^{3+} and Fe^{3+}, in an

aqueous solution (0.9 μM). A competition study also was carried out using aqueous solutions containing mixed metal ions.

2.8. Quantum yield measurements

Fluorescent quantum yield was examined by comparison with standard quinine sulfate dihydrate solution, using a reported method [18,25]. In brief, the stock solution (100 mg/L) was made by dissolving 5 mg quinine sulfate dihydrate in 50 ml 0.1 M H_2SO_4 solution. UV–vis and fluorescent spectra (excited at 325 nm) were measured for the same solution. The two newly produced nanochemosensors were dispersed in aqueous solution and further diluted to 1 mg/L then subjected to the same measurements. The quantum yields of the nanochemosensors were calculated using Eq. (1):

$$\Phi = \Phi_R \frac{I A_R n^2}{I_R A n_R^2} \tag{1}$$

where Φ is the quantum yield of the nanoparticles, I is the integrated intensity, A is the optical density from the UV–vis measurement and n is the refractive index of the solvent. The subscript, R, refers to the reference fluorophore, quinine sulfate dihydrate, with a known quantum yield [18]. In this expression, it is assumed that the sample and reference are excited at the same wavelength, so that it is not necessary to correct for the different excitation intensities of different wavelengths.

2.9. Job plot measurements

Various volumes (5, 4.5, 4, 3.5, 3, 2.5, 2, 1.5, 1 and 0.5 ml) of the produced nanochemosenors (0.3 μM, aqueous) were taken and transferred to separate vials, to which Zn^{2+} solutions (0.3 μM, aqueous) with volumes of 0, 0.5, 1, 1.5, 2, 2.5, 3, 3.5, 4 and 4.5 ml, respectively, were added. Therefore, each vial had a total volume of 5 ml solution. The fluorescent intensity of each solution was recorded and plotted against the molar fraction of Zn^{2+}.

2.10. Recovery test

The recovery of $Fe_3O_4@SiO_2$-PEG-DnS was carried out by following these four steps: 1) placing 5 ml suspension of $Fe_3O_4@SiO_2$-PEG-DnS (0.3 μM) into a vial; 2) mixing it with 5 ml Zn^{2+} solution (0.9 μM); 3) adding an equivalent amount of EDTA (5 ml, 0.9 μM) into the step 2 mixture; and 4) recovering and resuspending $Fe_3O_4@SiO_2$-PEG-DnS in 5 ml water by use of an external magnet followed by washing (3 × 5 ml D.I. water). The florescent intensity of the solution was recorded at each step. The procedure was repeated on the recovered nanosensor particles for another four cycles. In each cycle, three vials were used in parallel. The average of the three measurements was used for comparison. The mass of the recovered nanosensor particles also was recorded at the end of cycles 1, 3 and 5, each time using sample from one vial only.

3. Results and discussions

3.1. Synthesis and characterisation of $Fe_3O_4@SiO_2$-DnS and $Fe_3O_4@SiO_2$-PEG-DnS

Two nanostructured magnetic chemosensors were produced using a facile synthetic pathway, displayed in Scheme 1. The synthetic pathway involved, firstly, the preparation of magnetic iron oxide (Fe_3O_4) nanoparticles that were coated with a thin shell of silica, containing either 1-aminopropyl or 3-glycidyloxypropyl functional groups, for further functionalisation. TEOS and either APS or GPS were used simultaneously in these reactions [15]. The produced functionalised silica-iron oxide
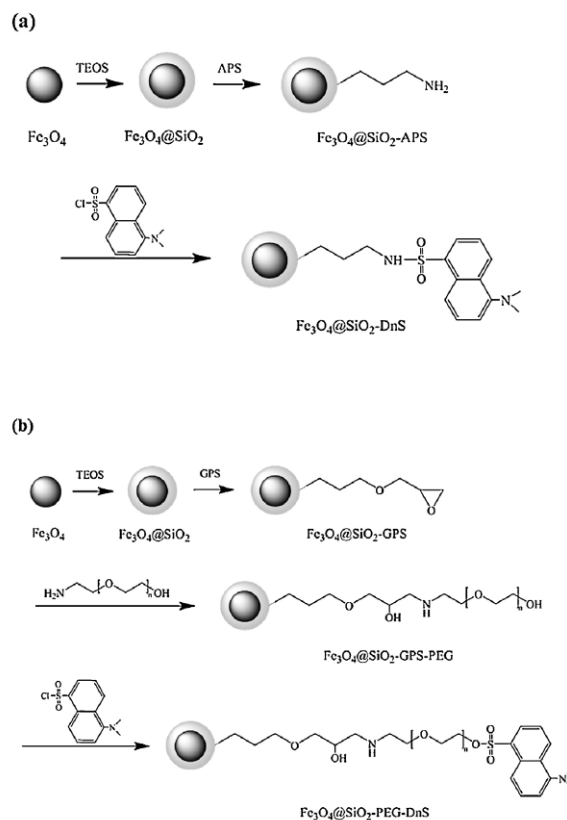
Scheme 1. Synthetic pathways for the dansylated magnetic nanochemosensors.

nanoparticles, $Fe_3O_4@SiO_2$-APS, were conjugated with dansyl chloride to produce the chemosensor, $Fe_3O_4@SiO_2$-DnS, containing no PEG spacer (Scheme 1(a)). The GPS-functionalised silica-iron oxide nanoparticles, $Fe_3O_4@SiO_2$-GPS, were first conjugated with aminated PEG, and then esterified with DnCl to produce the dansylated magnetic chemosensor containing PEG spacer, $Fe_3O_4@SiO_2$-PEG-DnS (Scheme 1(b)).

TEM micrographs of the nanoparticles produced at each stage of synthesis are shown in Fig. 1. The average size of the original Fe_3O_4 nanoparticles was 8 ± 3 nm. However, the size of nanoparticles increased at each subsequent stage of the chemical reactions, due to the added silica coating and organic functional groups on the surfaces of the nanoparticles. For the final products, $Fe_3O_4@SiO_2$-PEG-DnS and $Fe_3O_4@SiO_2$-DnS, the particle sizes were 33 ± 6 and 28 ± 4 nm, respectively. The presence of silica shell was well-demonstrated in all coated nanoparticles and is evident in the EDS spectrum of $Fe_3O_4@SiO_2$-GPS, compared with no silica present in the EDS spectrum of plain Fe_3O_4 nanoparticles.

Fig. 2(a) shows the FTIR spectra of $Fe_3O_4@SiO_2$-DnS and the related compounds. An absorbance at 561 cm^{-1}, which can be seen in all compounds, is associated with the stretching and vibration of Fe-O bonds. The typical vibration and stretching band of Si-O-Si at 1079 cm^{-1} can be seen in both $Fe_3O_4@SiO_2$-APS and $Fe_3O_4@SiO_2$-DnS. For the former, absorption bands at 2927 and 2861 cm^{-1} can be attributed to the C—H asymmetric and symmetric stretching vibrations of the C—H within the APS. The characteristic band at 1524 cm^{-1} is attributable to the N—H bending of primary amines. For $Fe_3O_4@SiO_2$-DnS, the S—O stretching vibrations at 1210 cm^{-1}

(a)

(b)

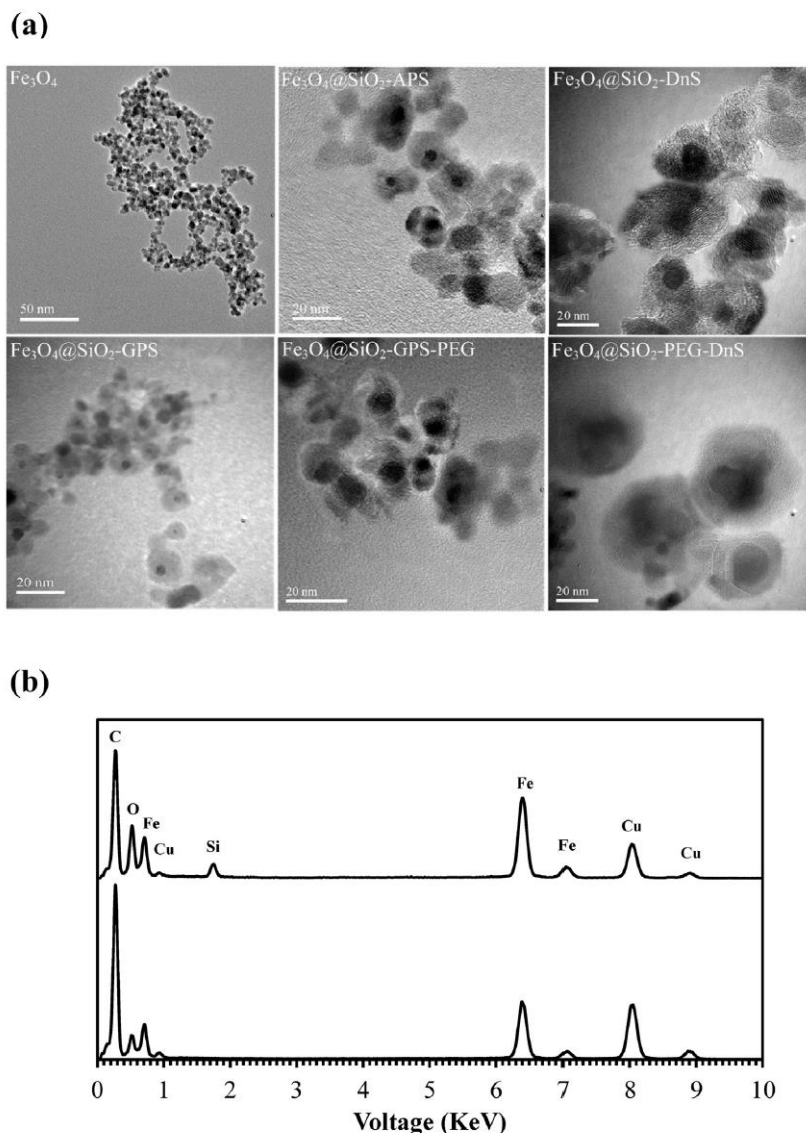
Fig. 1. (a) TEM images of magnetic nanoparticles, (b) EDS spectrum of Fe_3O_4 and Fe_3O_4@SiO_2-GPS. Cu and C in EDS spectrum are from the copper grid and carbon coating on the copper, respectively.

and the C—N vibrations at $1150\,cm^{-1}$ due to the presence of the dansylate group are well-demonstrated.

Fig. 2(b) displays FTIR spectra of all compounds related to the production of Fe_3O_4@SiO_2-PEG-DnS. The existence of GPS on Fe_3O_4@SiO_2 is confirmed by the presence of a new band at $903\,cm^{-1}$, representing the epoxy group. Absorption bands at 2927 and $2861\,cm^{-1}$ also can be observed, attributable to the C—H stretching vibrations of GPS. After conjugation of PEG moieties onto the Fe_3O_4@SiO_2-GPS, the absorption band corresponding to the epoxy group disappears and an additional band at $3248\,cm^{-1}$ is apparent, which supports the existence of N—H bending of the secondary amine. The stretching vibrations of S-O at $1210\,cm^{-1}$ and C—N at $1150\,cm^{-1}$ also can be seen in the spectra, denoting the attachment of dansyl groups.

The powder X-ray diffraction patterns of Fe_3O_4 nanoparticles and the functional nanosensors, Fe_3O_4@SiO_2-DnS and Fe_3O_4@SiO_2-PEG-DnS, are shown in Fig. 3. As can be seen, all samples possess the characteristic diffraction peaks at (2 2 0), (3 1 1), (4 0 0), (4 2 2), (5 1 1) and (4 4 0), which are in good agreement with pure cubic Fe_3O_4 [26]. The broad peak appearing at 20–28° in the spectra for the two nanosensors corresponds to the amorphous-state silica layer and the spacer/linker attached to it, which indicates that the Fe_3O_4 magnetic cores have been successfully coated by a layer of SiO_2 and other functional groups. The XRD patterns of the nanosensors are similar to that of plain Fe_3O_4, demonstrating that the organic modification process does not induce any phase change of the Fe_3O_4 nanoparticles.
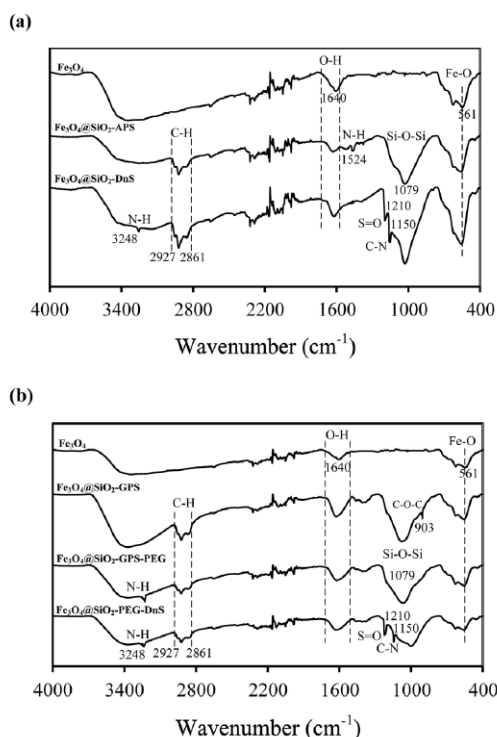
(a)

(b)

Fig. 2. FTIR spectra of all nanoparticles related to (a) $Fe_3O_4@SiO_2$-DnS and (b) $Fe_3O_4@SiO_2$-PEG-DnS.

Fig. 3. XRD patterns of Fe_3O_4, $Fe_3O_4@SiO_2$-DnS and $Fe_3O_4@SiO_2$-PEG-DnS.

The UV–vis spectra displayed in Fig. 4(a) further reveal the successful synthesis of $Fe_3O_4@SiO_2$-DnS and $Fe_3O_4@SiO_2$-PEG-DnS. As can be seen from the figure, free dansyl chloride exhibits absorption bands at λ_{max} = 230 and 325 nm, which correspond to π-π^* and n-π^* orbital transitions, respectively [11]. Both bands appear in $Fe_3O_4@SiO_2$-DnS and $Fe_3O_4@SiO_2$-PEG-DnS, due to the formation of dansylated species.

TGA analysis of $Fe_3O_4@SiO_2$-PEG-DnS, and its intermediates (Fig. 4(b)), revealed a weight loss at 35–100 °C, corresponding to the evaporation of the physically adsorbed water, and a more significant weight loss at the temperature range of 200 °C to 800 °C. An estimation based on these data indicates that the mole concentration of dansyl group on the surface of $Fe_3O_4@SiO_2$-PEG-DnS was approximately 6.66×10^{-6} mmol/mg nanoparticles. A similar analysis was performed on $Fe_3O_4@SiO_2$-DnS. The obtained mole concentration of dansyl group was only 3.13×10^{-6} mmol/mg
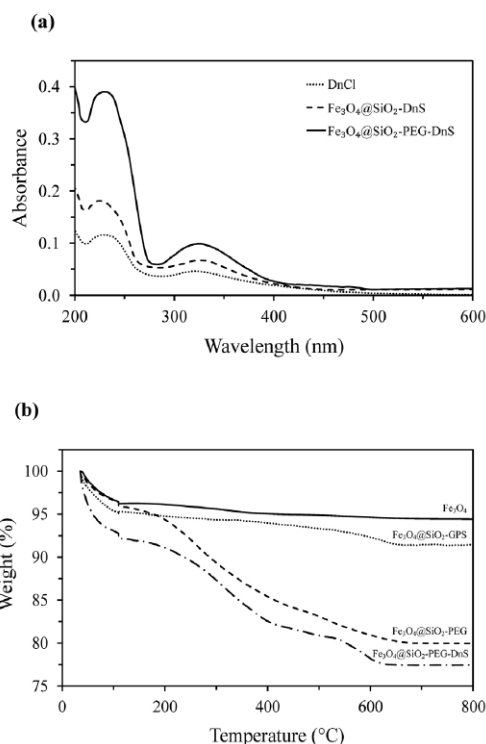
(a)

(b)

Fig. 4. (a) UV–vis spectra of DnCl, $Fe_3O_4@SiO_2$-DnS and $Fe_3O_4@SiO_2$-PEG-DnS and (b) thermal curves showing thermogravimetric loss of $Fe_3O_4@SiO_2$-PEG-DnS at various temperature ranges.

nanoparticles, which is half the value demonstrated by the DnS attached to $Fe_3O_4@SiO_2$-PEG-DnS.

The presence of the DnS fluorophore on the surfaces of nanoparticles was further quantified by establishing a UV–vis calibration curve at λ_{max} = 325 nm, with different molar concentrations of DnCl. The numbers of DnCl molecules attached to chemosensors were then calculated by taking the ratios of the molar concentration of DnCl obtained from the UV-calibration curve (at λ = 325 nm) to each of the initial mass concentrations of chemosensors, resulting in the numbers for $Fe_3O_4@SiO_2$-DnS and $Fe_3O_4@SiO_2$-PEG-DnS, respectively, being 3.00×10^{-6} mmol/mg and 6.92×10^{-6} mmol/mg. These results are in agreement with those obtained from TGA.

Thus, the number of DnS molecules attached to a unit mass of $Fe_3O_4@SiO_2$-PEG-DnS is twice that for $Fe_3O_4@SiO_2$-DnS. This could be attributed to the presence of the PEG spacer in the former. Having PEG as an inert and hydrophilic spacer causes the dansylation reaction to be more facile in an aqueous environment. On the other hand, the direct attachment of DnS onto the surface of the core-shell nanostructure could be sterically hindered. For the examinations via fluorescent microscopy, discussed in the following sections, equal molar concentrations of DnS fluorophore were used for comparison.

3.2. Fluorescence studies

Fig. 5(a) shows the fluorescent responses of DnCl, $Fe_3O_4@SiO_2$-PEG, $Fe_3O_4@SiO_2$-DnS and $Fe_3O_4@SiO_2$-PEG-DnS in aqueous solutions. The fluorescent spectra were obtained using compounds containing the same amounts of DnS (0.3 μM), with the exception
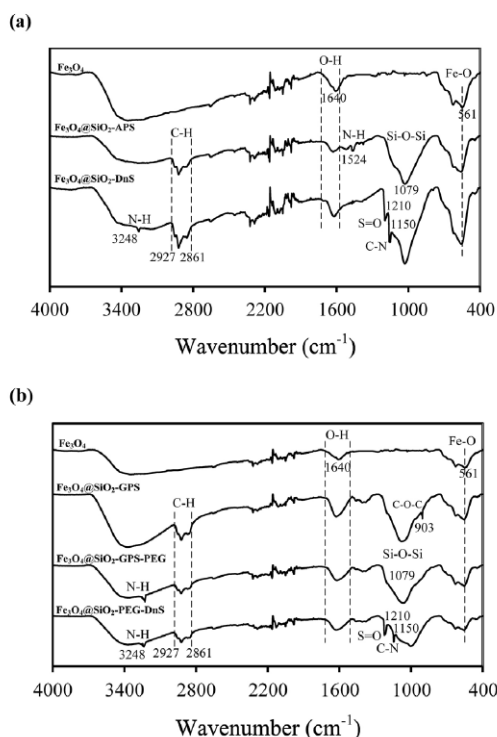
(a)

(b)

Fig. 2. FTIR spectra of all nanoparticles related to (a) $Fe_3O_4@SiO_2$-DnS and (b) $Fe_3O_4@SiO_2$-PEG-DnS.

Fig. 3. XRD patterns of Fe_3O_4, $Fe_3O_4@SiO_2$-DnS and $Fe_3O_4@SiO_2$-PEG-DnS.

The UV–vis spectra displayed in Fig. 4(a) further reveal the successful synthesis of $Fe_3O_4@SiO_2$-DnS and $Fe_3O_4@SiO_2$-PEG-DnS. As can be seen from the figure, free dansyl chloride exhibits absorption bands at λ_{max} = 230 and 325 nm, which correspond to π-π^* and n-π^* orbital transitions, respectively [11]. Both bands appear in $Fe_3O_4@SiO_2$-DnS and $Fe_3O_4@SiO_2$-PEG-DnS, due to the formation of dansylated species.

TGA analysis of $Fe_3O_4@SiO_2$-PEG-DnS, and its intermediates (Fig. 4(b)), revealed a weight loss at 35–100 °C, corresponding to the evaporation of the physically adsorbed water, and a more significant weight loss at the temperature range of 200 °C to 800 °C. An estimation based on these data indicates that the mole concentration of dansyl group on the surface of $Fe_3O_4@SiO_2$-PEG-DnS was approximately 6.66×10^{-6} mmol/mg nanoparticles. A similar analysis was performed on $Fe_3O_4@SiO_2$-DnS. The obtained mole concentration of dansyl group was only 3.13×10^{-6} mmol/mg
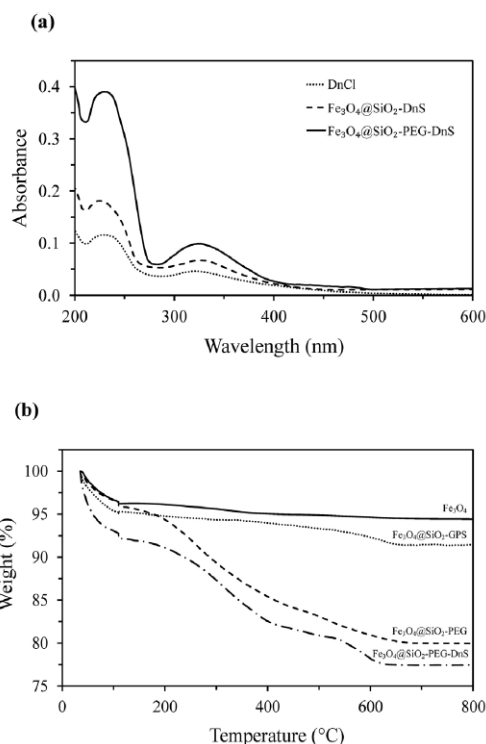
(a)

(b)

Fig. 4. (a) UV–vis spectra of DnCl, $Fe_3O_4@SiO_2$-DnS and $Fe_3O_4@SiO_2$-PEG-DnS and (b) thermal curves showing thermogravimetric loss of $Fe_3O_4@SiO_2$-PEG-DnS at various temperature ranges.

nanoparticles, which is half the value demonstrated by the DnS attached to $Fe_3O_4@SiO_2$-PEG-DnS.

The presence of the DnS fluorophore on the surfaces of nanoparticles was further quantified by establishing a UV–vis calibration curve at λ_{max} = 325 nm, with different molar concentrations of DnCl. The numbers of DnCl molecules attached to chemosensors were then calculated by taking the ratios of the molar concentration of DnCl obtained from the UV-calibration curve (at λ = 325 nm) to each of the initial mass concentrations of chemosensors, resulting in the numbers for $Fe_3O_4@SiO_2$-DnS and $Fe_3O_4@SiO_2$-PEG-DnS, respectively, being 3.00×10^{-6} mmol/mg and 6.92×10^{-6} mmol/mg. These results are in agreement with those obtained from TGA.

Thus, the number of DnS molecules attached to a unit mass of $Fe_3O_4@SiO_2$-PEG-DnS is twice that for $Fe_3O_4@SiO_2$-DnS. This could be attributed to the presence of the PEG spacer in the former. Having PEG as an inert and hydrophilic spacer causes the dansylation reaction to be more facile in an aqueous environment. On the other hand, the direct attachment of DnS onto the surface of the core-shell nanostructure could be sterically hindered. For the examinations via fluorescent microscopy, discussed in the following sections, equal molar concentrations of DnS fluorophore were used for comparison.

3.2. Fluorescence studies

Fig. 5(a) shows the fluorescent responses of DnCl, $Fe_3O_4@SiO_2$-PEG, $Fe_3O_4@SiO_2$-DnS and $Fe_3O_4@SiO_2$-PEG-DnS in aqueous solutions. The fluorescent spectra were obtained using compounds containing the same amounts of DnS (0.3 μM), with the exception
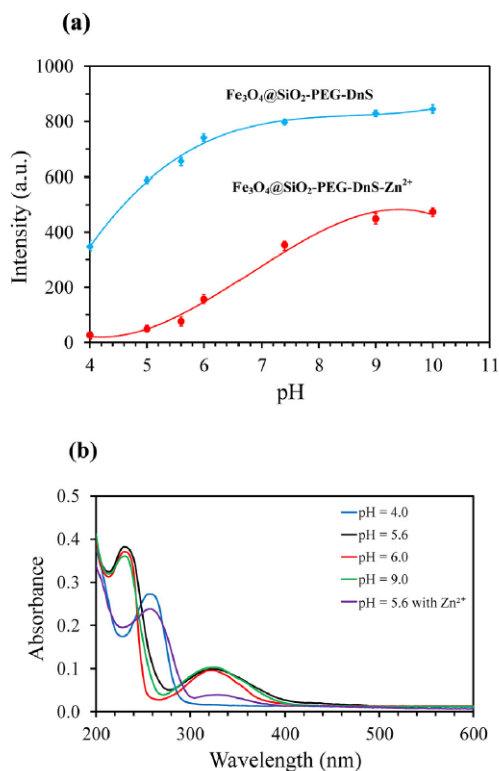
Fig. 6. (a) Fluorescent intensity of $Fe_3O_4@SiO_2$-PEG-DnS at different pH values and (b) absorption spectra of $Fe_3O_4@SiO_2$-PEG-DnSunder various conditions. Both are contrasted with results upon the addition of 3.0 equiv. of Zn^{2+}.

the pH value upon the absorption wavelength. The n-π^* absorption band at $\lambda = 325$ nm completely disappears at pH = 4. Only the π-π^* transition of the naphthalene ring is present. However, at pH = 6 and 9, there are no significant changes in the absorption spectra, indicating no modification within the naphthalene ring [19,22]. Similar results were observed for $Fe_3O_4@SiO_2$-DnS.

It should be noted that fluorescent quenching by Cu^{2+} and Fe^{3+} also is demonstrated in Fig. 5(a) and (b), but by a much smaller amount. This can be attributed to the redox activity of these cations, owing to their partially filled 3d shells, which allows an electron exchange between the fluorophore and the cation via nonradiative energy transfer [12,24,34,35]. There was no significant change in the emission intensity after the addition of other metal ions, indicating a lack of interaction between those cations and the dansylated chemosensors. Moreover, both chemosensors

could selectively distinguish between Zn^{2+} and Cd^{2+}, which is an extra benefit of the produced chemosensors. Cd^{2+} often demonstrates coordination properties similar to those of Zn^{2+}, due to both having a d^{10} electron configuration [36].

The fluorescent quantum yield also was determined using quinine sulfate in 0.1 M H_2SO_4 ($\Phi = 0.57$) [18] as a reference standard. The results obtained from Eq. (1) show the highest emission quantum yield for $Fe_3O_4@SiO_2$-PEG-DnS ($\Phi = 0.39$), when compared with those of $Fe_3O_4@SiO_2$-DnS ($\Phi = 0.28$) and free DnCl ($\Phi = 0.07$). A Job plot was obtained to demonstrate the stoichiometry of the complexation between the nanosensors and Zn^{2+} (Fig. 7(a)). A stoichiometric ratio of 2:1 was confirmed between the nanosensors and Zn^{2+}.

To further investigate sensing properties quantitatively, fluorescence titration was performed on both nanochemosensors (0.3 μM) by varying the concentrations of Zn^{2+} (0–5 μM) in aqueous solution. Briefly, 2.5 ml of each of the Zn^{2+} concentrations was added to 2.5 ml of nanochemosensor solution to make a 5 ml total solution of each. The fluorescent responses of $Fe_3O_4@SiO_2$-DnS and $Fe_3O_4@SiO_2$-PEG-DnS are shown in Fig. 7(b) and (c), respectively. A gradual decrease is seen in the fluorescent intensity of both chemosensors upon the addition of Zn^{2+}, until saturated, indicating quantitatively that Zn^{2+} is bonded to the dansyl units. A detection limit was determined by comparing the fluorescent intensities of the produced nanochemosensors with those of quenched solutions. The minimum Zn^{2+} concentration that resulted in a distinguishable intensity difference (confirmed by students using a t-test with p < 5%) was taken as the detection limit. This is equivalent to 12.5 nM for $Fe_3O_4@SiO_2$-DnS and 6.25 nM for $Fe_3O_4@SiO_2$-PEG-DnS, which are both much lower values than that reported for Zn^{2+} detection (18.2 nM) in the open literature [37–39].

Competition studies also were carried out by treating the nanochemosensor with 3.0 eq. of Zn^{2+} in the presence of identical amounts of other metal ions (as listed earlier) at the same concentrations. As shown in Fig. 8(a) and (b), most background metal ions demonstrated little or no obvious interference with the detection of Zn^{2+} ions. An apparent interference by Fe^{3+} and Cu^{2+} was shown to be due to the previously explained quenching nature of the two metal ions, indicating a more favourable interaction of the nanofluorophore with Fe^{3+} and Cu^{2+} and, therefore, a reduced quenching effect by the Zn^{2+}. The interference by Fe^{3+} and Cu^{2+} was less effective when the pegylated nanochemosensor was used, which is attributable to its more sensitive nature.

Reusability and regeneration is one the key factors in designing nanosensors for practical applications. The recovery of $Fe_3O_4@SiO_2$-PEG-DnS was examined throughout five cycles. For each cycle, the nanosensor was freed from the Zn^{2+} ions by treating each solution with EDTA in base (pH = 8) conditions. The fluorescent intensity was examined and a 98.3% recovery was observed after five cycles (Fig. 8(c)). The mass recoverability also was examined, and was found to be 94.0%, 88.8% and 76.4% after the 1st, 3rd and 5th cycles, respectively. The results demonstrated the excellent

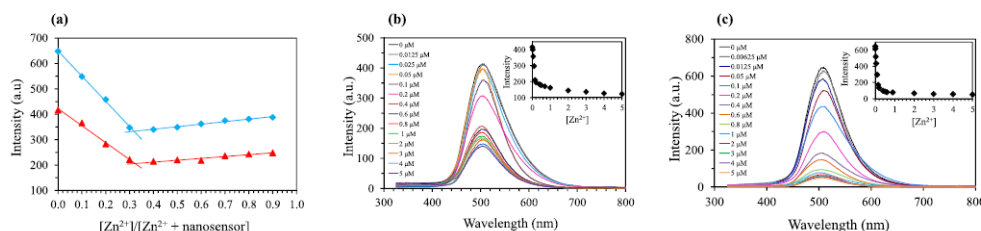**Fig. 7.** (a) The Job plot of $Fe_3O_4@SiO_2$-DnS and $Fe_3O_4@SiO_2$-PEG-DnS, and fluorescence spectra of (b) $Fe_3O_4@SiO_2$-DnS and (c) $Fe_3O_4@SiO_2$-PEG-DnS, all upon the addition of Zn^{2+} (0–5 μM) in aqueous solution. Sensor concentration is 0.3 μM.
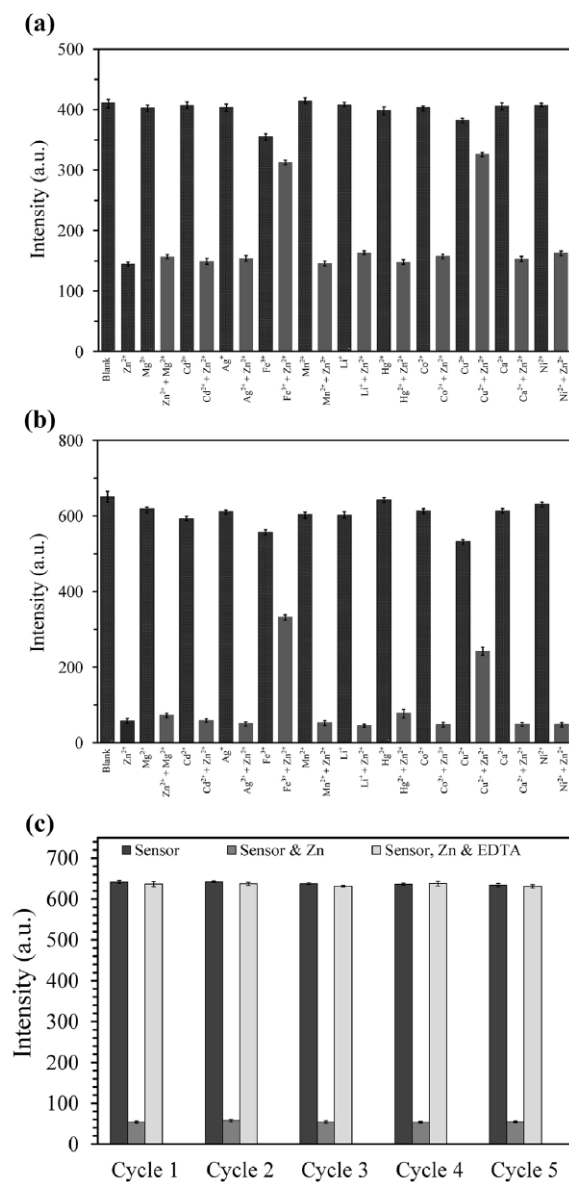
Fig. 8. Fluorescent emission changes of (a) Fe_3O_4@SiO_2-DnS and (b) Fe_3O_4@SiO_2-PEG-DnS at 0.3 μM upon the addition of various metal cations (3.0 equivalents), and (c) the recoverability of Fe_3O_4@SiO_2-PEG-DnS with Zn^{2+}.

stability of the nanochemosensor and its recyclability for practical applications.

4. Conclusions

In summary, this communication reports the successful fabrication and characterisation of a novel magnetic nanochemosensor, namely Fe_3O_4@SiO_2-PEG-DnS, and includes the investigation results in regard to its sensitivity, selectivity, detection limit and pH dependence, as well as its stability and reusability in relation to a series of metal ions. A strong and selective fluorescent quenching was obtained in regard to Zn^{2+} in aqueous solutions. The contributions from both zinc-complexation and/or protonation of the dimethylamine group in the dansyl fluorophore have been hypothesised, both of which are pH dependent. In comparison with Fe_3O_4@SiO_2-DnS, which contains no PEG spacer, Fe_3O_4@SiO_2-PEG-DnS showed a significantly improved sensitivity and selectivity towards zinc ions (Zn^{2+}). Fe_3O_4@SiO_2-PEG-DnS also displayed a noticeably higher value for the quantum yield (0.39) than that of the non-spacer chemosensor ($\Phi = 0.28$), and a very sensitive detection limit of 6.00 nM in regard to zinc ions, which is lower than the lowest reported value of 18.2 nM. In addition, the nanochemosensors displayed very good selectivity when in competition with other cations, except for Cu^{2+} and Fe^{3+}. Furthermore, the novel Fe_3O_4@SiO_2-PEG-DnS nanosensor has proven to be very stable and highly recoverable. Both chemosensors selectively distinguished Zn^{2+} from Cd^{2+}, which is an additional benefit.

References

[1] P. Jiang, Z. Guo, Fluorescent detection of zinc in biological systems: recent development on the design of chemosensors and biosensors, Coord. Chem. Rev. 248 (2004) 205–229.
[2] Z. Xu, J. Yoon, D.R. Spring, Fluorescent chemosensors for Zn^{2+}, Chem. Soc. Rev. 39 (2010) 1996–2006.
[3] J. Wu, W. Liu, J. Ge, H. Zhang, P. Wang, New sensing mechanisms for design of fluorescent chemosensors emerging in recent years, Chem. Soc. Rev. 40 (2011) 3483–3495.
[4] J. Cao, C. Zhao, X. Wang, Y. Zhang, W. Zhu, Target-triggered deprotonation of 6-hydroxyindole-based BODIPY: specially switch on NIR fluorescence upon selectively binding to Zn^{2+}, Chem. Commun. 48 (2012) 9897–9899.
[5] Y. Wu, X. Peng, B. Guo, J. Fan, Z. Zhang, J. Wang, et al., Boron dipyrromethene fluorophore based fluorescence sensor for the selective imaging of Zn(II) in living cells, Org. Biomol. Chem. 3 (2005) 1387–1392.
[6] I. Ravikumar, P. Ghosh, Zinc(II) and PPi selective fluorescence OFF–ON–OFF functionality of a chemosensor in physiological conditions, Inorg. Chem. 50 (2011) 4229–4231.
[7] X. Zhou, B. Yu, Y. Guo, X. Tang, H. Zhang, W. Liu, Both visual and fluorescent sensor for Zn^{2+} based on quinoline platform, Inorg. Chem. 49 (2010) 4002–4007.
[8] Z. Xu, X. Liu, J. Pan, D.R. Spring, Coumarin-derived transformable fluorescent sensor for Zn^{2+}, Chem. Commun. 48 (2012) 4764–4766.
[9] Y. Wang, X. Peng, J. Shi, X. Tang, J. Jiang, W. Liu, Highly selective fluorescent chemosensor for Zn^{2+} derived from inorganic-organic hybrid magnetic core/shell Fe_3O_4@SiO_2 nanoparticles, Nanoscale Res. Lett. 7 (2012) 1–13.
[10] M. Park, S. Seo, I.S. Lee, J.H. Jung, Ultraefficient separation and sensing of mercury and methylmercury ions in drinking water by using aminonaphthalimide-functionalized Fe_3O_4@SiO_2 core/shell magnetic nanoparticles, Chem. Commun. 46 (2010) 4478–4480.
[11] G. Liu, H. Wu, H. Zheng, L. Tang, H. Hu, H. Yang, et al., Synthesis and applications of fluorescent-magnetic-bifunctional dansylated Fe_3O_4@SiO_2 nanoparticles, J. Mater. Sci. 46 (2011) 5959–5968.
[12] X. Feng, S. Zhang, X. Lou, Controlling silica coating thickness on TiO_2 nanoparticles for effective photodynamic therapy, Colloids Surf. B 107 (2013) 220–226.
[13] A.H. Lu, E.e.L. Salabas, F. Schüth, Magnetic nanoparticles: synthesis, protection, functionalization, and application, Angew. Chem. Int. Ed. 46 (2007) 1222–1244.
[14] L. Tian, X. Lou, Z.Q. Pan, Q.M. Huang, H. Zhou, Synthesis, characterisation and catalase-like activity of silica-coated magnetite nanoparticles modified by a Schiff base Mn complex, Micro Nano Lett. 8 (2013) 159–162.
[15] X. Lou, T. Schumacher, H. Yang, A. Ding, Synthesis and characterisation of silica–polymer hybrid core–shell and hollow spheres for drug delivery applications, J. Controlled Release 152 (2011) e65–e67.
[16] H. Wu, P. Zhou, J. Wang, L. Zhao, C. Duan, Dansyl-based fluorescent chemosensors for selective responses of Cr(III), New J. Chem. 33 (2009) 653–658.
[17] G.G. Talanova, N.S. Elkarim, V.S. Talanov, R.A. Bartsch, A calixarene-based fluorogenic reagent for selective mercury(II) recognition, Anal. Chem. 71 (1999) 3106–3109.
[18] J.R. Lakowicz, B.R. Masters, Principles of fluorescence spectroscopy, J. Biomed. Opt. 13 (2008) 9901.
[19] M. Montalti, L. Prodi, N. Zaccheroni, G. Falini, Solvent-induced modulation of collective photophysical processes in fluorescent silica nanoparticles, JACS 124 (2002) 13540–13546.
[20] Q.Y. Chen, C.F. Chen, A new Hg^{2+}-selective fluorescent sensor based on a dansyl amide-armed calix [4]-aza-crown, Tetrahedron Lett. 46 (2005) 165–168.
[21] M. Schuster, M. Šandor, N-Dansyl-N′-ethylthiourea for the fluorometric detection of heavy metal ions, Fresenius J. Anal. Chem. 356 (1996) 326–330.

[22] L. Prodi, F. Bolletta, M. Montalti, N. Zaccheroni, Searching for new luminescent sensors: synthesis and photophysical properties of a tripodal ligand incorporating the dansyl chromophore and of its metal complexes, Eur. J. Inorg. Chem. 1999 (1999) 455–460.

[23] B.H. Shankar, D. Ramaiah, Dansyl-naphthalimide dyads as molecular probes: effect of spacer group on metal ion binding properties, J. Phys. Chem. B 115 (2011) 13292–13299.

[24] X. Feng, S. Zhang, H. Wu, X. Lou, A novel folic acid-conjugated TiO_2–SiO_2 photosensitizer for cancer targeting in photodynamic therapy, Colloids Surf. B 125 (2015) 197–205.

[25] G.A. Crosby, J.N. Demas, Measurement of photoluminescence quantum yields. Review, J. Phys. Chem. 75 (1971) 991–1024.

[26] J. Feng, J. Mao, X. Wen, M. Tu, Ultrasonic-assisted in situ synthesis and characterization of superparamagnetic Fe_3O_4 nanoparticles, J. Alloys Compd. 509 (2011) 9093–9097.

[27] L. Prodi, F. Bolletta, M. Montalti, N. Zaccheroni, Luminescent chemosensors for transition metal ions, Coord. Chem. Rev. 205 (2000) 59–83.

[28] B.P. Joshi, C.R. Lohani, K.-H. Lee, A highly sensitive and selective detection of Hg(II) in 100% aqueous solution with fluorescent labeled dimerized Cys residues, Org. Biomol. Chem. 8 (2010) 3220–3226.

[29] V. Tharmaraj, K. Pitchumani, An acyclic, dansyl based colorimetric and fluorescent chemosensor for Hg(II) via twisted intramolecular charge transfer (TICT), Anal. Chim. Acta 751 (2012) 171–175.

[30] H. Maeda, T. Maeda, K. Mizuno, Absorption and fluorescence spectroscopic properties of 1-and 1, 4-silyl-substituted naphthalene derivatives, Molecules 17 (2012) 5108–5125.

[31] G. Weber, F.J. Farris, Synthesis and spectral properties of a hydrophobic fluorescent probe: 6-propionyl-2-(dimethylamino) naphthalene, Biochemistry 18 (1979) 3075–3078.

[32] W. Schmidt, Optical Spectroscopy in Chemistry and Life Sciences, Wiley-VCH, 2005.

[33] T. Koike, T. Watanabe, S. Aoki, E. Kimura, M. Shiro, A novel biomimetic zinc(II)-fluorophore dansylamidoethyl-pendant macrocyclic tetraamine 1, 4, 7, 10- tetraazacyclododecane (cyclen), JACS 118 (1996) 12696–12703.

[34] L. Fabbrizzi, M. Licchelli, P. Pallavicini, D. Sacchi, A. Taglietti, Sensing of transition metals through fluorescence quenching or enhancement. A review, Analyst 121 (1996) 1763–1768.

[35] B. Valeur, I. Leray, Design principles of fluorescent molecular sensors for cation recognition, Coord. Chem. Rev. 205 (2000) 3–40.

[36] K. Hanaoka, K. Kikuchi, H. Kojima, Y. Urano, T. Nagano, Development of a zinc ion-selective luminescent lanthanide chemosensor for biological applications, JACS 126 (2004) 12470–12476.

[37] G.J. Park, Y.J. Na, H.Y. Jo, S.A. Lee, A.R. Kim, I. Noh, et al., A single chemosensor for multiple analytes: fluorogenic detection of Zn^{2+} and OAc^- ions in aqueous solution and an application to bioimaging, New J. Chem. 38 (2014) 2587–2594.

[38] Y. Ma, H. Chen, F. Wang, S. Kambam, Y. Wang, C. Mao, et al., A highly sensitive and selective ratiometric fluorescent sensor for Zn^{2+} ion based on ICT and FRET, Dyes Pigm. 102 (2014) 301–307.

[39] E.J. Song, H. Kim, I.H. Hwang, K.B. Kim, A.R. Kim, I. Noh, et al., A single fluorescent chemosensor for multiple target ions: recognition of Zn^{2+} in 100% aqueous solution and F^- in organic solvent, Sens. Actuators B 195 (2014) 36–43.

Biographies

Ghazaleh Pourfallah is PhD student in the Department of Chemical Engineering, Curtin University. She holds a BSc from the University Isfahan, a MSc from Arak University and a second MSc from Trent University.

Xia Lou (PhD, University of Dublin) is a professor in the Department of Chemical Engineering of Curtin University. Her research is focused on the development of novel polymeric and nanomaterials and their applications to medical devices, sensing, photocatalysis, drug delivery, cancer targeting, and gas separation/storage.